Comparison of microbially induced sedimentary structures in the Palaeoproterozoic Magaliesberg (Transvaal Supergroup) and Makgabeng (Waterberg Group) Formations, Kaapvaal craton, South Africa

by

Jude Onyekachukwu Okafor

Submitted in partial fulfillment of the requirements for the degree

Master of Science (Geology)

In the Faculty of Natural and Agricultural Sciences

University of Pretoria

Pretoria

05 December 2014

Declaration of originality

I, Jude Onyekachukwu Okafor declare that this thesis, which I hereby submit for the degree Master of Sciences at the University of Pretoria, is my own work and has not previously been submitted for a degree at this or any other tertiary institution.

Signature: ……...

Date: ……

Abstract

The MRS/MISS of the Makgabeng Formation encompasses sand cracks, wrinkle marks, mat fragments, mat chips and roll-ups and those of the Magaliesberg formation are wrinkle marks, petees/petee ridges, sand cracks, and multi-directional ripples. The sedimentary process that moderated the formational mechanism of the MISS of the Makgabeng Formation is (descriptively allochthonous) of high energy (inter-dune depositional setting) that eroded, transported and re-deposited mat bound sediments. The genetic mechanism of the MISS of the Magaliesberg Formation is descriptively authochthonous because of enhanced resistance of biostabilized sediments to being reworked.

XRF (major and trace) and XRD analysis (qualitative and quantitative) was done on MISS bearing sedimentary rock layers (A) and underlying sedimentary sections (B) of Magaliesberg and Makgabeng samples. Result show high quartz content of all the analyzed samples compared to average sandstones. This premise suggests a relation of microbes (e.g. cyanobacteria) to phototrophy and/photoautotrophy because of the conduction properties of translucent quartz. Also plausible inference is that the intense chemical weathering that produced the quartz arenite was positively influenced by microbes, as noted in some Proterozoic basins. There is higher concentration of Ba in all A samples compared to B (Makgabeng and Magaliesberg) which might be emblematic of biogenicity. The Magaliesberg analyzed samples (MAG 101, 102, 103) exhibit homogeneity by the higher concentration of Al_2O_3, TiO_2, K_2O, and P_2O_5, and lower concentration of SiO_2 in the A compared to the B subsamples of a particular sample. Also, Magaliesberg analyzed samples (MAG 101, 102, 103) exhibit homogeneity by the lower concentration of quartz and higher concentration of muscovite in the A compared to the B subsamples. This exact established negative correlation between the duo of SiO_2 and quartz, and the quartet of Al_2O_3, TiO_2, K_2O, and P_2O_5, and muscovite as in Magaliesberg samples pertains also to a Makgabeng sample (MKG 102; roll-up). MKG 101 (mat fragment) deviates from this mineralogical and geochemical trend. Each of the A samples of MAG 101, 102, 103, are uniformly of higher concentration in Ce, Cr, Nb, Th, V, Y, Zn, Zr compared to the B version of that sample. MKG 101 and 102 are uniformly of lower concentration of Ce, Cr, Nb, Th, V, Y, Zn, Zr in A compared to the B version of that sample. The A of each of the samples MAG 101, 102, and 103 has higher concentration of Hf and Rb compared to its B; a character that is also

exhibit in MKG 102, and MKG 101 is vice versa. Microscopy shows that A of all the samples is of smaller grain size compared to B, espousing affinity of microbes to fine-medium grained sandstones. Microscopy of the Magaliesberg Formation samples show Pseudo petee ridges and pseudo cross lamination which reflect biostabilization, and microscopy of the Makgabeng Formation show roll-ups, mat chips and composite mat chips.

The MISS genetic difference of the two formations is related to energy, water residence time (emergence and inundation), Ph, and similarity is related to mutuality in shallow water environment. Mat types are inferred to be biologically, physically and chemically moderated adaptations of microbial communities to specific *cum* peculiar locally prevailing environmental conditions; factors that are premised on taphonomy and ecology.

Keywords: cyanobacteria, phototrophy, photoautotrophy, arenite, Proterozoic, allochthonous, autochthonous, emergence, inundation, shallow water, ph, taphonomy, ecology.

Oh! True God that is everlastingly faithful; to thy all is geared!

Dedication

This work is dedicated to the valediction of Emeritus Prof. P.G Eriksson from lectureship who supervised my honors and M.Sc. degrees, rekindled my love for soft geology and who inculcated in me the hard work, diligence, humility and concordant futuristic dividends of life as an academic, and to my sons; Som and Kosi who bore the pains of a physically absentee father.

Acknowledgement

My elderly parents; Sir and Lady B.E.C Okafor (K.S.J) that worked so hard to make all of us nine siblings graduates. My uncle Prince (Engr.) Arthur Eze for his gratuitous quest and contributions directed towards the elevation of sciences in Nigeria. Prof. Louis Van Rooy that was helpful at the twilight of this academic trudge.

Table of Contents

CHAPTER 4: PHYSICAL SEDIMENTARY GRAIN ANALYSIS

CHAPTER 5: GEOCHEMISTRY AND MINERALOGY OF MISS SAMPLES

CHAPTER 6: DISCUSSION

List of Figures

List of Tables

Appendix

Chapter 1

INTRODUCTION

1.1 Aim of thesis

The aim of the thesis is the characterization of the prolific microbially induced sedimentary structures (MISS) that occur within the Magaliesberg Formation (*ca.* 2.1 Ga, Pretoria Group, Transvaal Supergroup) of the Transvaal basin, particularly in the Pretoria region, and of those that occur in the Makgabeng Formation (*ca.* 2.06-1.8 Ga, Waterberg Group) of the Makgabeng Plateau, Limpopo Province. The former MISS occur in shallow marine tidal-distal braid-delta settings (e.g. Eriksson *et al*., 2012) while those of the Waterberg are from lenticular playa lake deposits within a palaeodesert setting (e.g. Eriksson *et al.,* 2000). The initial aims of this dissertation are thus the creation of a MISS catalogue for the two Formations, the determination of relationships between different types of MISS in each formation, and also the recording of the approximate proportions to each other (i.e. relative importance) of the various MISS types in each unit. In addition, their relationship to the sedimentary processes and products of their respective palaeoenvironments will be examined.

The basic research question at the end is: how do the MISS from these two different formations and environments compare with each other? What were the shared/similar features and what was different, and why did these similar and different features occur?

1.2 Methodology

1.2.1 Field work

Field work in the Makgabeng and Magaliesberg Formations study areas was carried out through field navigation by the utilization of a G.P.S. (global positioning system) receiver. A MISS catalogue of each of the Formations was created and primary sedimentary structures were also identified. Identification of MISS was based on features that are not compatible with the primary sedimentary structure classification scheme of Pettijohn and Potter (1964).

1.2.2 Digital photographs of inferred MISS and other sedimentary structures

Numerous digital photos of inferred MISS structures and other primary sedimentary structures were taken in the field areas of each of the formations, so as to allow megascopic comparison of the MISS structures and other concordant physical sedimentary structures.

1.2.3 Geochemical and mineralogical analysis

Five samples were studied from the two Formations (MAG 101, MAG 102, MAG 103, MKG 101, and MKG 102). Each sample was segregated into a directly MISS-bearing section and an underlying sediment section. The MISS-bearing section and underlying sediment section were analyzed through standard methods of X-ray fluorescence spectrometry (XRF) in the Council for Geosciences Laboratory in Silverton, Pretoria and Qualitative X-ray diffraction at the University of Pretoria X-ray Laboratory to determine the geochemistry and mineralogy, respectively.

1.2.4 Microscopic analysis

Iterative processes involving the utilization of cut slabs and thin sections of each of the samples were carried out with the basic aim of deciphering and understanding peculiar textural attributes. The slab sections particularly showed unusual features of MISS under examination by non-transmitted light microscopy and were thus utilized extensively in this thesis.

1.3 Geological Background

The geological background of this research project is presented separately for the two studied formations because of the comparative aim of the project. Figure 1.1 is a sketch map depicting the relationship between the Transvaal Basin, Waterberg basins (Main and Middelburg Basins) and Bushveld Igneous Complex (BIC). Geological processes leading to the volcano-sedimentary successions of these basin in-fills and also the extrusive and intrusive igneous rocks of the Bushveld Igneous Province are all Palaeoproterozoic with the exception of the lower part of the Transvaal succession which is Neoarchaean. The Neoarchaean-Palaeoproterozoic period in Earth's history is one of large-scale changes related to the supercontinent cycle, allied to development of the sedimentary palaeoenvironments, and also to changes in palaeo-atmospheric composition (e.g., Eriksson *et al.*, 2004).

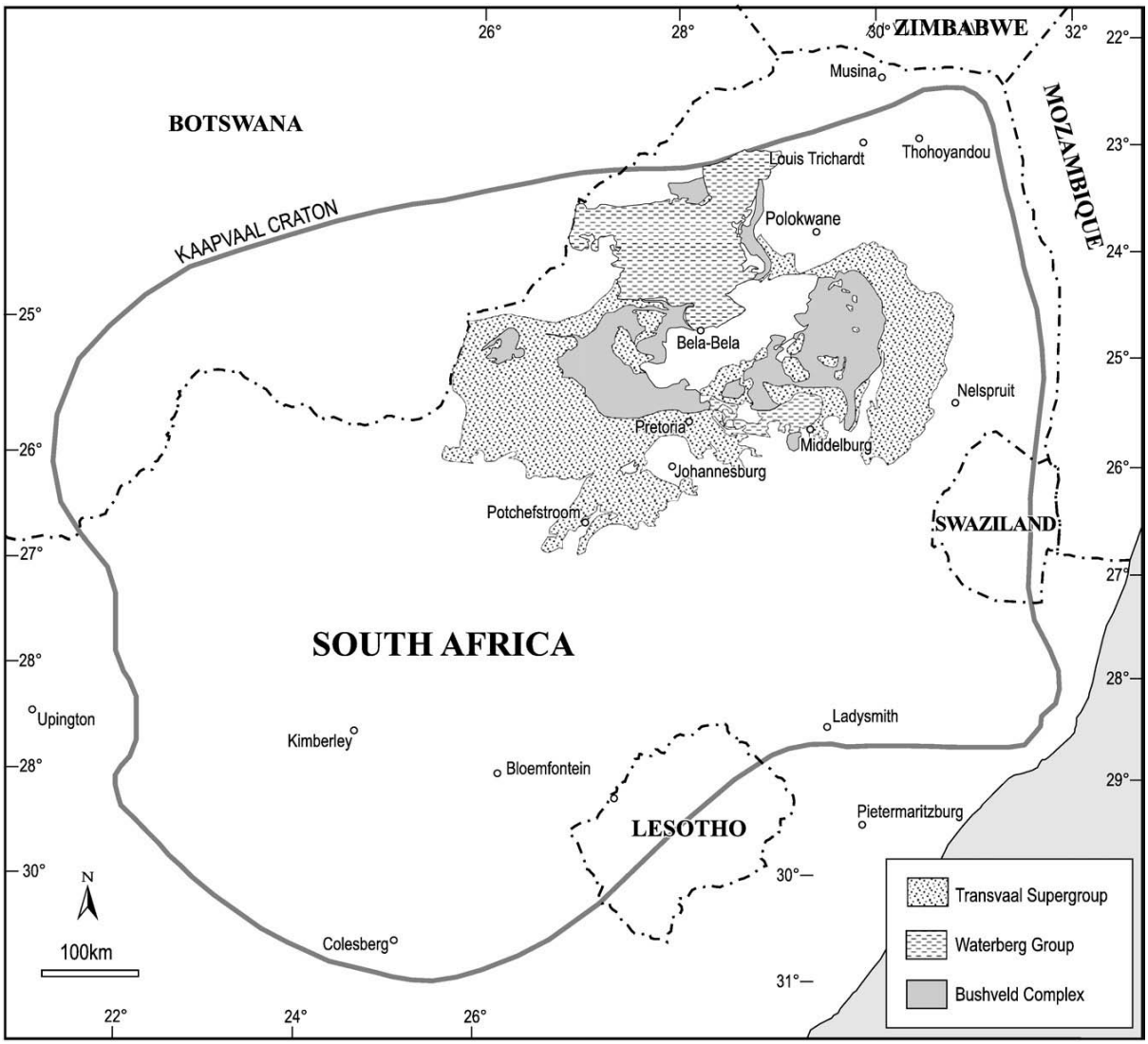

Figure 1.1: The Map of the Kaapvaal craton of Southern Africa showing the Transvaal Basin of South Africa, Bushveld Complex and the Waterberg Group (two basins) (Eriksson *et al.*, 2009).

1.3.1 Magaliesberg Formation of the Transvaal Supergroup

The Magaliesberg Formation forms part of the Pretoria Group of the Transvaal Supergroup (*ca.* 2.67-2.1 Ga) (Bosch and Eriksson, 2008). The Transvaal Supergroup is preserved in three basins of the Kaapvaal craton of southern Africa: Transvaal and Griqualand West Basins in South Africa and Kanye Basin in south-eastern Botswana (Eriksson *et al.*, 2001, 2006a) (Figure 1.2). The evolution of the Neoarchean-Palaeoproterozoic Transvaal basin is ascribed predominantly to magmatism, palaeoclimate and eustasy, with plate tectonics probably playing a lesser role (Eriksson *et al.*, 2001). The Transvaal Supergroup unconformably overlies the Kaapvaal basement, Witwatersrand and Ventersdorp Supergroups (Eriksson *et al.*, 2001) and exhibits stratigraphic and lithological similarities to the relatively coeval Hammersley and Turee Creek Groups of the Pilbara craton of Australia

(Nelson *et al.*, 1999). Based on these stratigraphic and lithological similarities, there are many suggestions for a common evolution of these successions on a greater Kaapvaal-Pilbara craton (e.g. Cheney, 1996), although this is also disputed (e.g., Wingate, 1998; Nelson *et al.*, 1999; Eriksson *et al.*, 1999).

The Transvaal Basin is located in the north-central part of the craton, is the best preserved succession of the Transvaal Supergroup and contains one of the thickest (*ca.* 15 km; Button, 1986) and most complete sequences of Neoarchean-Palaeoproterozoic rocks globally. The Transvaal basin-fill comprises the basal protobasinal rocks (a descriptive term), succeeding the Black Reef Formation, the Chuniespoort Group and the Pretoria Group (e.g. Eriksson *et al.*, 2009) (Figures 1.2, 1.3 and 1.4). The uppermost Rooiberg Group volcanic rocks, often assigned to the Supergroup, are related petrogenetically to the 2.05 Ga Bushveld Complex and are thus more logically a constituent of this inferred large mantle plume event (e.g. Eriksson *et al.*, 2006a).

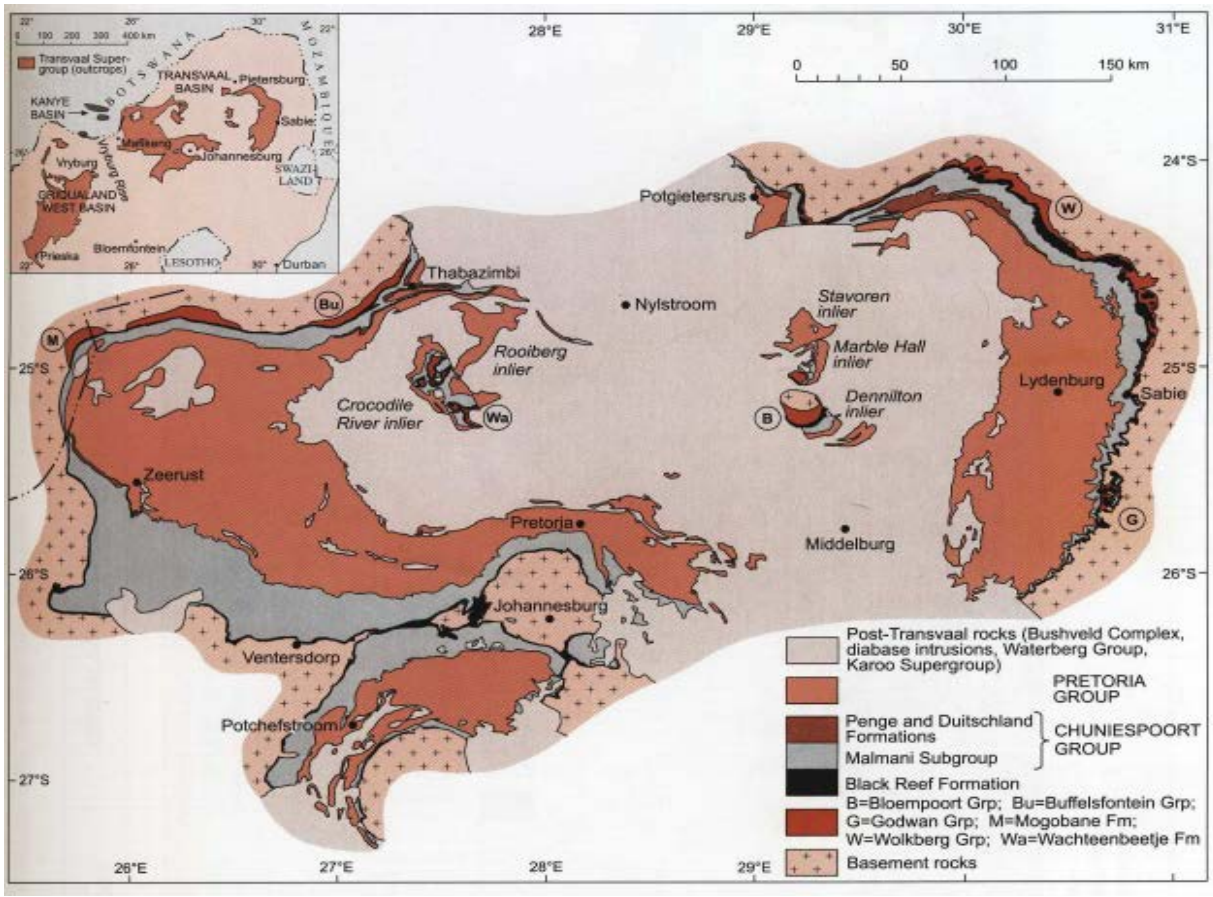

Figure 1.2: Geological Map of the Transvaal Basin of the Transvaal Supergroup. The entire distribution of the Supergroup is shown in the inset map including the Kanye Basin in south-eastern Botswana and the Griqualand West Basin in South Africa (Eriksson *et al.*, 2006a).

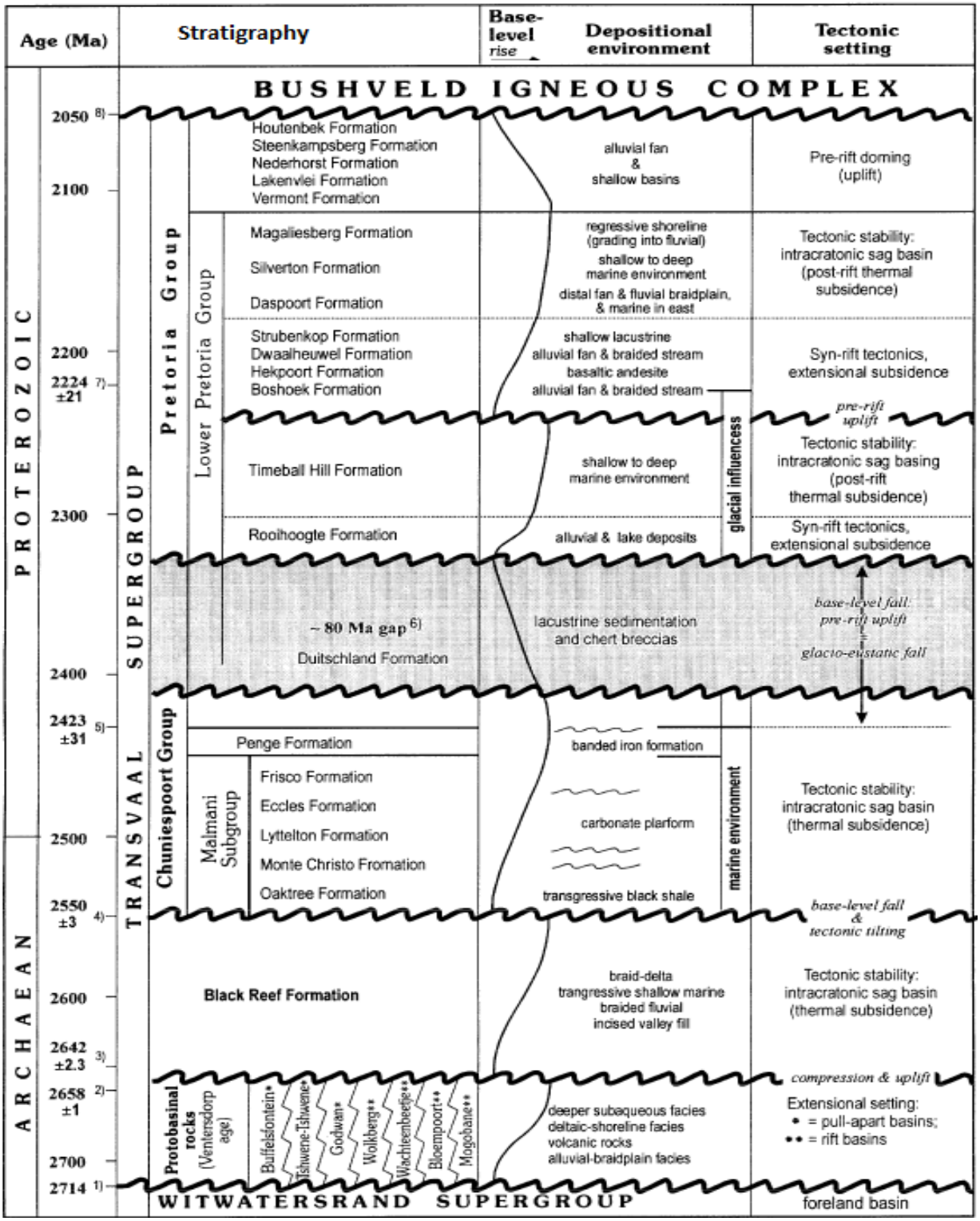

Figure 1.3: Summary of Transvaal Supergroup stratigraphy, geochronology, inferred depositional palaeoenvironments, tectonic settings and the interpreted base-level changes. Wavy lines suggest unconformable contacts (Catuneanu and Eriksson, 1999; Eriksson *et. al.*, 2001 and references therein).

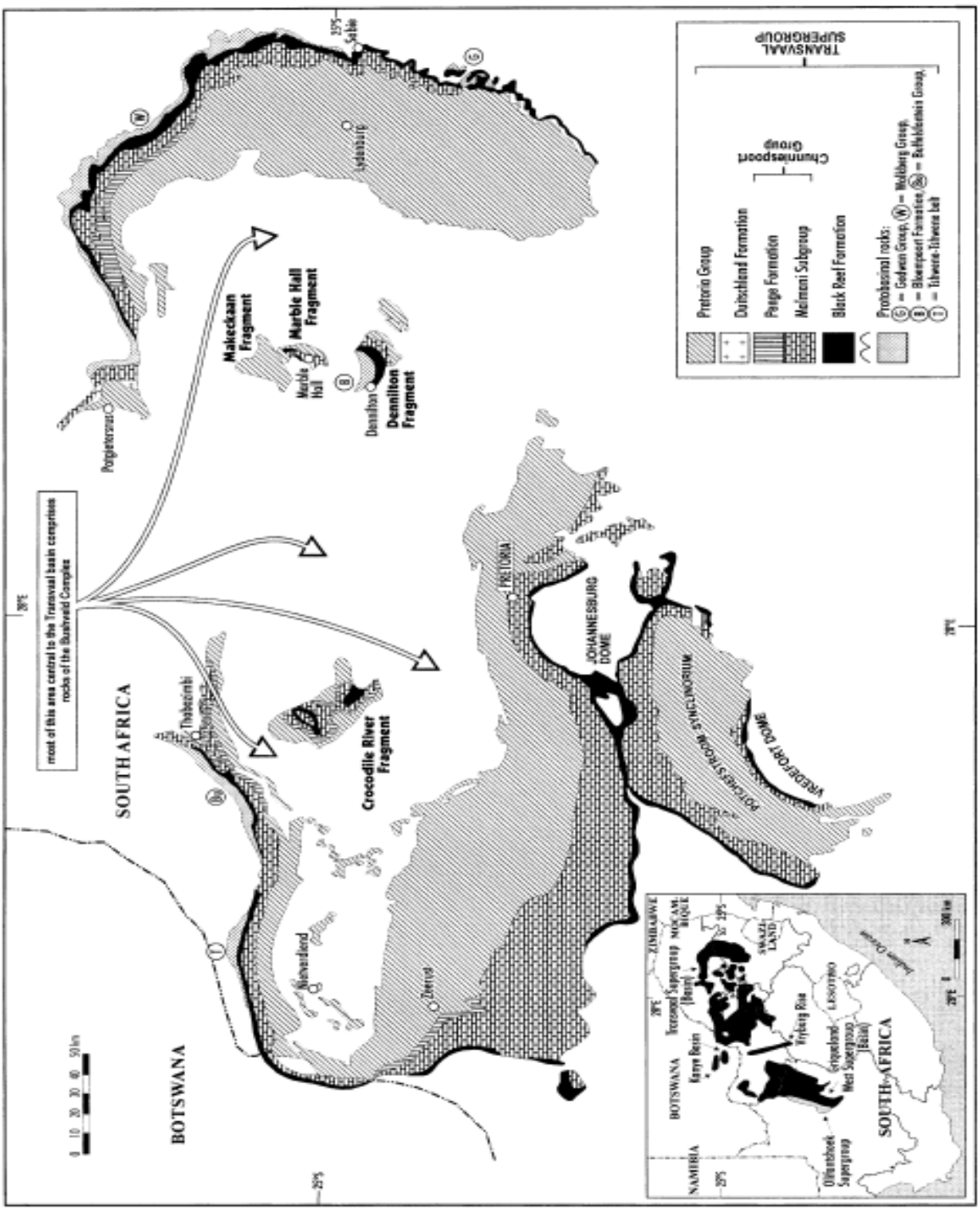

Figure 1.4: Geological map of the Transvaal basin, Transvaal Supergroup, showing basal protobasinal rocks succeeding the Black Reef Formation, Chuniespoort Group and the uppermost Pretoria Group. The centrally located Bushveld Complex is not shown on map in order to avoid complexity. Note fragments of Transvaal rocks (surrounded by Bushveld intrusives) at Crocodile River, Makeckaan, Marble Hall and Dennilton (Eriksson *et al.*, 2001).

The discrete, immature, clastic-volcanic rift-related basin-fills of the so-termed "protobasinal rocks" are thought to reflect a wide zone of rifting that was possibly related to the *ca.* 2.7 Ga Ventersdorp Supergroup mantle plume (e.g. Tyler, 1979a and b; Eriksson *et al.*, 2001, 2006a). These basal protobasinal rocks occur as separate, commonly fault-related units around the margins of the preserved Transvaal basin (Tshwene-Tshwene belt, Buffelsfontein Group, Godwan Group and Wolkberg Group) and are also preserved in two fragments of Transvaal rocks within the Bushveld complex (the Wachteenbeetje Formation in the Crocodile River fragment and the Bloempoort Group in the Dennilton fragment). Thin (generally 30-60 m) widespread fluvial sandstones of the undated Black Reef Formation overlie a basal subaerial unconformity and generally comprise a sheet-like geometry, with thicknesses mostly between a few meters and *ca.* 30m. In eastern Botswana these can be up to 60 m thick (e.g., Henry *et al.*, 1990; Catuneanu and Eriksson, 1999).

An unconformity at the top of the Black Reef Formation is overlain by transgressive black shale which is at the base of the Chuniespoort dolomite-BIF succession (Catuneanu and Eriksson, 1999). The Chuniespoort Group comprises the basal Malmani Subgroup (almost 1200 m thick) that comprises five formations made up of stromatolitic dolomites, subordinate limestone, chert and minor mudrocks and chert-in-shale breccias (Eriksson *et al*., 2001). The Malmani Subgroup and its constituent formations are characterized by a sheet-like geometry (Eriksson and Altermann, 1998) and form a part of a much larger *ca.* 2642-2430 Ma carbonate platform that is also preserved in the Kanye and Griqualand West Basins on the Kaapvaal craton (e.g., Eriksson *et al.*, 2001, 2006a). This carbonate succession in the Transvaal basin grades up into the Penge banded iron formation (BIF), which also appears to have a sheet-like geometry (Eriksson and Reczko, 1995). The Duitschland Formation is the uppermost part of the Chuniespoort Group and has bounding angular unconformities, narrow basin-fill preserved geometry and very local occurrence only in the NE of the Transvaal basin. Catuneanu and Eriksson (1999) interpret the Duitschland sedimentation as largely comprising continental facies resulting from rapid shoreline retreat related to a base level fall driven-regression (falling stage systems tract).

Clastic sedimentary and volcanic rocks of the Pretoria Group (Figures 1.3-1.5) unconformably overlie the Chuniespoort chemical sedimentary rocks (and the Duitschland Formation) with a major angular unconformity which may have encompassed a time gap up to *ca*. 80 million years (Eriksson and Reczko, 1995). The Pretoria Group comprises of an

alternation of mudrocks, quartzose and less mature sandstones, and lesser volcanic rocks (Eriksson *et al.*, 1995b). Figure 1.3 shows the stratigraphy of the Pretoria Group which is made up of 14 formations in the east of the preserved basin where a maximum thickness of 8 km is recorded.

The Pretoria Group has five "post-Magaliesberg formations" preserved in the east of the basin, with the centrally located Rayton and westerly Woodlands Formations suggested as equivalent successions elsewhere in the depository (e.g., Eriksson *et al.*, 1998; Figure 1.5). Boshoek and Dwaalheuwel Formations are best preserved in the northeast and northwest of the preserved basin and wedge out towards the Pretoria area (see Figure 1.4). The general geometry of the lower nine Pretoria Group units (up to and including the Magaliesberg Formation) is predominantly tabular (except, however, the Boshoek and Dwaalheuwel Fms. which are wedge-shaped) (Eriksson and Reczko, 1995). The Pretoria Group in the central part of the Transvaal basin (Gauteng Province area) is subdivided into the basal Rooihoogte Formation, followed upwards by the Timeball Hill, Boshoek, Hekpoort, Strubenkop, Daspoort, Silverton, Magaliesberg and Rayton Formations (SACS, 1980; Eriksson *et al.*, 2001). The sedimentation of the Pretoria Group is ascribed to two cycles of rifting and subsequent thermal subsidence (Eriksson *et al.*, 2001) with the Magaliesberg Formation being deposited late in the second episode of thermal subsidence within an overall intra-cratonic sag basin (Catuneanu and Eriksson, 1999; Eriksson *et al.*, 2001).

The Magaliesberg Formation is composed of alternating successions of sandstones with minor thin (a few dm.) mudrock beds, and the thickness of the Formation in the vicinity of Pretoria is *ca.* 300m (Eriksson *et al.*, 1995b). The quartzose sandstones of the Magaliesberg Formation are horizontally stratified; some are cross-bedded, with abundant ripple marks (Van der Neut, 1990). The Magaliesberg Formation (and other Transvaal basin rocks) formed the floor to the *ca.* 2.56 Ga Bushveld Complex (Eriksson *et al.*, 1998) and consequently underwent contact metamorphism producing hornfels in the thin mudrock interbeds and much more commonly recrystallised quartzitic sandstones from the original arenaceous sedimentary rocks. The dip of the bedding of the Magaliesberg Formation and other Transvaal basin strata, is mostly about 10-15^{o} towards the centrally-located Bushveld Complex, in addition to deformation caused by open interference folds (Eriksson *et al.*, 1998) and faulting (Van der Merwe *et al.*, 1988).

Age dating (Rb-Sr, whole rock) gave an Early Proterozoic Age of about 2250 Ma (Burger and Walraven, 1980) for the lower Pretoria Group, which has been supplemented by more accurate dating of the Timeball Hill (2316±7 Ma) and Hekpoort (2224±21 Ma) Formations (refer to Eriksson *et al.*, 2006a and references therein for succinct discussion). Three architectural elements (cf. Miall, 1985) are identified in the Magaliesberg Formation (e.g. Parizot *et al.*, 2005; Eriksson *et al.*, 2008): (1) Medium- to coarse-grained sandstone sheets with unimodal palaeocurrent trends; (2) Fine- to medium-grained sandstone sheets with bi- to polymodal palaeocurrent modes; (3) Mudrock elements. Both arenaceous elements are dominated by horizontal laminations and planar cross-bedding, with subordinate trough cross-bedding, channel-fills, wave ripple marks, minor double-crested and flat-topped ripples and desiccated mudrock partings (Eriksson *et al.*, 1995b).

The *ca.* 2.1 Ga Magaliesberg Formation is ascribed to formation through a combination of ephemeral braid-delta systems (first architectural element above) debouching into high energy peritidal flats (cf., architectural element 2). This fluvial-tidal setting was situated at the periphery of a shallow epeiric sea then occupying the Transvaal Basin (Eriksson *et al.*, 2002), leading to reworking through small waves and meso- to locally macro-tidal conditions (Eriksson *et al.*, 1995). The subordinate mudrock element suggests abandonment of braid-delta channels, or uppermost tidal flat sedimentation. The sandstones of the Magaliesberg Formation are interpreted as reflecting a second order highstand systems tract within a clastic marine setting, where sediments were fed into a tidally dominated coastline setting by episodic braided fluvial systems (Eriksson *et al.*, 2012).

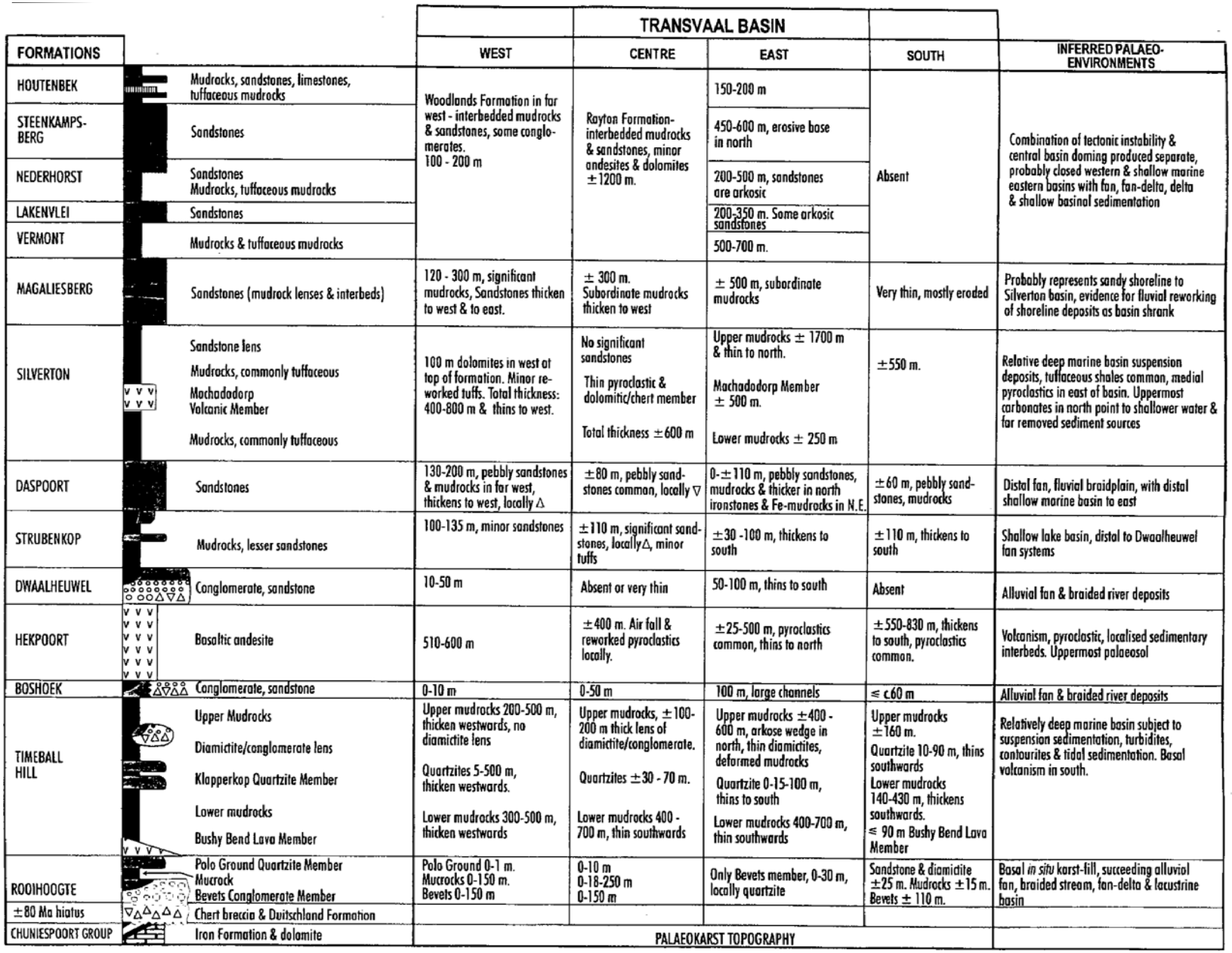

FORMATIONS		TRANSVAAL BASIN: WEST	TRANSVAAL BASIN: CENTRE	TRANSVAAL BASIN: EAST	TRANSVAAL BASIN: SOUTH	INFERRED PALAEO-ENVIRONMENTS
HOUTENBEK	Mudrocks, sandstones, limestones, tuffaceous mudrocks	Woodlands Formation in far west - interbedded mudrocks & sandstones, some conglomerates. 100 - 200 m	Rayton Formation- interbedded mudrocks & sandstones, minor andesites & dolomites ±1200 m.	150-200 m	Absent	Combination of tectonic instability & central basin doming produced separate, probably closed western & shallow marine eastern basins with fan, fan-delta, delta & shallow basinal sedimentation
STEENKAMPS-BERG	Sandstones			450-600 m, erosive base in north		
NEDERHORST	Sandstones Mudrocks, tuffaceous mudrocks			200-500 m, sandstones are arkosic		
LAKENVLEI	Sandstones			200-350 m. Some arkosic sandstones		
VERMONT	Mudrocks & tuffaceous mudrocks			500-700 m.		
MAGALIESBERG	Sandstones (mudrock lenses & interbeds)	120 - 300 m, significant mudrocks, Sandstones thicken to west & to east.	± 300 m. Subordinate mudrocks thicken to west	± 500 m, subordinate mudrocks	Very thin, mostly eroded	Probably represents sandy shoreline to Silverton basin, evidence for fluvial reworking of shoreline deposits as basin shrank
SILVERTON	Sandstone lens Mudrocks, commonly tuffaceous Machadodorp Volcanic Member Mudrocks, commonly tuffaceous	100 m dolomites in west at top of formation. Minor re-worked tuffs. Total thickness: 400-800 m & thins to west.	No significant sandstones Thin pyroclastic & dolomitic/chert member Total thickness ±600 m	Upper mudrocks ± 1700 m & thin to north. Machadodorp Member ± 500 m. Lower mudrocks ± 250 m	±550 m.	Relative deep marine basin suspension deposits, tuffaceous shales common, medial pyroclastics in east of basin. Uppermost carbonates in north point to shallower water & far removed sediment sources
DASPOORT	Sandstones	130-200 m, pebbly sandstones & mudrocks in far west, thickens to west, locally △	±80 m, pebbly sandstones common, locally ▽	0-±110 m, pebbly sandstones, mudrocks & thicker in north ironstones & Fe-mudrocks in N.E.	±60 m, pebbly sandstones, mudrocks	Distal fan, fluvial braidplain, with distal shallow marine basin to east
STRUBENKOP	Mudrocks, lesser sandstones	100-135 m, minor sandstones	±110 m, significant sandstones, locally△, minor tuffs	±30 -100 m, thickens to south	±110 m, thickens to south	Shallow lake basin, distal to Dwaalheuwel fan systems
DWAALHEUWEL	Conglomerate, sandstone	10-50 m	Absent or very thin	50-100 m, thins to south	Absent	Alluvial fan & braided river deposits
HEKPOORT	Basaltic andesite	510-600 m	±400 m. Air fall & reworked pyroclastics locally.	±25-500 m, pyroclastics common, thins to north	±550-830 m, thickens to south, pyroclastics common.	Volcanism, pyroclastic, localised sedimentary interbeds. Uppermost palaeosol
BOSHOEK	Conglomerate, sandstone	0-10 m	0-50 m	100 m, large channels	≤ c60 m	Alluvial fan & braided river deposits
TIMEBALL HILL	Upper Mudrocks Diamictite/conglomerate lens Klapperkop Quartzite Member Lower mudrocks Bushy Bend Lava Member	Upper mudrocks 200-500 m, thicken westwards, no diamictite lens Quartzites 5-500 m, thicken westwards. Lower mudrocks 300-500 m, thicken westwards	Upper mudrocks, ±100-200 m thick lens of diamictite/conglomerate. Quartzites ±30 - 70 m. Lower mudrocks 400 - 700 m, thin southwards	Upper mudrocks ±400 - 600 m, arkose wedge in north, thin diamictites, deformed mudrocks Quartzite 0-15-100 m, thins to south Lower mudrocks 400-700 m, thin southwards	Upper mudrocks ±160 m. Quartzite 10-90 m, thins southwards Lower mudrocks 140-430 m, thickens southwards. ≤ 90 m Bushy Bend Lava Member	Relatively deep marine basin subject to suspension sedimentation, turbidites, contourites & tidal sedimentation. Basal volcanism in south.
ROOIHOOGTE	Polo Ground Quartzite Member Mucrock Bevets Conglomerate Member	Polo Ground 0-1 m. Mucrocks 0-150 m. Bevets 0-150 m	0-10 m 0-18-250 m 0-150 m	Only Bevets member, 0-30 m, locally quartzite	Sandstone & diamictite ±25 m. Mudrocks ±15 m. Bevets ± 110 m.	Basal *in situ* karst-fill, succeeding alluvial fan, braided stream, fan-delta & lacustrine basin
±80 Ma hiatus	Chert breccia & Duitschland Formation					
CHUNIESPOORT GROUP	Iron Formation & dolomite	PALAEOKARST TOPOGRAPHY				

Figure 1.5: Variations in lithology, thickness and inferred depositional conditions of the Pretoria Group across the Transvaal Basin represented in a schematic summary profile (Eriksson *et al.*, 2006).

1.3.2 Makgabeng Formation of the Waterberg Group

The Makgabeng Formation forms part of the Main Basin of the Waterberg Group. The Waterberg Group is preserved within a large Main Basin in North-Northwestern South Africa and adjacent eastern Botswana and within a smaller Middelburg Basin, east of Pretoria (SACS, 1980; Jansen, 1982; Eriksson *et al.,* 2008) (Figure 1.6). Jansen (1982) divided the larger northern basin into the Nylstroom Protobasin and the immediately adjacent Main Basin. The Main Waterberg basin occupies an area of approximately 22,000 km^2 (Jansen, 1971) and the Makgabeng Formation is a part of the Waterberg Main basin-fill. There is controversy pertaining to the thickness of the Waterberg succession: between *ca.* 2700m and 7000m or more (Hall, 1932; Jansen, 1982; Tankard *et al.,* 1982; Cheney and Twist, 1986; Du Plessis, 1987; Stettler, 1991), The Waterberg Group consists of a succession of coarse siliciclastic rocks that show two upward-fining sequences (Callaghan *et al.,* 1991).

The Waterberg Group in the Main Basin is comprised of eleven Formations (Eriksson *et al.,* 2000 and references therein). The lowest Formation of the Main Basin rests unconformably on the Blouberg Formation, a lone-standing unit of pre-Waterberg age (Bumby, 2000), as well as on granites and mafic rocks of the Archaean granitic-gneissic basement; the Karoo Supergroup rocks overlie the Waterberg Group in the North of the basin (Eriksson *et al.,* 1991). A complex stratigraphy comprises 11 Formations, many of which pass laterally into others and are thus presumed to be coeval, with the Vaalwater fault essentially separating the coeval stratigraphy (Figures 1.7 and 1.8).

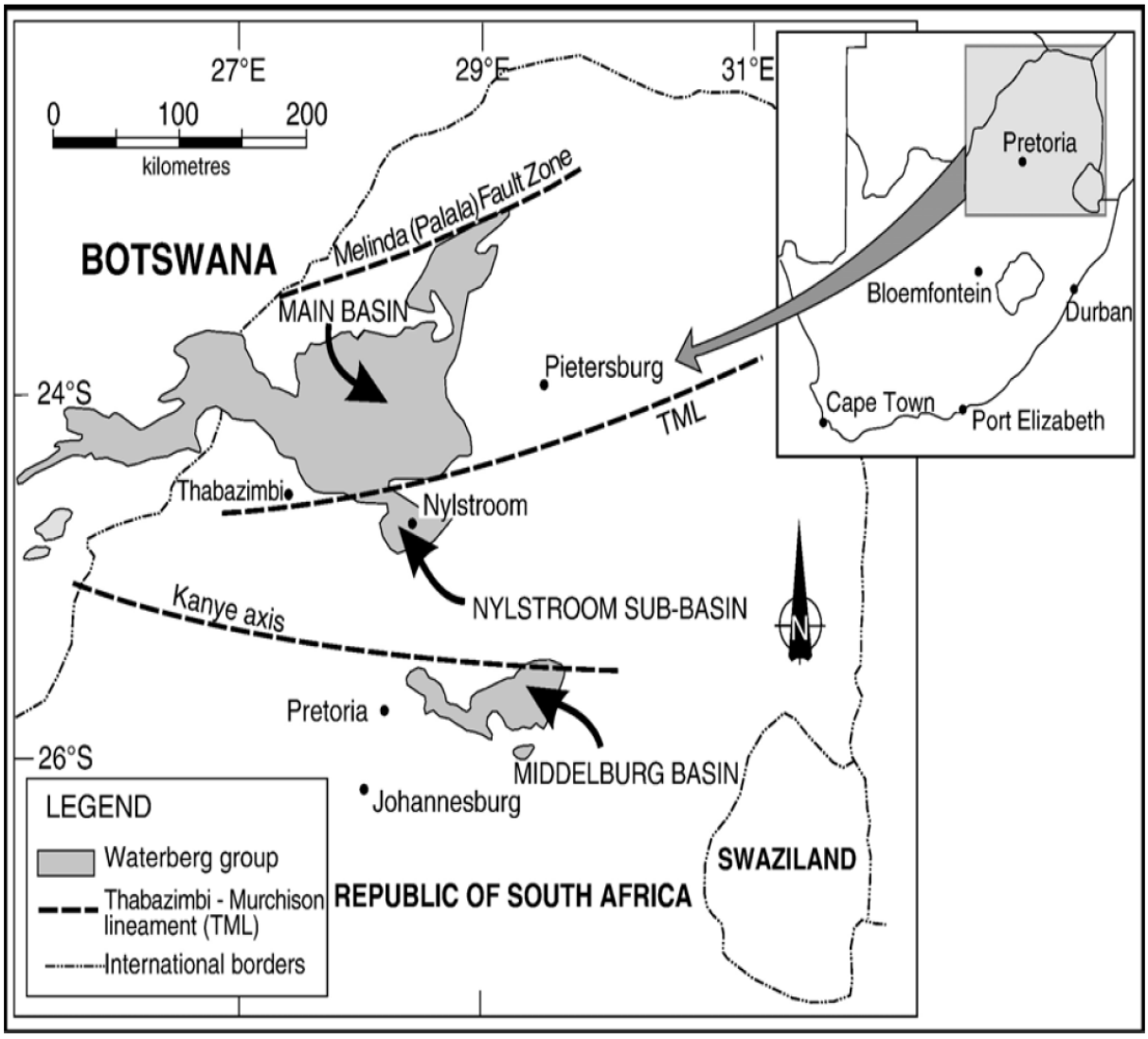

Figure 1.6: Sketch map showing the location of the Waterberg Group in South Africa; larger Main Basin in the northeast and smaller Middelburg Basin east of Pretoria. Main Basin bounded by Melinda (Palala) fault and Thabazimbi-Murchison lineament (TML), and Middelburg Basin bounded by the Kanye axis (Eriksson *et al.*, 2006b).

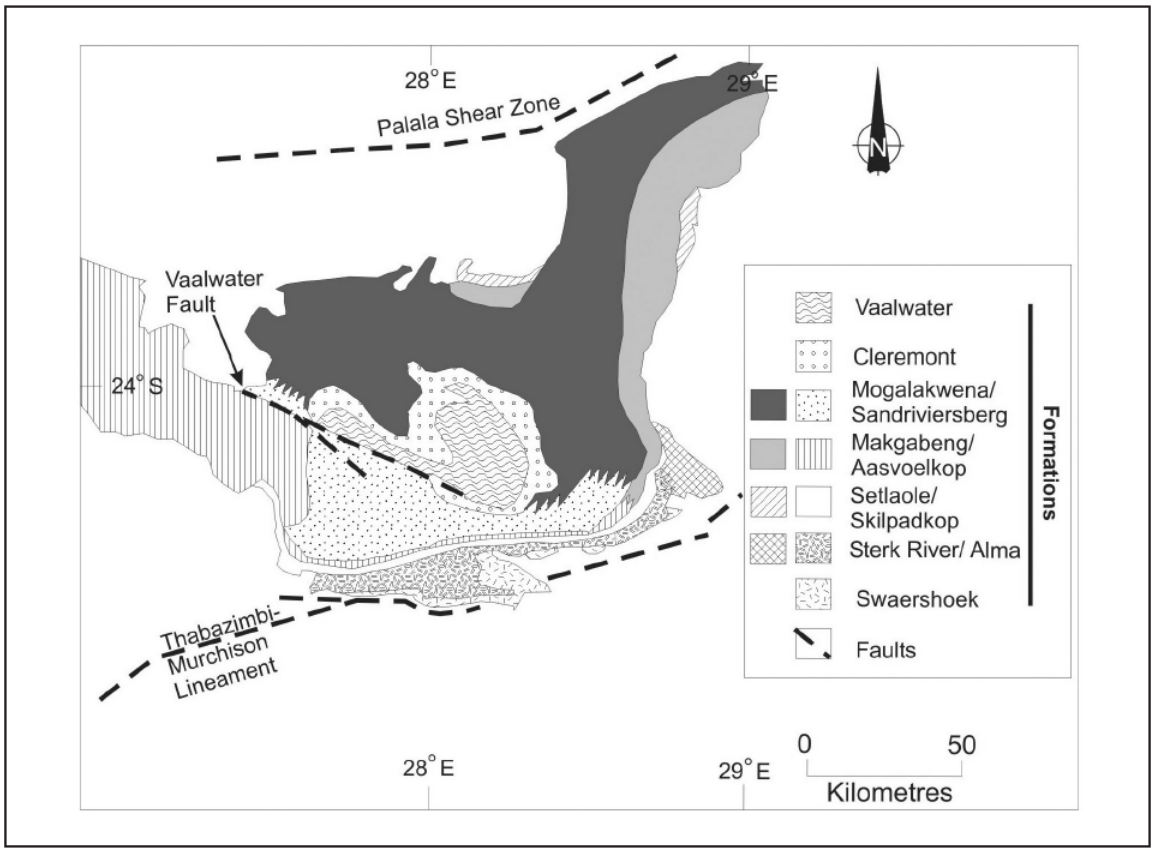

Figure 1.7: Geological sketch map of the Waterberg Group Main Basin, showing individual formations and their three-dimensional stacking relationships (see legend box). Note Vaalwater fault and three correlated pairs of medial Waterberg Group formations (Setlaole/Skilpadkop; Makgabeng/Aasvoelkop; Mogalakwena/Sandriviersberg) respectively to the northeast and southwest of this fault (Eriksson *et al.*, 2006b).

The deposition of the Waterberg Group took place mainly within alluvial settings (Vos and Eriksson, 1977; Bumby, 2000), with lesser lacustrine and desert palaeoenvironments, and possible terminal littoral marine influences towards the south of the preserved basin (Callaghan *et al.*, 1991); subordinate volcanic rocks occur locally (Eriksson *et al.*, 1991).

The age of the Waterberg Group is confined approximately between 2.06 and 1.88 Ga (Simpson *et al.*, 2013 and references therein), and it is comprised of red pigmented, coarse clastic sedimentary rocks that generally display a fining-upward sequence throughout the succession, from basal rudites, through arenites and lutaceous arenites (Callaghan, 1987a). The Main Waterberg basin is a fault-controlled basin bounded by two major and fundamental

structural lineaments within the Kaapvaal craton (Callaghan *et al.*, 1991): the long-lived Thabazimbi Murchison lineament (TML) and the Melinda (Palala) fault zone of the Limpopo mobile belt (Figure 1.6); the latter represents a Himalayan-style collisional event between the Zimbabwe craton in the north and the Kaapvaal craton in the south (e.g., Treloar *et al.*, 1992; Rigby *et al.*, 2008). The TML was reactivated in the Palaeoproterozoic to accommodate the Waterberg sediments (Button, 1972; Jansen 1975a, 1982).

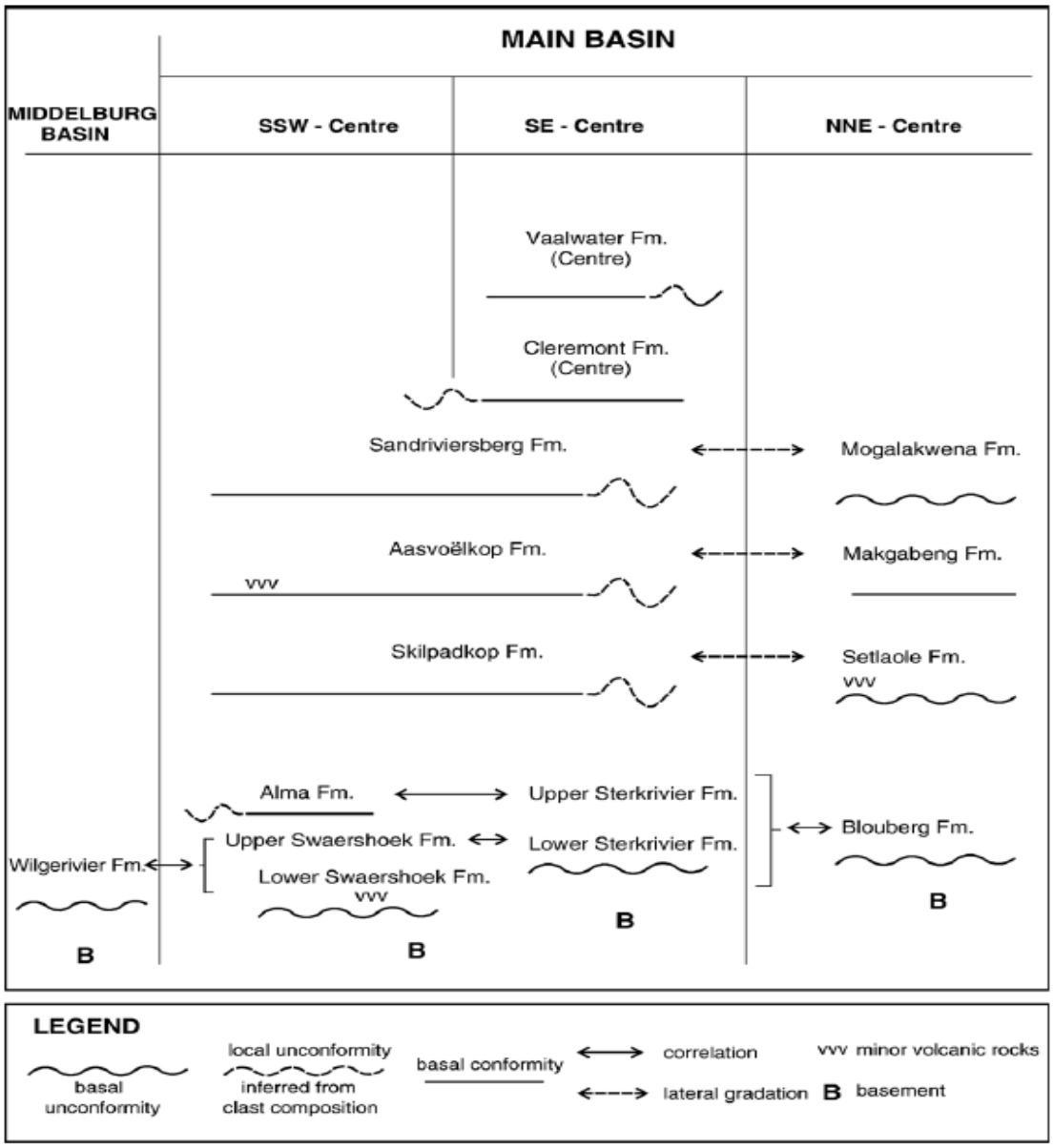

Figure 1.8: Details of the stratigraphic subdivision of the Waterberg Group in different areas of the Main Basin; inferred correlations/unconformable contacts are also shown (Eriksson *et al.*, 2006b).

The Waterberg Group is one of the sedimentary units which mark the first appearance globally of red beds (*sensu stricto* - i.e. those where clast surfaces are partially stained by red-coloured iron minerals, as opposed to matrix-staining) and also of large erg deposits worldwide, at *ca.* 1.9 to 1.8 Ga (e.g., Eriksson and Cheney, 1992; Eriksson and Simpson, 1998).

The Makgabeng Formation occurs in the northern and eastern parts of the Main Waterberg Basin where it conformably overlies the Setlaole Formation where they are both present and is unconformably overlain by the Mogalakwena Formation (Jansen, 1982) (Figure 1.8). The Formation is made up of fine- to medium-grained arenites which display very large scale cross-bedding (Eriksson *et al.*, 2000; Simpson *et al.*, 2002). The maximum thickness of the Formation is 1200m (Jansen, 1982) to 1000m (SACS, 1982). The lithofacies distribution of the Makgabeng Formation and their relationship to climatic shift is reviewed in Hennes *et al.* (2014) and Simpson *et al.* (2013).

1.4 Study areas

1.4.1 Magaliesberg Formation study area

The study location is the Bronx Glass and Sand Mine and silica quarry on the farm Vlakfontein in the District of Bronkhorstspruit, which is about 50 km east of Pretoria (Figure 1.9 A and B). At this location, only the finer-grained sandstone sheet and mudrock architectural elements identified by Eriksson *et al.* (1995; see also Parizot *et al.*, 2005) are evident.

The study area is located in the southern part of the Transvaal Supergroup exposures, and here the Magaliesberg Formation is separated from the Bushveld Igneous Complex intrusion only by the Rayton Formation (uppermost Pretoria Group; e.g., Parizot *et al.*, 2005). As a consequence of this factor, the Magaliesberg Formation lies within the Bushveld contact aureole and some individual beds have consequently been recrystallized to quartzite, with interbeds not affected. Most of the samples with MISS are not *in situ* because of continuous quarrying activity that is negatively affecting its preservation, and the majorities are taken from unrecrystallised beds. The samples exhibit peculiar structures on microscopic and megascopic scales that are not recorded by the Pettijohn and Potter (1964) classification of sedimentary structures (see also Noffke *et al*, 2001a).

Figure 1.9: Google Earth map view of the Magaliesberg Formation study area (25°52'20.04"S, 28°39'28.75"E; pinkish bulb). Note the whitish colour of the freshly quarried sandstone which underlines the high mineralogical maturity (quartz >99%) of the sandstones.

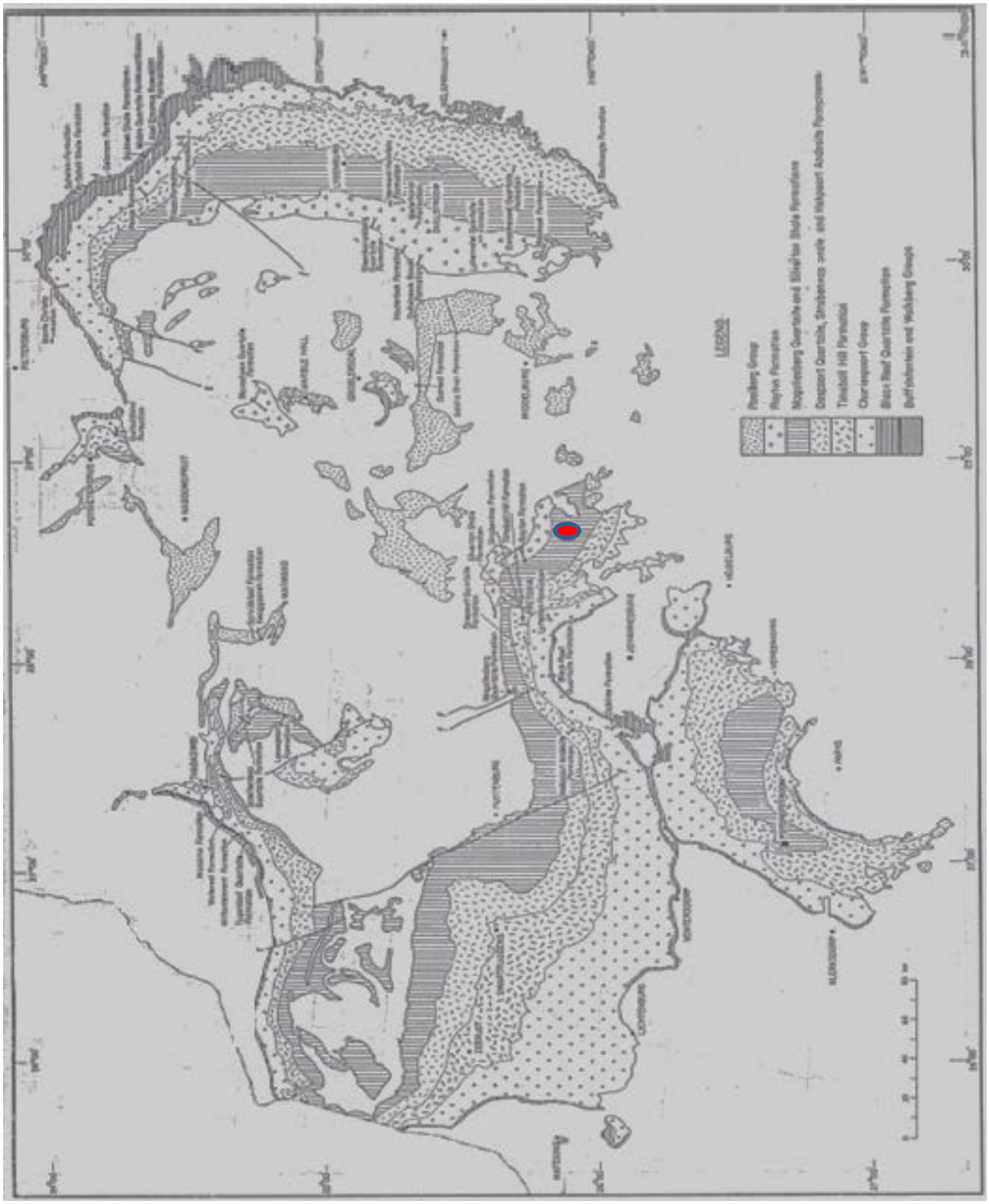

Figure 1.10: Map of the Transvaal Basin, also showing the Pretoria Group. Note that the location of the study area is given by the red coloured dot (after Eriksson *et al.*, 1995).

1.4.2: Makgabeng Formation study area

The study area is located in the Limpopo Province of the Republic of South Africa and lies in the exposures around the Makgabeng Plateau (Fig. 1.10 A and B); the lithology of the area is characterized by red-coloured fine- to medium-grained quartz arenites and also minor finer siliciclastics and localized pebbly sandstones.

Figure 1.11: Google Earth map view of the Makgabeng Plateau study area (23°13'53.36"S, 28°52'59.95"E) which forms a topographic high crossed by dykes, easily visible on the image, with study area marked by the a pinkish bulb along the northern marginal cliffs of the plateau.

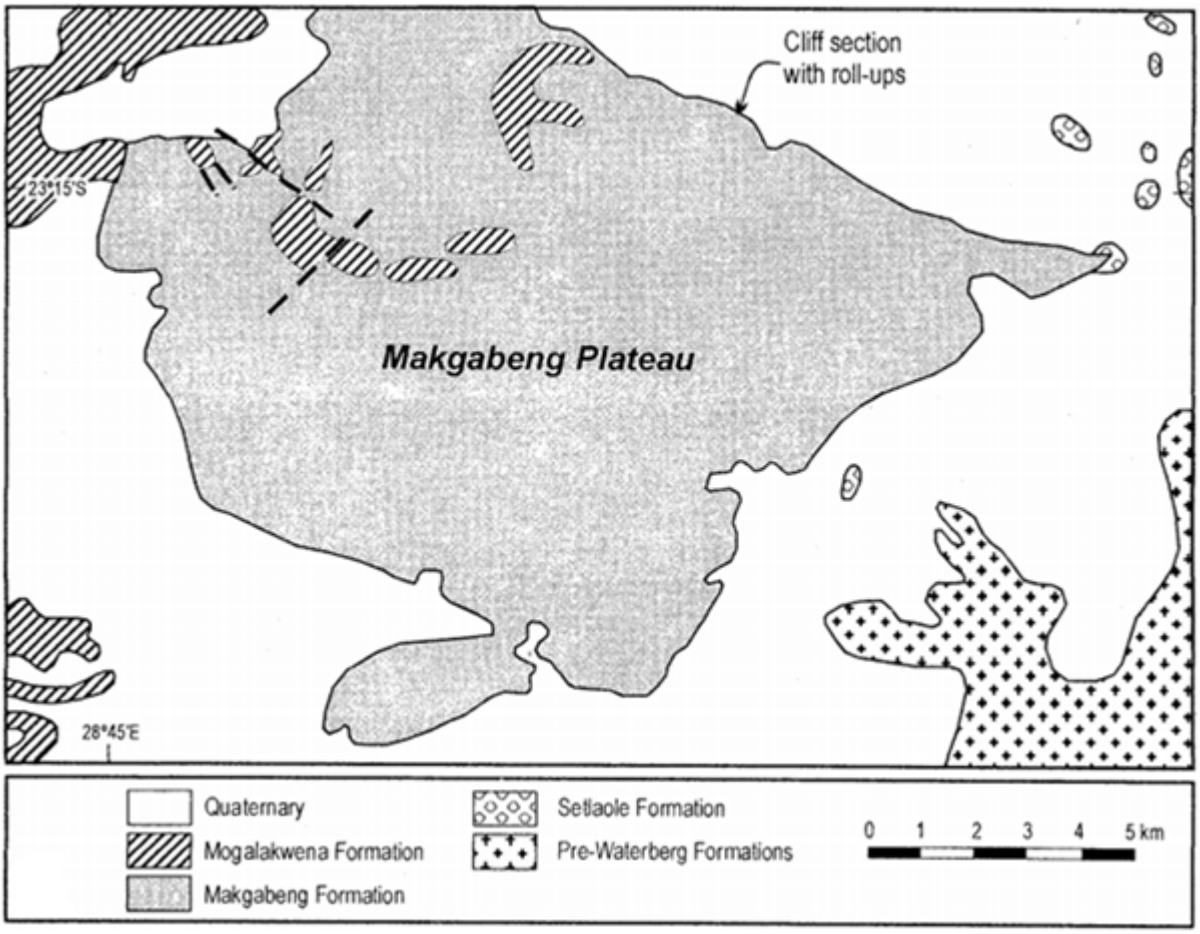

Figure 1.12: Map of the Makgabeng Plateau study area showing the location of the cliff section with preservation of MISS/MRS features (Eriksson *et al.*, 2000).

Chapter 2

MICROBIALLY-INDUCED SEDIMENTARY STRUCTURES (MISS)

The wide variety of sedimentary structures observed in sedimentary rocks is the result of a large range of physical, chemical, and biological processes characterizing sedimentary depositional systems (e.g., Noffke *et al.*, 2001a). Physical sedimentary structures are formed by the strictly physical processes of erosion, transport, deposition, and deformation (Pettijohn and Potter, 1964) and include various forms of bedding, markings on bedding surfaces (both upper and lower), structures within beds (such as cross-strata) and deformational phenomena (see Reid *et al.*, 2000 for recent overview). The classification scheme of Pettijohn and Potter (1964) formed the basis for the classification of sedimentary structures and was later augmented by the addition of microbial structures in siliciclastic sediments and rocks. The scheme of Pettijohn and Potter (1964) records stromatolites as positive growth structures projecting from former depositional surfaces, recognizing the fact that microbes construct them in conjunction with syn-sedimentary sedimentation (e.g., Altermann, 2004).

Microbial related features (cf. stromatolites) from carbonate rock-forming palaeoenvironments are well known, but microbial mat features preserved within the clastic sedimentary record are much less so (e.g., Eriksson *et al.*, 2008). Kalkowsky (1908) described stromatolite as a layered rock. Buick *et al.* (1981) describe stromatolite as any up-domed sedimentary structure that has layered internal texture independent of the origin of the structure and utilized the acronym for structures that are definitely of biological origin (organo-sedimentary structures). Awramik and Margulis (1974) define stromatolites as laminated microbialites that are produced by sediment trapping, binding, and/or *in situ* precipitation of minerals (most especially, carbonate minerals) as a consequence of the growth and metabolic activity of microorganisms, principally cyanobacteria. Noffke (2010 ; see also Noffke *et al.*, 2001a) defines MISS as sedimentary structures that are of organo-physico-chemical origin and which are also primary sedimentary structures that are products of syn-depositional interaction of biofilms and microbial mats with the physical sediment dynamics in the siliciclastic system. Eriksson *et al.* (2010) utilized mat-related structures (MRS) as a broader definition to encompass even those structures that are not directly induced by microbes. MISS are formed by baffling, trapping of sediment, microbial growth, biostabilization and the interaction of some/all of these parameters (e.g., Eriksson *et al.*,

2007a and references therein; Noffke, 2010) with little or no primary mineral precipitation but probable secondary mineral accretion (caused by microbial decay). The extrapolymeric substances (proteins and polysaccharides) colonized by millions of microbes as biofilms and consequent/probable microbial mats that are inherent in the formation of stromatolites are also the genetic starting point and norm for MISS. As stromatolites and MISS are formed by relatively similar fundamental iterative processes and mechanisms (equivalents to a certain degree), but with more restriction of stromatolites to chemical lithologies and MISS to siliciclastic environments, Noffke (2013) describes MISS and stromatolite as "relatives" of each other.

The low preservation potential of MISS in mudstone and sandstone (high porosity and permeability) reflects poor carbon preservation because of enhanced decomposition of carbon materials; therefore the fundamental fact is that evidence for microbial mats in mudrocks and sandstones is generally indirect (e.g., Schieber, 1998a), comprising proxies rather than direct observations (e.g., Eriksson *et al.*, 2012), and thus often contentious (e.g., Buick *et al.*, 1981; Schieber, 1999). It can be complex to interpret these features from the sedimentary record, especially in environments whose configuration and sedimentary dynamics can change in relatively short time periods (days to decades), such as coastal areas (deltas, estuaries, lagoons, evaporitic flats, dunes, etc.; e.g., Hamblin and Christiansen, 2007), or in going from aquatic to non-aquatic environments in a few centimeters or meters of preserved rock strata. Eriksson *et al.* (2008, and references therein) define mat-related features (MRS, cf. MISS) as sedimentary features that *sensu stricto* may form from several microbial genetic influences and stress that analogous features may also form by non-biological means or through a mixture of physical-chemical and microbial influences. One of the most important effects of mats on sandstones and mudstones is the increase in cohesion and change in the rheology of sediments caused by microbe-sediment interaction.

Prior to the incursion of grazing metazoans that is coincident with the Neoproterozoic-Phanerozoic boundary; the influence of microbial mats would have been prolific on Earth (Schieber, 2004). Microbial mats would probably have colonized most sedimentary surfaces, clastic and chemical, where their water/moisture, light and nutrition requirements could be met (e.g., Schieber *et al.*, 2007 and references therein). A relatively large number of clastic sedimentary features that are directly and indirectly related to the presence of such mats are identified in the rock record (e.g., Schieber, 1998; Schieber *et al.*, 2007 for an atlas of MISS)

and is emblematic of a genetic continuum from mat growth, through mat metabolism, mat destruction, to mat decay and diagenesis, within either mudstones or sandstones (e.g., Schieber, 2004 and references therein) (Figures 2.1 and 2.2). In modern environments, microbial mats are commonly found in a relatively wide range of depositional settings, on sandy and finer siliciclastic surfaces (Schieber, 1998a). Microbes can be expected in all (Precambrian) environments and in the long term, they may have strongly influenced the regional topography, sedimentation rates, sedimentary dynamics, and the reworking of previously emplaced materials (Beraldi Campesi, 2013). Noffke *et al.* (2003, 2006a and b) have shown that MISS occur as far back as at least 3.2 Ga in the rock record, in the Moodies Group of the Barberton greenstone belt of South Africa. Noffke *et al.* (2013) similarly record an active, ancient ecosystem in the *ca*. 3. 48 Ga Dresser Formation, of the Pilbara craton, in Western Australia.

Microbial mats are common in supratidal facies, but also spread from deeper subtidal examples right through to palaeodesert mat-related features (e.g., Eriksson *et al.,* 2002). The utilization of MISS in palaeoenvironmental interpretation is hitherto controversial. Noffke *et al.* (2006a) use MISS to interpret shallow marine siliciclastic environments, and more specifically regression-transgression turning points. Catuneanu (2007; see also, Bose *et al.*, 2007) argues in favour of a wider palaeoenvironmental distribution, but more specifically for mats having had a more complex effect on sequence architecture, systems tract preservation and sedimentation rates.

2.1 MISS on clastic sedimentary surfaces

The sedimentary surface is an interface for the interaction of gaseous, fluid and solid phases (e.g., Noffke, 2010); these essentially open systems have complex thermodynamic and chemical characteristics. Recent studies have shown that surficial organisms interacted with physical agents of erosion, sedimentation and deformation (Noffke *et. al.*, 2001a) in clastic settings (e.g., Schieber, 1999, 2004; Hagadorn *et al*., 1999; Eriksson *et al*., 2000), similar to processes in carbonate-depositing settings (e.g., Awramik, 1984). Microbial-sediment interaction was important in shaping Precambrian continental landscapes (e.g., Buick, 1992; Bosch and Eriksson, 2008; Sheldon, 2012) and this interaction of microbial organisms with physical agents of erosion, sedimentation and deformation in clastic settings is the basis of MISS features. This microbe-sediment interaction in clastic settings can produce proxy evidence by isotope or/and major element geochemistry of palaeosols and marine sediments

(Gutzmer and Beukes, 1998; Watanabe *et al.*, 2000; Retallack, 2001) and is physically manifested by a number of clastic sedimentary structures identified from the Precambrian rock record that are indirectly or directly indicative of microbial mats. (e.g., Hagadorn *et al*., 1999; Schieber *et al*., 2004).

The role of microbes (e.g., fungi, cyanobacteria, micro-algae, etc.) and their influence on rocks and structures formed in sedimentary environments is significant (Ehrlich, 1996; Krumbein e*t al.*, 1994; Riding, 2000; Riding and Awramik, 2000; Nisbet and Sleep, 2001). Microbes affect the sedimentary system by their tendency to grow, and by their ability to biostabilize, baffle and trap, and bind sediments. The fixation of sediments by micro-organisms (e.g. cyanobacteria, diatoms, etc.) is described as biostabilization (see Paterson, 1994 for further elucidation) and baffling, trapping and binding describe the accumulation of sediments by activities related to bacteria and consequent incorporation of the grains into the mat fabrics (see Noffke *et al*., 2001a for further explanation). MISS are constructed through these and other processes (e.g., Eriksson *et al.*, 2007a; Schieber *et al*. 2007; Noffke, 2010). Other MISS genetic milieus range from mat destruction, mat burial to mat diagenesis (Schieber *et al*., 2007 and references therein) (Figures 2.1 and 2.2).

MISS are a product of the growth of biofilms, their transition into a meshwork of microbial mat, and lastly preservation, and can only actuate by the overlap of these parameters. Microbial mats are larger biofilms (Costerton and Stoodley, 2003) and comprise integrated clusters of microorganisms that are attached to a surface and embedded in EPS. Extrapolymeric substances (EPS) are very adhesive substances that bacteria are embedded in, and this EPS can grow to thick carpet-like layers (e.g. Noffke, 2010). Microbial related sedimentary structures (MISS; Noffke *et al*., 2001a) comprise a genetic continuum from mat growth, through mat metabolism and mat destruction, to mat decay and diagenesis, within either sandstones or mudrocks (Schieber, 2004 and references therein) (Figures 2.1 and 2.2). Biofilms and microbial mats are generally not particularly facies-specific as they can be found in almost all modern sedimentary environments, but MISS are most commonly preserved in upper intertidal and lower supratidal flats because of intermittent inundation and exposure fostering benthic growth of photosynthetic microbes which are very important mat builders (e.g. Schieber *et al*., 2007 and references therein).

Artificial mat cultivation has shown that the transition of a thin and fragile biofilm to a consistently dense meshwork of mat requires sufficient time of non-burial for mat coherence

that homogeneously covers the substrate (Gerdes and Klenke, 2003). Garcia-Pichel and Castenholz (1994) suggest that a high level of light intensity on mat surfaces can lead to an organic productivity increase some millimeters beneath the sedimentary surface and again emphasize that sufficient time prior to burial is imperative for widespread mat development. Mat colonization in siliciclastic environments is enhanced by translucent, clear and fine-grained quartz sands (e.g., Noffke, 2010) where hydrodynamic flow is moderate in the sense that it can sweep clay minerals from mat surfaces but can't erode biostabilized laminae (Gerdes *et al.*, 1985). The translucent quartz acts as light conductors for parts of the microbial mats that are not on the surface and the moderate hydrodynamic flow ensures that there are no clay laminae to obstruct the conduction of light by the upper-most quartz veneer. Both light conduction and low sedimentation rate are thus important for the good establishment of a strong meshwork of microbial mat and concordant MISS, and for probable MISS preservation too, which is however subject to other factors.

The type of MISS constructed is also related to the importance of filamentous and coccoidal cyanobacteria. The most successful biofilm integrators, mat builders and consequently most important microbes in MISS construction are cyanobacteria. The signatures of cyanobacteria are replete in Archaean, Proterozoic and Phanerozoic sedimentation records (e.g., Noffke 2003; 2006a and b) as they contribute to sediment and sedimentary structures through the establishment of accretions, layered accretions and filamentous biomass. Cyanobacteria are endowed with this unique role as they utilize all existential metabolic pathways on Earth (Krumbein *et al.*, 2003), have extensive morphological variability (e.g., Stal. 2000) and are as yet the oldest known photoautotroph. Stal (2000) suggests that the success of cyanobacteria in mat-building is based on the uniqueness of certain characteristics: (a) they are oxygenic phototrophic prokaryotes, (b) they are endowed with resilience to changes of environmental conditions (see Eriksson *et* al., 2000 for extremophiles of the Makgabeng palaeo-desert), and (c) since their predominant metabolism is oxygenic photosynthesis, they can utilize light as an energy source and water as an electron donor. Noffke (2010) posits that cyanobacteria can utilize long-wave and low-energy light in photosynthesis and an electron donor (e.g., H_2S) which is a further advantage on adaptation.

Three main genetic classifications of MISS have appeared in recent years (e.g., Eriksson *et al*., 2007 for summary), those of Gerdes *et al*. (2000a), Noffke *et al*. (2001a), and Schieber (2004). A fourth was promoted recently by Sarkar *et al*. (2008). These classifications overlap

as they tend to describe the same physical-microbe interactions which result in mat formation through different classification scheme modalities. In this thesis use will primarily be made of the MISS classification of Noffke *et al*. (2001a). This scheme effectively sub-divides MISS into structures atop bedding planes (class A) and structures within bedding plane (class B). The classification of Schieber (2004) summarizes the continuum of genetic mechanisms of mat forming processes in sandstones, as well as in mudstones (Figures 2.1 and 2.2), and encompasses the same range of MISS features described by Noffke *et al.* (2001a).

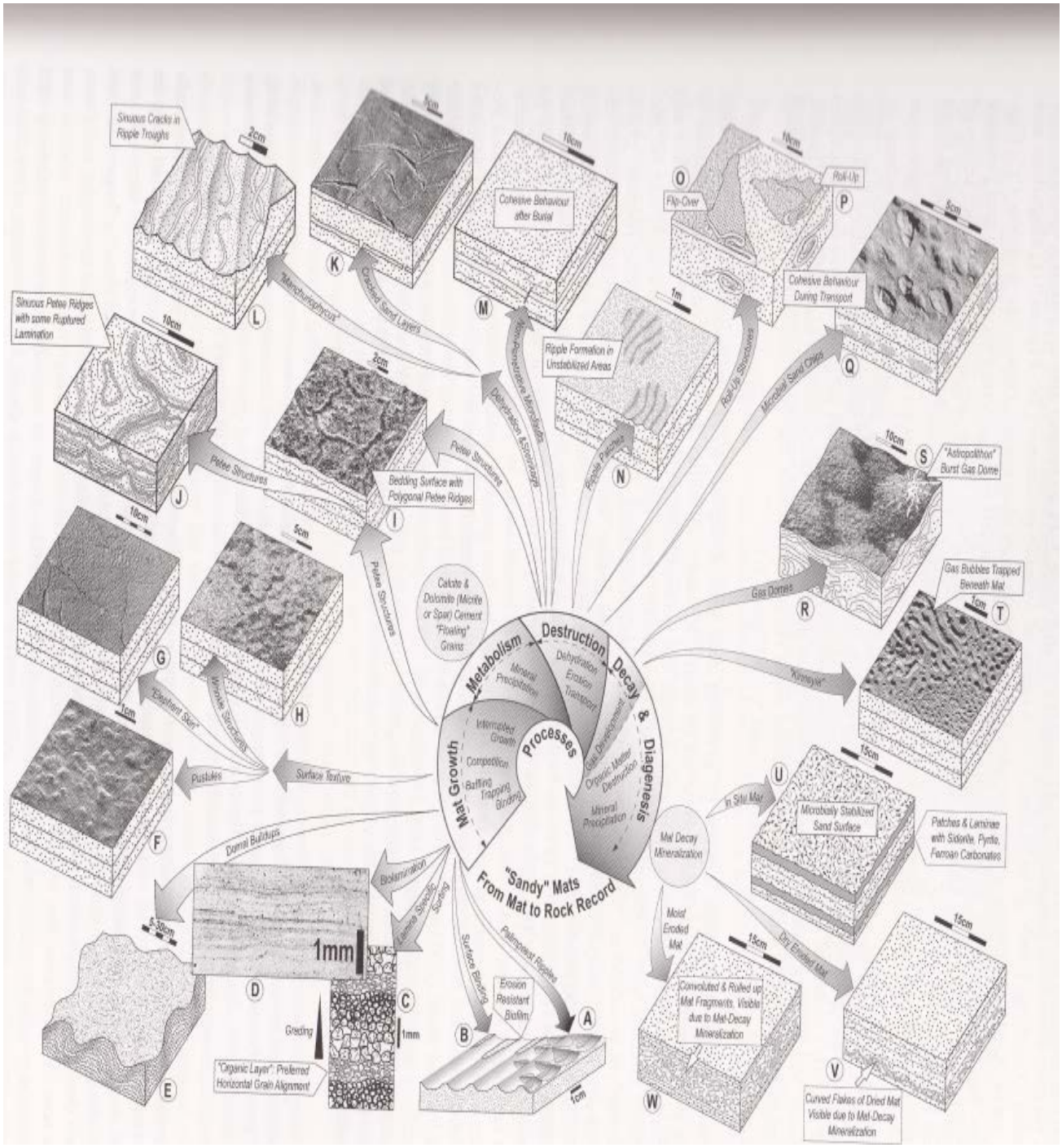

Figure 2.1: Chart showing features found in sandstones where microbial mats flourished in the environment. Note that the genetic processes are arranged clockwise along a continuum from active growth of mats to final destruction during diagenesis (Schieber, 2004).

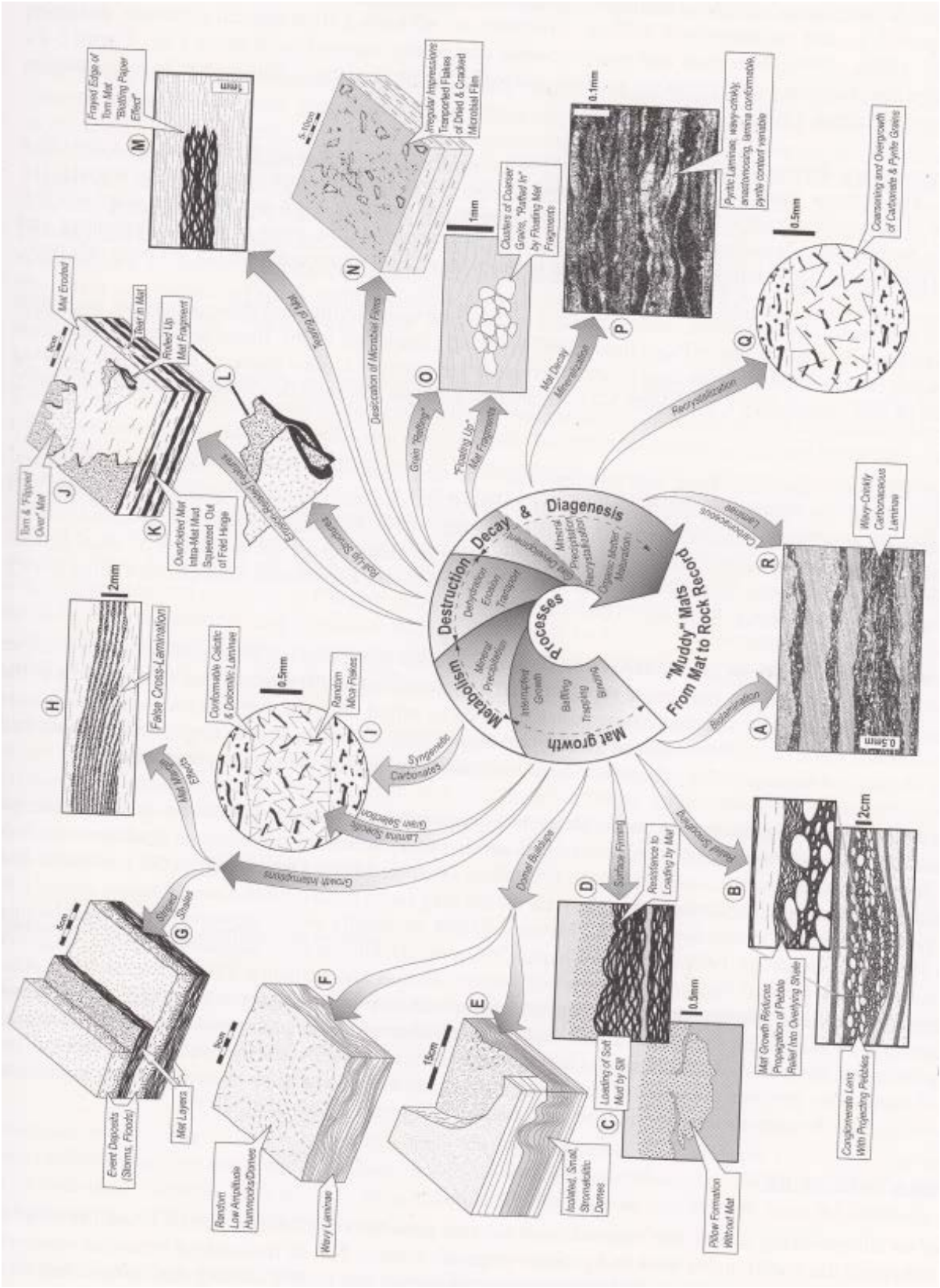

Figure 2.2: Chart showing features found in mudstones where microbial mats flourished in the environment. Note that the genetic processes are arranged clockwise along a continuum from active growth of mats to final destruction during diagenesis (Schieber, 2004).

2.2 MISS on bedding planes (class A structures of Noffke *et al*., 2001a)

Multi-directed ripple marks (a and b in Fig. 2.1) are a type of MISS on bedding planes, formed due to biostabilization of sediments by microbial mats. Genetically, it is assumed that the first generation of ripples was biostabilized by microbial mats which would have been the reason for their resistance to re-working and these first ripple marks were thus preserved with the second generation of ripple marks (cf., Noffke 2003c). Such ripple overprints also lead to formation of palimpsest ripples (a in Fig. 2.1) (Schieber, 2004).

Patchy ripples (n in Fig. 2.1) comprise flat sandstone surfaces exhibiting patches marked by ripples of variegated types and also ripples that grade into the surrounding sandstone surfaces (Bottjer and Hagadorn, 2007). The localized exposures of sandy beds with ripples form because of the selective removal of overlying protective mats in certain places; the absence of the mat in such patches leaves the exposed sand vulnerable to sedimentary reworking and concordant formation of ripple marks within those patches by wave, current or tidal action.

Cracked ripple crests are probably caused by the dewatering of biofilms on rippled sandy surfaces, with greater tension exerted on mats above ripple crests as shrinking takes place in the mat, cracking preferentially over the ripple crests (Bottjer and Hagadorn, 2007).

Exfoliating sand laminae (fig. d) are ≤ 1mm thick successive sandy veneers, lacking mud interlayers and showing no evidence of veneer amalgamations. This suggests that biofilms separated each successive thin layer of sand, providing the relevant enhanced cohesion (Bottjer and Hagadorn, 2007).

Wrinkle structures (h in Fig. 2.1) are wrinkled sandy bedding planes. It is essentially an umbrella acronym used to define various patterned bedding plane structures related to the corrugation of the surface of a sand bed. It is probably a reflection of microbial mat binding allowing weak currents or winds to wrinkle partially loose mats and their sediment substrates locally. It may also reflect small-scale loading of microbial bound sediments (Bottjer and Hagadorn, 2007). Wrinkle structures are a type of MISS genetically related to leveling within class A in the classification scheme of Noffke *et al*. (2001a). Leveling refers to the overgrowth of a depositional surface by a microbial mat so that prior structures like ripple marks are covered by biomass, thus the original depositional surface entirely or partly invisible under the mat tissue. Leveling is usually attributed to the growth of microbial mats and usually takes place during times of low erosion and deposition. Wrinkle structures can be

divided into three types: "runzelmarken" or wrinkle marks, *Kinneyia* structures and "old elephant skin" (O.E.S) textures (e.g., Porada *et al*., 2007). **Old elephant skin textures** (g in Fig. 2.1) are a reflection of growth of microbial mats which predominantly occurs on argillaceous veneers on top of fine-grained sandy bed surfaces. **Kinneyia structures (**fig. e**)** are characterized by sinuously curved, bifurcating and flat-topped crests that are usually separated by parallel, and round bottomed depressions, inferred to form beneath microbial mats and *Kinneyia* troughs and ripples are typically overlain by dark, fine-grained sediment, usually silty argillite characterized by carbonaceous lamina and isolated sand grains (Porada and Bouougri, 2007).

Sand cracks/shrinkage cracks (k in Fig. 2.1) reflect the onset of mat destruction as a result of desiccation of mat-bound sediments (e.g., Eriksson *et al*., 2007b and references therein). The elevated cohesiveness given to underlying sand by microbial mats and the consequent cracking of the mat due to desiccation can lead to cracks also penetrating the underlying sand layer. **Filled sand cracks** as the name implies are sand cracks that have been filled by sediments after formation. The essential difference between sand cracks and filled sand cracks is that filled sand cracks are positive features while sand cracks are negative features. **Manchuriophycus** (l in Fig. 2.1) is a peculiar type of microbial shrinkage crack that exhibits sinuous to circular geometry and is sympathetic to ripple troughs (Eriksson et *al*., 2007b). This MISS structure is probably formed due to desiccation of thickened mat layers within ripple troughs (Pflüger, 1999; Gehling, 2000).

Petees/petee ridges (i and j in Fig. 2.1) are upwardly concave ridges, often with polygonal geometry in plan view or lone-standing positive spindle-like forms (e.g., Eriksson *et al*., 2007b and references therein). Gehling (1999) collectively named these anti-formal structures "petees" and discriminated them into petees *sensu stricto* and petees *sensu lato*; he related the genesis of the former to mat growth expansion and pressure underlying mat layers derived from gases from decaying older mats, and the latter to cracks in microbial mats. Gavish *et al*. (1985) and Reineck *et al*. (1990) define petees as domes, buckles and folds developed on a supple mat surface. Eriksson *et al*. (2007b) suggest that they probably have a synaeresis-like origin (post-burial movement of sands from below the mat into cracks in the mat caused by overlying beds' pressure), or form by lateral movement of liquefied sand into the cracks in microbial mats from below, because of pressure from overlying water or spring-tidal oscillation. Noffke (2010) argues that the genetic mechanism of petees is biostabilization and the consequent arrangement of microbial mat into folds occurs because mat portions exposed

to sunlight have differential growth rates to those not exposed to sunlight. She also argues that many coccoidal cyanobacteria are resistant to solar radiation and desiccation (e.g., *Synechnocossus*) and predominates on petee surface portions exposed to sunlight, while the folds of a petee are composed of filamentous taxa (e.g., *Oscillatorialimosa* or *Microcoleuschthonoplastes*).

Curled crack margins, **flipped over mat edges and rolled-up mat fragments.** These mat destruction features (o in Fig. 2.1; j, k, l and m in Fig.2.2) are caused by the erosion of mat bound sediments (Eriksson *et al*., 2007b). **Curled crack margins are** the first feature in a continuum followed by flipped over mat edges and rolled-up mat fragments (e.g. Eriksson *et al*., 2007b). **Flipped over mat edges and rolled-up mat fragments** are formed due to erosive currents affecting partially loose mats and their bound sandy sediments, with the cohesion of the underlying sandy sediments enabling formation of either "flip–overs" or "roll- ups". **Flipped over mat edge** (fig. j) is probably formed by the complete inversion of a mat edge by water, or possibly wind currents. A flipped over mat edge is suggestive of localized physical mat destruction without the mat being completely detached from its sandy substrate. **Rolled-up mat fragments comprise** sandstone or mudrock (inferred to have covered the original mats and been trapped therein) that is rolled up within thinly bedded clastic sediments **(**Eriksson *et al*., 2007b). Examples known include aeolian fine-grained sand and/or flash-flood reworked sandy playa deposits. The inference is that a high energy sedimentation event can roll up a curling mat, normally a detached portion thereof, so that it resembles the rolled tobacco leaves in a cigar, and this feature is then incorporated into the sandy sediments resulting from the specific sedimentation event. Such inferred sedimentation events can be within almost any sedimentary environment or setting where sudden high energy events affect loose or partially desiccating mats.

Microbial mat chips and **microbial sand chips** (q in Fig. 2.1) are genetically related to flip-overs and roll-ups but reflect more intensive sediment reworking. Due to longer reworking, they are smaller, rounded, and mostly current-aligned microbially bound sand clasts. Preservation of the clast forms normally excludes survival of any mat material, leaving only the sand clasts themselves within a surrounding clastic sediment host. Microbial mat chips (n in Fig. 2.2) represent strongly desiccated mat-bound sediment surfaces forming relatively rigid and curved clasts. Microbial mat chips are not as rounded as roll-ups and have a resemblance to dried-up mud clasts that are formed as a consequence of desiccation and breaking up of a thin mud layer.

Spheroidal pliable sand clasts or algal balls (Bottjer and Hagadorn, 2007) are relatively larger spherical clasts of sandstone, often associated with ripple marks. Their genesis is ascribed to mat growth in shallow marine settings, with high wave energy and current action transporting cohesive fragments of mat bound sand which are rounded by transport and deposition (e.g., Eriksson *et al.*, 2007b and references therein). **Domal sand buildups or sand stromatolites** (e in Fig. 2.1) in sandy siliciclastic settings reflect locally significant topography which may build up on tidal flats, etc (Bottjer and Hagadorn, 2007). The patterns may range from larger domes in the middle surrounded by smaller ones to clustered associations exhibiting no preference for size distribution. Sand stromatolites are comparative to stromatolites of the carbonate setting because of similarity in cauliflower-like growth morphology, but with a lower vertical relief. This lower vertical relief morphology of the sand stromatolite compared to the stromatolite of the carbonate setting may be due to their lack of bacteria-induced carbonate precipitation (e.g., Bottjer and Hagadorn, 2007). Sand stromatolites can be dominated by either of two categories; clustered heads or non-clustered small pea-sized heads; this may reflect biological affinities aligned to different life histories, and/or interactional history with the physical environment (cf. Bottjer and Hagadorn, 2007). Clustered sand stromatolites may be representative of an older/faster growing enclave compared to the unclustered heads because the clustered sand stromatolite type can be observed in rippled and non-rippled surfaces, and can also exist as part of a mixture with unclustered ones. Domal MISS features also occur within muddy sediments (e and f in Fig. 2.2).

Sand shadow structures (Bottjer and Hagadorn, 2007) are cohesive surface bumps on sandy bed surfaces which also occur as bed-sole features. Sand shadow structures resemble sand stromatolites, but with drumlin-like sand shadows which accumulated in a down-current direction relative to the sand bed surface bumps. Microbial binding of sand with consequent fallout of wind - or water-borne sand particles leading to the formation of leeward tails is inferred as the genetic formational mechanism of this MISS structure (Bottjer and Hagadorn, 2007). **Erosional remnants and pockets** (Noffke, 1999) reflect mat-protected, flat topped rises that are several centimetres in height (erosional remnants) alternating with sediment surface parts that are deeper-lying (erosional pocket). It is inferred to reflect partial erosion and destruction of mat covered tidal surfaces (Noffke, 1999).

2.3 MISS within bedding planes (class B structures of Noffke *et al.*, 2001a)

The most important features in this MISS class are detailed briefly below. **Sponge pore fabric** (cf. fenestral fabrics; r in Fig. 2.2) (Noffke *et al.*, 2001a) is an internal bedding structure that owes its genesis to biostabilization. This MISS structure is formed due to the covering of sediment by a microbial mat which consequently restricts gaseous exchange between the water or atmosphere and the underlying deposits. This is reflected by voids within sediments that are visible in thin sections.

Oriented grains (c in Fig. 2.1) (Noffke *et al.*, 2001a) is a MISS structure that is induced by grain separation promoted by upward transportation of mineral grains due to ongoing growth of minerals that coat the particles (Noffke *et al.*, 2001a). This is evinced in thin section by single sand grains floating without contact to other grains in the developed mat layer. Thin sections showing micro-vertical successions show that the grains are oriented with the long axis parallel to the depositional surface and that there is randomized grain orientation in the fabrics of the underlying substrate.

Biolaminites (d in Fig. 2.1; e, f and g in Fig. 2.2) form by the baffling and trapping of clastic grains by sediment-agglutinating bacteria, forming sediment lamina that are visible in thin section (Noffke *et al.*, 2001a). Biolaminite can be easily recognized by mat lamina-specific selection of heavy- mineral grains (e.g. Gerdes *et al.*, 2000b). **Mat-layer bound grains** owe their genesis to baffling and upward growth of a developing organic component of microbial layer. This is indicated by mat layer bound grains that are comparatively of smaller size when compared to the constituents of the sediments that are below the mat and devoid of vertical gradation of grain size (Noffke *et al*., 2001a and references therein).

2.4 Previous work on microbial-induced sedimentary structure of the Makgabeng and Magaliesberg Formations

2.4.1 MISS of the Magaliesberg Formation

The Magaliesberg Formation is imbued with very good exposures of various forms of crack-like features and their casts within thin mineralogically mature and texturally immature sandstone beds. These sand crack features extend to possibly related petee ridges and also those of both cracks and petee ridges (filled cracks) with a reticulate network, with lesser vermiform geometries (e.g., *Manchuriophycus*) which are commonly sympathetic to ripple

troughs (Parizot *et al.*, 2005; Bosch and Eriksson, 2008; Eriksson *et al.*, 2010, 2012). Circular imprints resembling concretions, or possibly oncolites on sand sheet surfaces are also recorded in the Magaliesberg Formation (Bosch and Eriksson, 2008). Earlier workers interpreted the inferred MISS in the Magaliesberg Formation sandstones as possible desiccation cracks (Visser, 1969; Van der Neut, 1990), with the muddy layer having being removed through erosion and/or weathering prior to the deposition of the second and overlying sandstone layer. Eriksson *et al.* (2008) interpreted these features as sand cracks of different geometries (e.g., branching and sinuous, vermiform, etc.) arguing that the large variety in size, shape and density of the supposed desiccation structures, and their positive and negative relief and occurrence on relatively mature sandstone beds of the Magaliesberg Formation cannot be satisfactorily explained by ordinary mudcracks or desiccation cracks. As such special conditions must have been pertinent for their formation. Sand on its own does not have enough cohesiveness to crack, unless it contains a significant proportion of clay minerals or is bound by a microbial mat growing on and within its upper surface (e.g., Schieber, 1998).

2.4.2 MISS of the Makgabeng Formation

Roll-up structures, mat chips and desiccated mat fragments are some of the MISS/MRS structures recorded in the Makgabeng Formation (Eriksson *et al*., 2000, Porada and Eriksson, 2009). Eriksson *et al.* (2007) described the roll-ups as constituted of silty mudstone laminations that are coiled through 2-3 revolutions (>720° and <1060°). Isolated and inter-connecting sand cracks, wrinkle structures (e.g., Eriksson *et al.*, 2000) and tufted mat, biological soil crust and gas escape features (Simpson *et al* ., 2013) are also recorded in the Makgabeng Formation.

The significance of the Makgabeng Formation roll-ups is that they are the first known (Eriksson *et al.*, 2000) example of desiccated microbial mat in a wholly continental and fully intracratonic palaeoenvironment; an environment that is interpreted as a harsh desert setting, and amongst the oldest such settings known (one located within the central parts of the craton; e.g., Eriksson and Simpson, 1998). The roll-ups of the Makgabeng Formation palaeodesert suggest colonization of Precambrian terrestrial settings by microbes and that even the harshest palaeoenvironments were able to support flourishing microbial communities (Porada and Eriksson, 2009; Simpson *et al.*, 2013).

Chapter 3

CATALOGUE OF INFERRED MISS/MRS (AND ASSOCIATED SEDIMENTARY STRUCTURES) FOUND IN THE STUDY AREA (MAGALIESBERG AND MAKGABENG FORMATIONS)

The MISS are identified based on Schieber *et al.* (2004; refined and updated in Schieber *et al*., 2007) and Noffke *et al.* (2001a; refined and updated in Noffke, 2010).

3.1 Magaliesberg Formation MISS catalogue and megascopic description

The Magaliesberg Formation MISS/MRS predominantly comprise sand cracks and filled sand cracks (positive polygons) embedded within or above the uppermost bedding planes of sandstones (*ca.* <3mm relief above/below bedding planes).

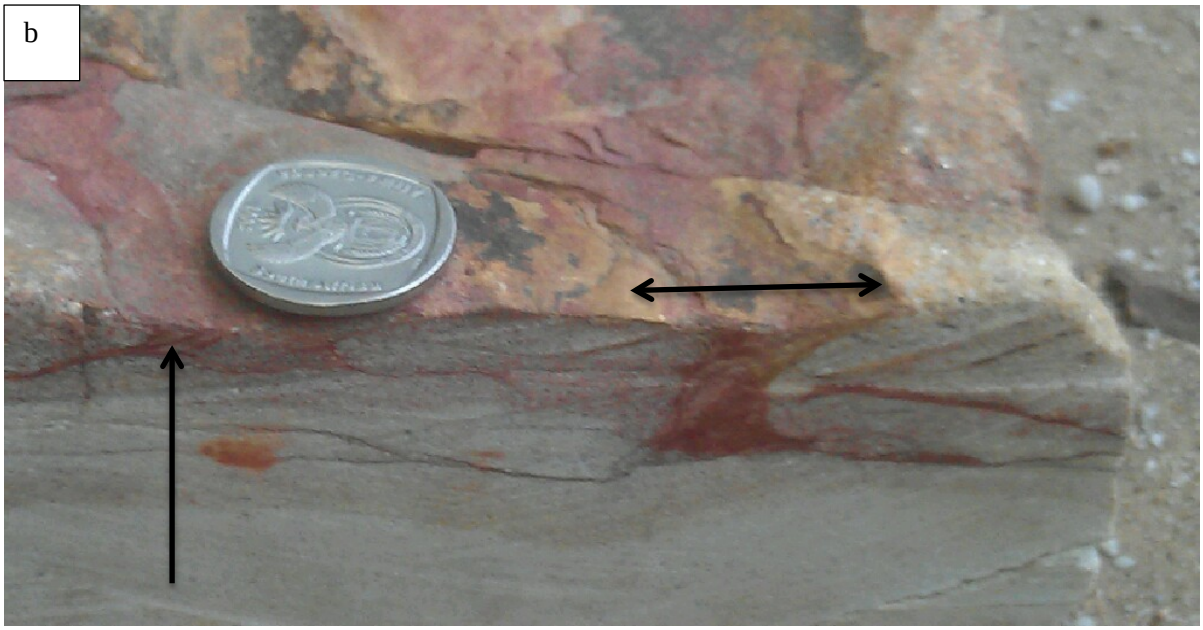

Figure 3.1: Sandstone bed sample showing inferred mat related features on the upper bedding plane (a), and in section (b). Smaller sample in (a) is the plan view of the cut section. The rippled sandstone shows evidence of leveling of the ripple topography, best seen in the cut section of the sandstone bed sample (b). The single -headed arrow in (b) shows a partially filled or leveled ripple trough. Note that the leveled ripple trough is more iron rich than the other portions of the section. Note the resultant muted ripple crest relief shown in (b) by double headed arrow. (Coin for scale in the two photographs: 2.2cm in diameter).

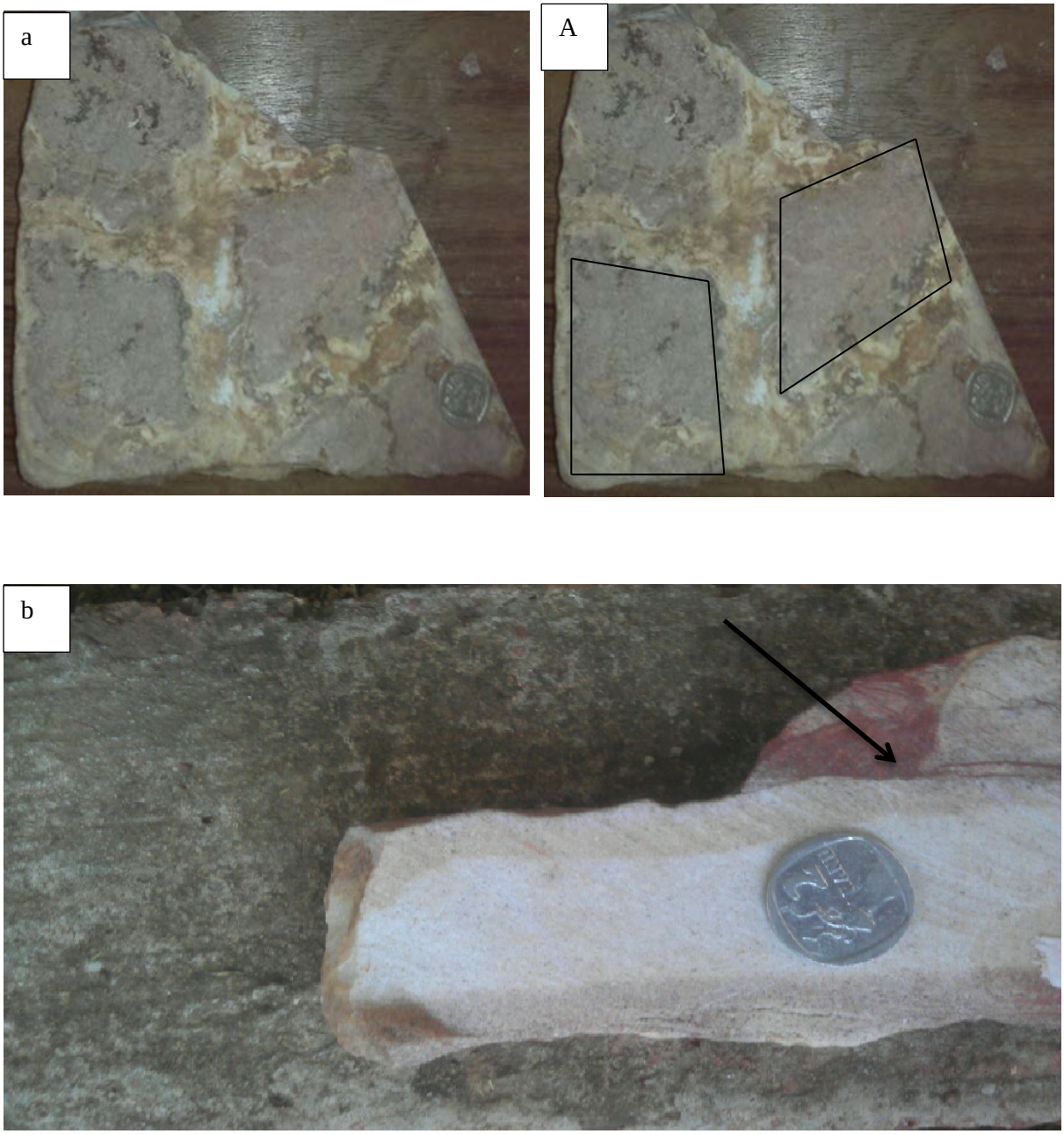

Figure 3.2: Sandstone sample showing inferred mat related features on both bedding planes (dorsal plane of the same sample shown in Figure 3.1). (a) is a sole view of the lowermost bedding plane of the sample showing a pattern of positive (NB, on the bed sole) polygonal features (shown with polygons between positive features in A for greater clarity); (b) is a cross-sectional view of (a), sole facing upwards, showing the feature (arrow) impinging into the underlying bed (Coin for scale in all two photographs: 2.2 cm in diameter).

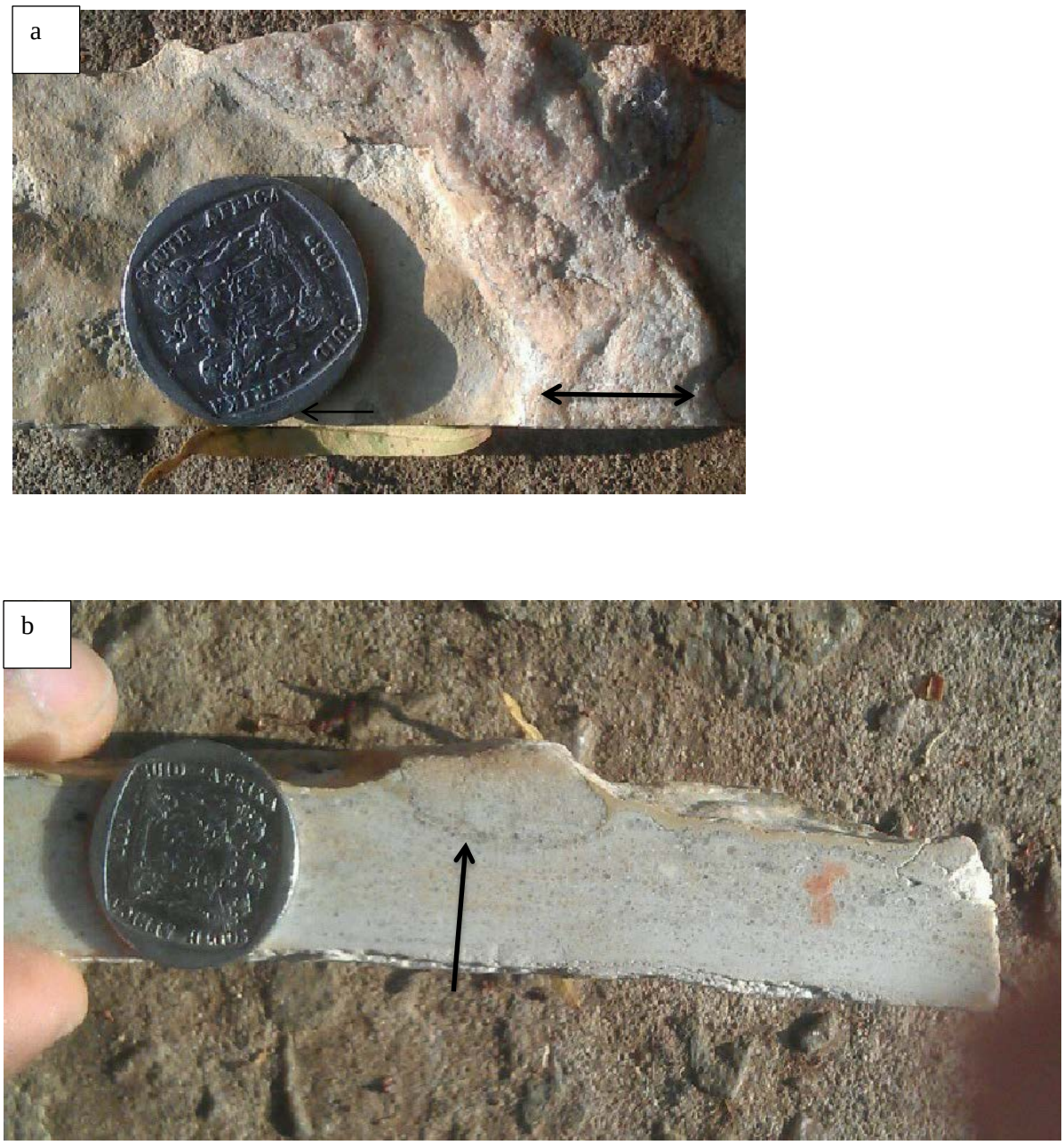

Figure 3.3: (a) is a plan view of a sandstone upper bed surface and (b) is a cross-sectional view cut through the same sample (sectional line of b forms base of sample in (a). (a) A robust presumed petee ridge structure (shown with double arrow). (b) Note the sharp contact between the inferred MISS structure (positive petee ridge) and the underlying bed (contact shown with arrow), and the concomitant megascopic change in grain size at the sharp contact. (Coin for scale: in a, and b is 2.2 cm in diameter).

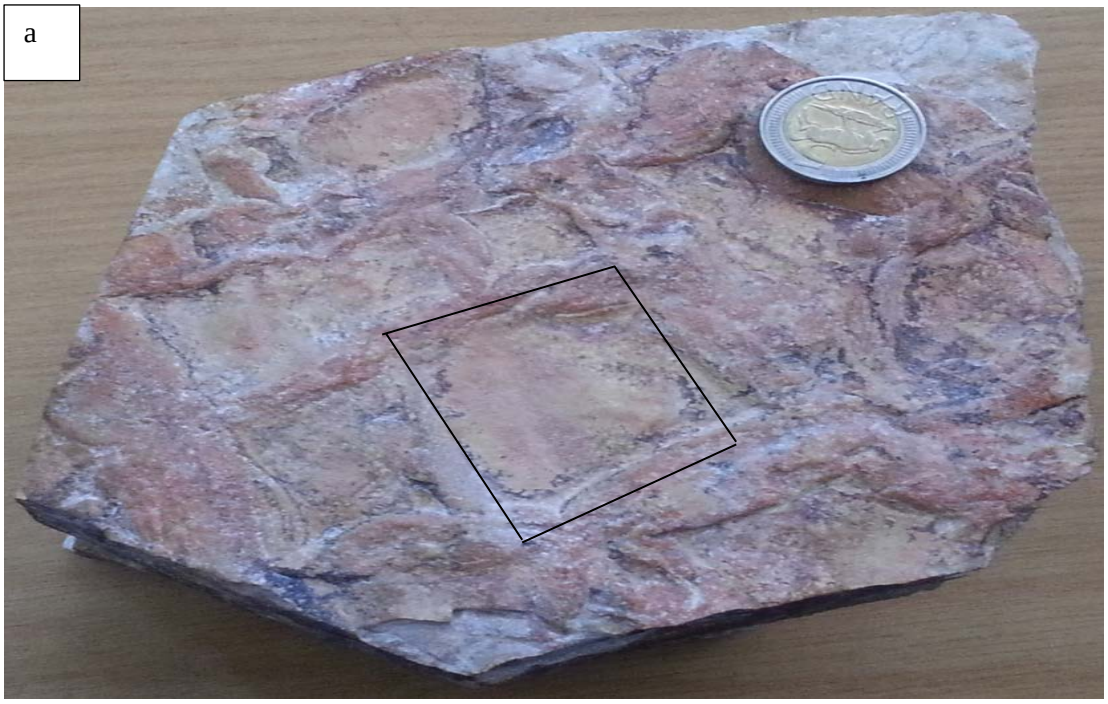

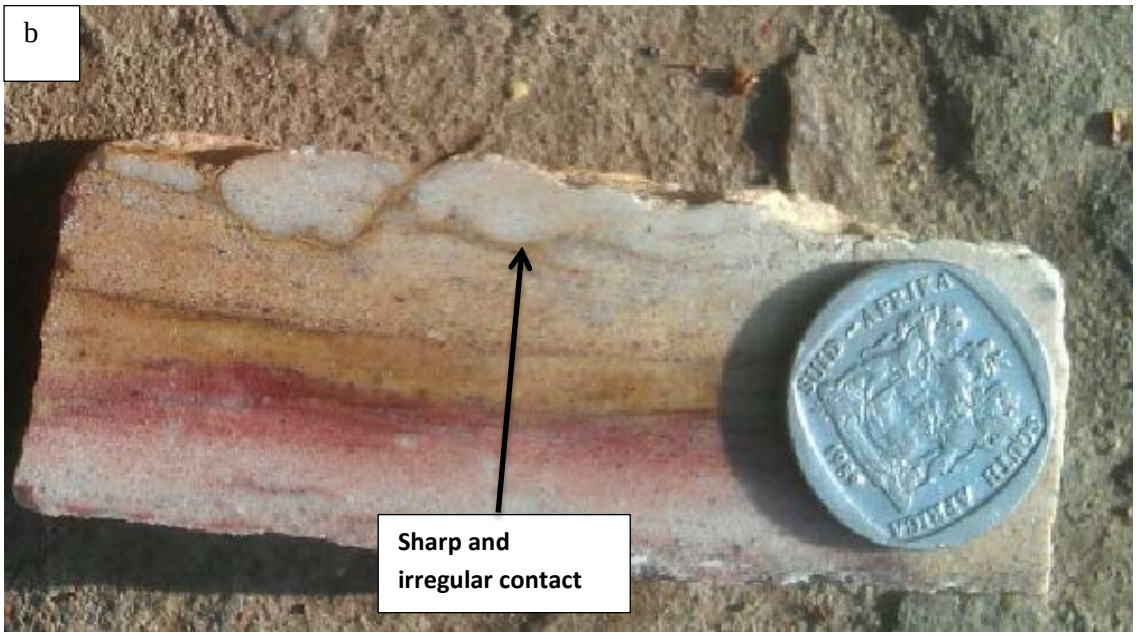

Figure 3.4: Sandstone bed with positive, reticulate polygonal structure inferred as petee ridges, on upper bedding surface. The plan view of the sample is shown as a, and the cross-sectional view of the cut sample (b) show a megascopically visible sharp and irregular contact (shown with arrow) between the inferred MISS (petee ridges?) and underlying horizontally laminated sandstone bed. (Coin for scale: a = 2.6cm, b = 2.2 cm in diameter).

Figure 3.5: Three orders of sand cracks denoted by decreasing width of crack-in fills (silty-sandy grey finer material than brownish sandstone). First-order cracks are the widest and show curvature, while second-order cracks tend to be straight, less wide and to connect the larger cracks. Third-order cracks have the smallest widths and divide the blocks defined by the second-order cracks. (Coin for scale is 2.6cm in diameter).

Figure 3.6: Positive relief structures forming a pattern of reticulate ridges (petees) on recrystallized sandstone upper bedding surface. They appear to be arranged in radiating patterns that connect circular ridges (shown by black arc) around a presumed central point (towards the thin end of sample), forming the overall reticulate and locally triangular (shown with arrow) to polygonal pattern through crossing of the ridges; note that the inferred radiating ridges are oriented approximately at 90° to the circular ones. (Coin for scale: 2.2 cm).

Figure 3.7: Ferruginous elongated ridges with relatively consistent polygonal geometry that might possibly be inferred as a filled sand crack type MISS. However, this structure is a dubious MISS, if it is one at all, and might better be interpreted as secondary ferruginous deposits formed along joints. (Pencil for scale is 12.5cm). This photograph illustrates the challenges in identifying MISS unequivocally from other geological features and also underlines the importance of examining cut cross-sections as done for most samples in this thesis.

Figure 3.8: Dense reticulate pattern of positive ridges (petee ridges, or alternatively, sand-filled cracks) on recrystallized sandstone upper bedding surface. The prominent ridges are of first-order character with second-order ridges less easily visible (e.g., at top of sample). (Pen for scale is 12.7cm).

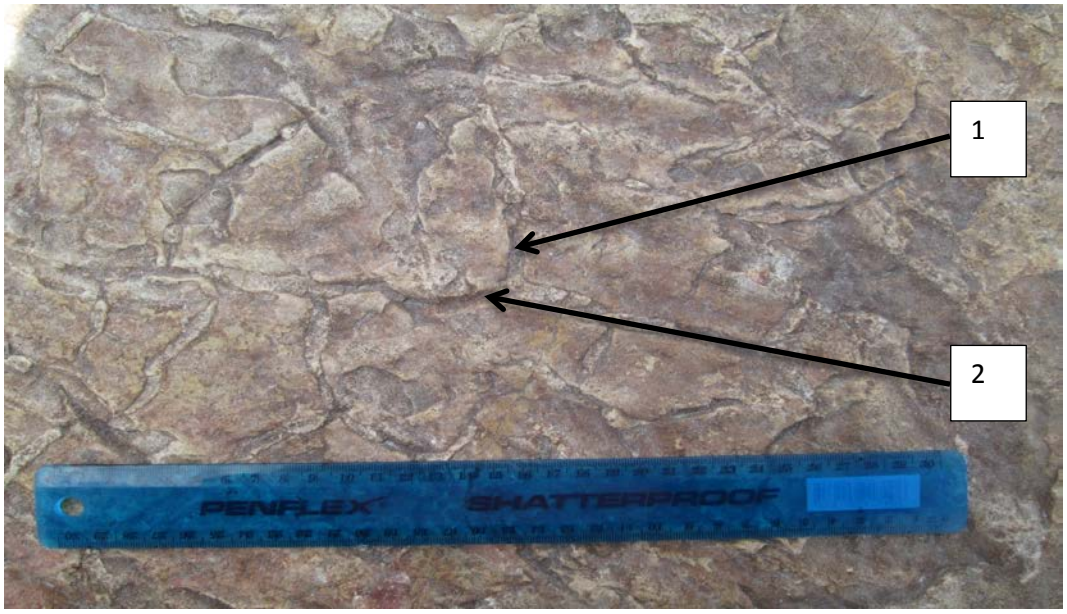

Figure 3.9: Inferred sand cracks (mat desiccation cracks that penetrated into microbially bound underlying sandy sediment) showing triradiate geometry defined by short dimension cracks (arrow 1) intersecting longer dimension cracks at approximately right angles (arrow 2). There are also hollows (e.g., to right and above ruler) that probably reflect erosion of the MISS or non-preservation of MISS. (Centimetric ruler for scale).

Figure 3.10: Upper sandstone bedding surface showing polygonal sand cracks with almost orthogonal intersections and curvilinear geometries (scale is pen: 12.5cm).

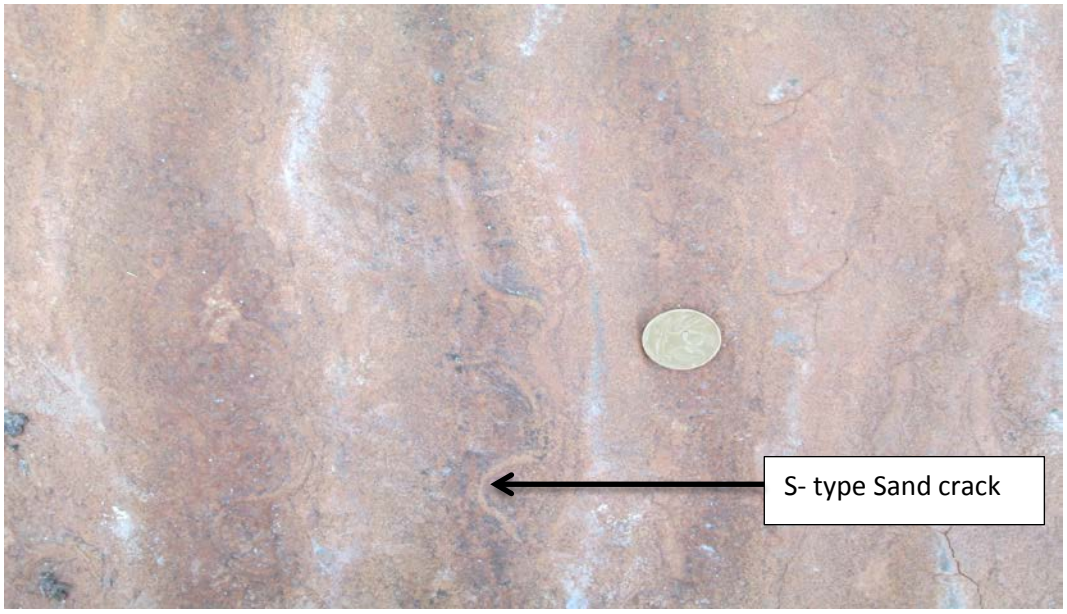

Figure 3.11: Ripple trough-sympathetic S-type sand cracks (cf. *Manchuriophycus*). Note that the sand cracks are strongly sinuous and follow the trough of the slightly sinuous ripples on the uppermost surface of a sandstone bed. Ripple crests appear white in photo and trough is of a slightly darker colour. (Coin for scale is 2.2cm in diameter).

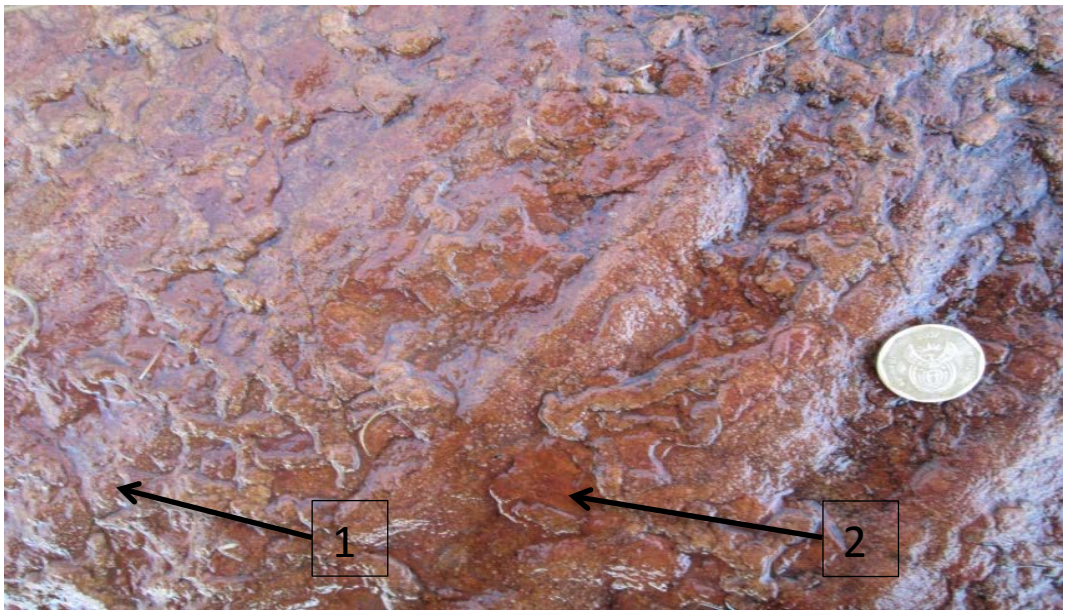

Figure 3.12: Possible leveling of rippled upper sandstone bedding surface that might be microbially related. Surface has been wet for clarity of photography. (1) Shows the relatively leveled surface of inferred pre-existing ripple troughs and crests. (2) Shows what might be a less complete leveling process whereby the inferred pustulose microbial growth seems to originate from the trough and graduate outwards to the two adjacent ripple crests as leveling proceeds. (Coin for scale is 2.2 cm).

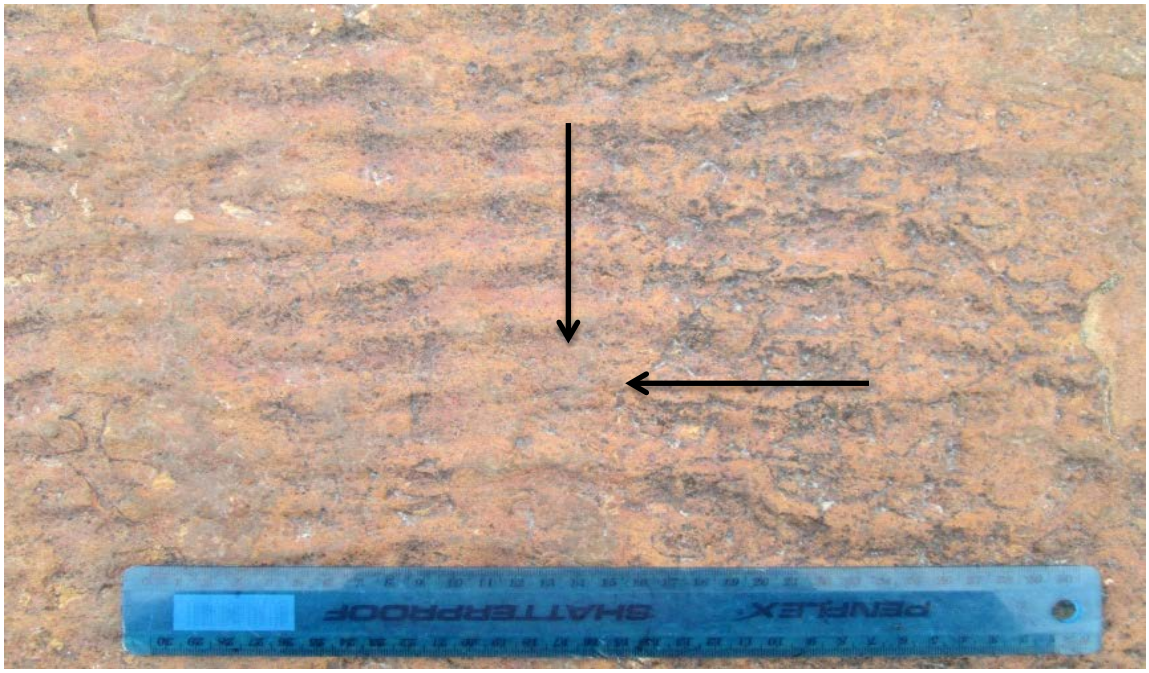

Figure 3.13: Interference ripples on sandstone upper bedding surface. Note that earlier ripples (example of ripple crest shown with right-to-left arrow) might have been biostabilized prior to the cross-cutting younger ripple crests (oriented at about right angles to the earlier ones, and an example of a ripple crest shown by top-to-bottom arrow). (Centimetric ruler for scale).

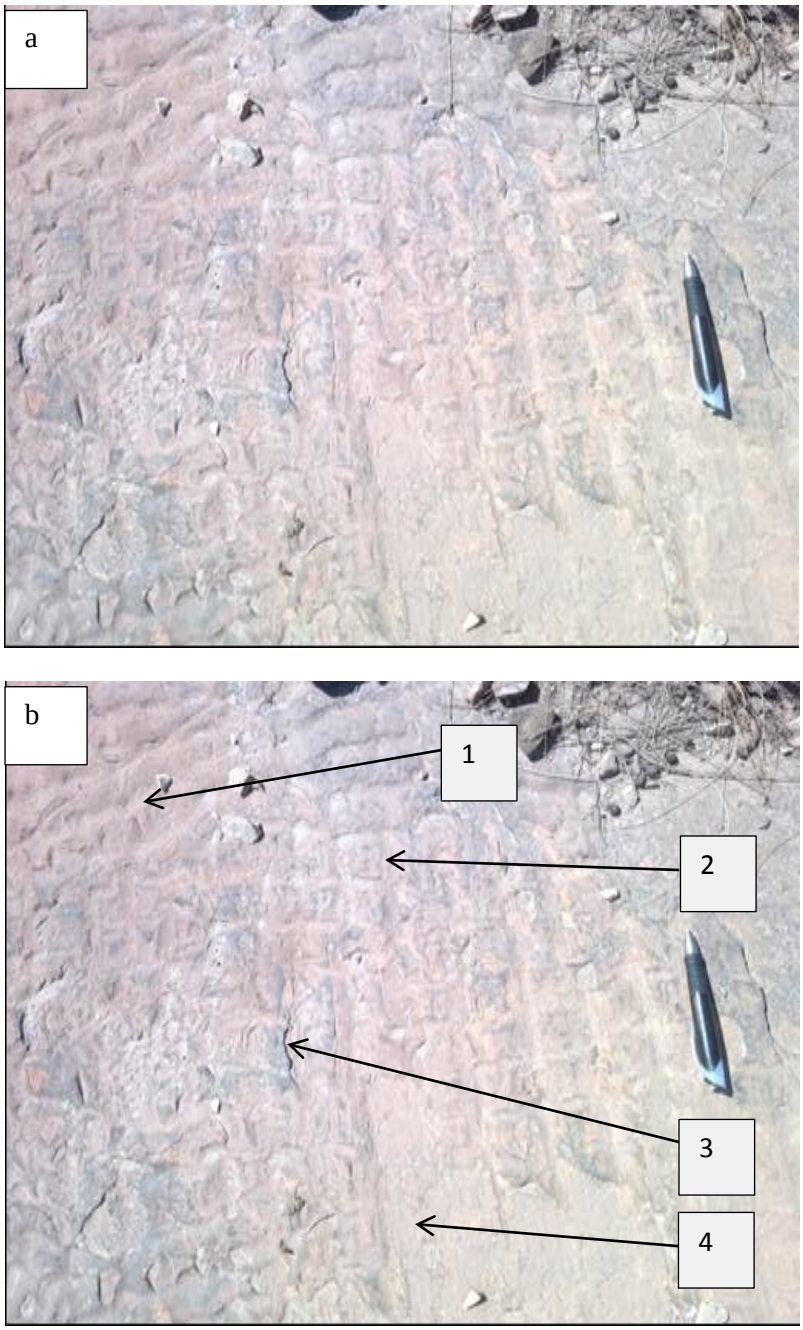

Figure 3.14a: Inferred MISS which reflect variable and complex influence of sediment re-working; (b) is labelled presentation of (a), shown separately for clarity of detailed features. (1) shows slightly sinuous ripples, which overlie and cross-cut at a low angle earlier interference ripples, shown well at (2) which can thus be described as palimpsest ripples; (3) there appear to be eroded hollows formed between palimpset interference ripple crests and position (4) resembles patchy ripples (erosional remnants of rippled surface surrounding an eroded pocket as shown by the smooth surface shown at (4). The relative order of the formation of the features at (3) and (4) relative to the youngest ripple set at (1) is unclear. (Pen for scale= 12.5cm).

Figure 3.14b: An inferred microbially bound upper sandstone bed surface marked by strongly sinuous petee ridges, and within the semi-circular hollows formed between ridges, what appears to be loosening of microbially bound sandy sediment chips (especially in the lower left portion of the photo), prior to full erosive removal, which might have formed subsequent hollows, deepening the "troughs" between the inferred petees (upper right of photo). (Pen for scale =12.5cm).

On the basis of the MISS catalogue for the Magaliesberg Formation, both petees and sand cracks (also filled sand cracks) are common features, with relatively minor occurrences of leveling, and few examples of a set of features: *Manchuriophycus*, interference ripples, palimpsest ripples, eroded hollows, patchy ripples, sand chips. Petees can also be related to cracks in microbial mats (Schieber *et al.*, 2007) and inferred dessication features are therefore predominant in this catalogue. However, mat destruction features (sand chips, hollows, patchy ripples) are uncommon, and pervasive mats appear to have covered many of the preserved thin sandstone beds of the Magaliesberg Formation, which were also dominated by various types of ripples (e.g., Bosch and Eriksson, 2008).

3.1 Makgabeng Formation MISS catalogue and megascopic description

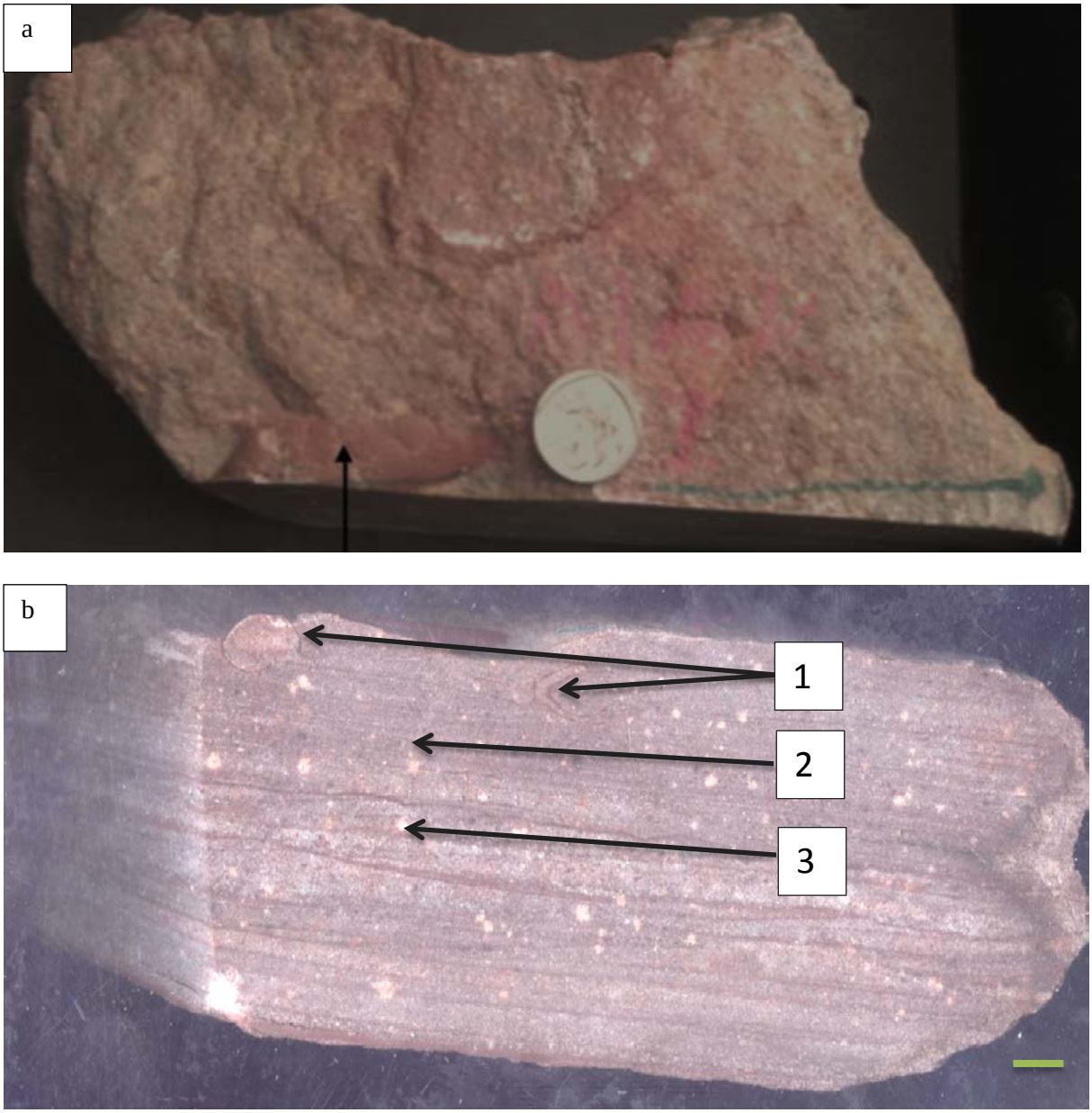

Figure 3.15: (a) sandstone upper bed surface with large embedded mat fragments (example shown with arrow). (b) Cut section of the same sandstone bed, showing that it contains concentric roll-ups made up of heavily iron rich mudrock (examples shown by arrow 1). The embedded mat fragment visible and arrowed in (a) is seen to be a large and elongated roll-up in the sectional view – see top left of cut face of sample. Note the very thin mm-scale planar lamination (arrow 2) interpreted as upper flow regime plane bedding. Note the white reduction spots (shown by arrow 3) which are emblematic of a redox zone. (Scale in a is 2.2 cm in diameter and in b is 1 cm).

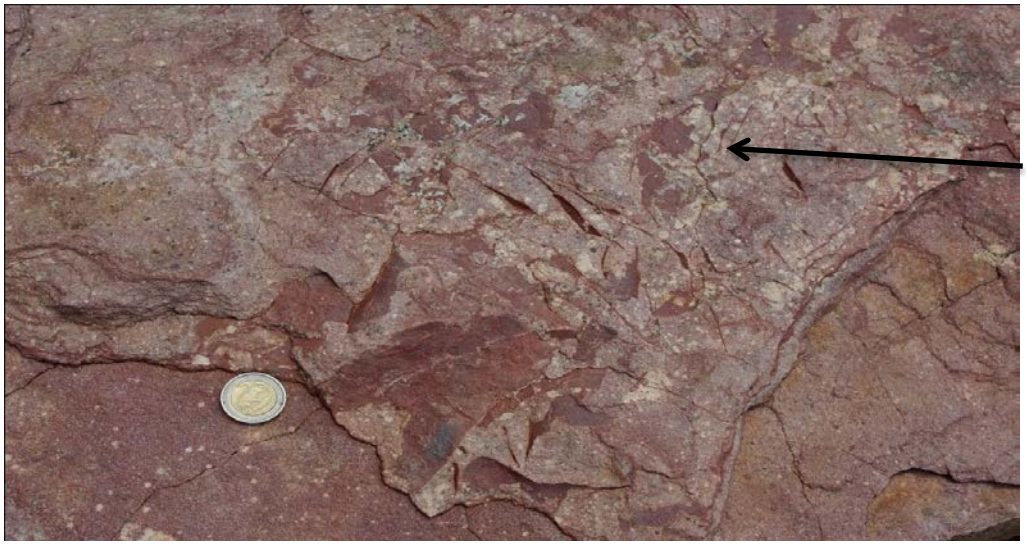

Figure 3.16: Sandstone upper bedding surface with numerous relatively large angular mat fragments. The fragments display no sorting and highly variable shapes and angularity. Note that the mat fragments are mud rich and more ferruginous than the arenaceous host sandstone exposed on the upper bedding surface (coin for scale=2.6 cm in diameter). These are inferred to reflect mat fragments (and trapped muddy sediment therein) rather than mudclasts due to the extreme angular shape of some fragments, given cohesion to preserve such fragment shapes by the binding mat material. Numerous white reduction spots also occur.

Figure 3.17: Cross-sectional photograph of poorly-sorted sandstone outcrop (larger grains stand out in weathering profile) showing variable iron concentration: (1) discontinuous wavy mudstone laminae within sandstone containing large clasts; (2) continuous relatively horizontal ferruginous mud-rich laminae: (3) reduction spots (Coin for scale is 2.6 cm in diameter). The wavy mudstone laminae are inferred to reflect mat-bound fine sediment which broke up into elongated portions without full destruction when relatively coarse enclosing sandstone bed was deposited.

Figure 3.18: Inferred petee ridges on exposed sandstone upper bed surface with cross-cutting patterns which locally define rounded hollows between ridges. (Hammer for scale: 27.5cm). The lack of any preferred orientations of ridge crests mitigates against an alternative interpretation as interference ripples; however, both interpretations would point to MISS features.

Figure 3.19: Two orders of sand cracks superimposed on interference ripples (with consistent orientation direction of sinuous crests); some cracks align with the crest line of the asymmetrical ripples (along both crests and troughs of ripples) and others cross-cut both ripple crests and the former group of cracks approximately orthogonally. (Coin for scale=2.6 cm in diameter).

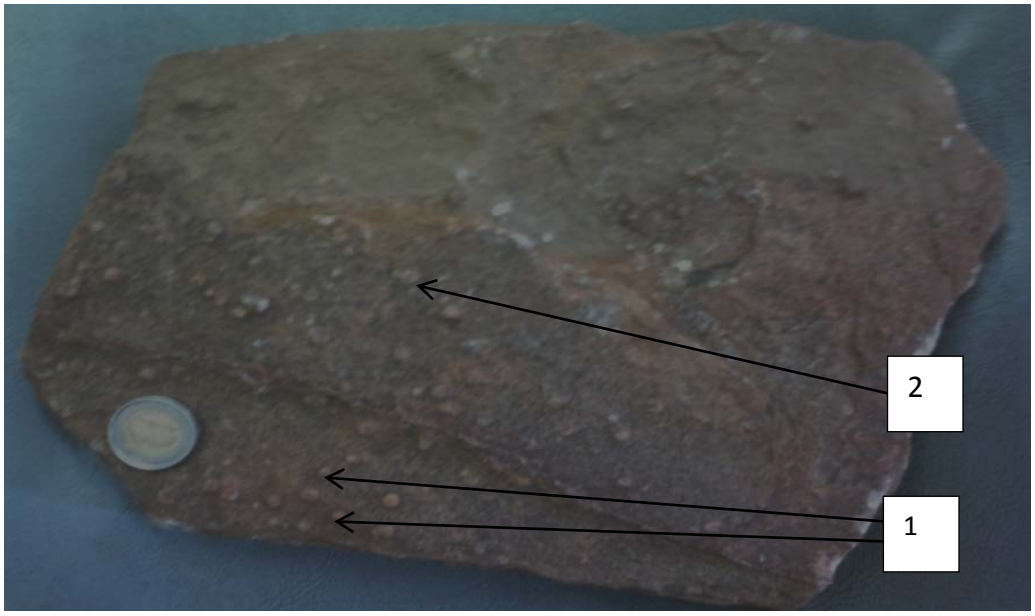

Figure 3.20: Pear-sized, concentrically layered, positive relief structures (domal sand buildups/sand stromatolites?) on two successive sandstone upper bedding surfaces, showing two types; clustered (shown with arrows 1) and non-clustered (shown with arrow 2). Coin for scale=2.6 cm in diameter).

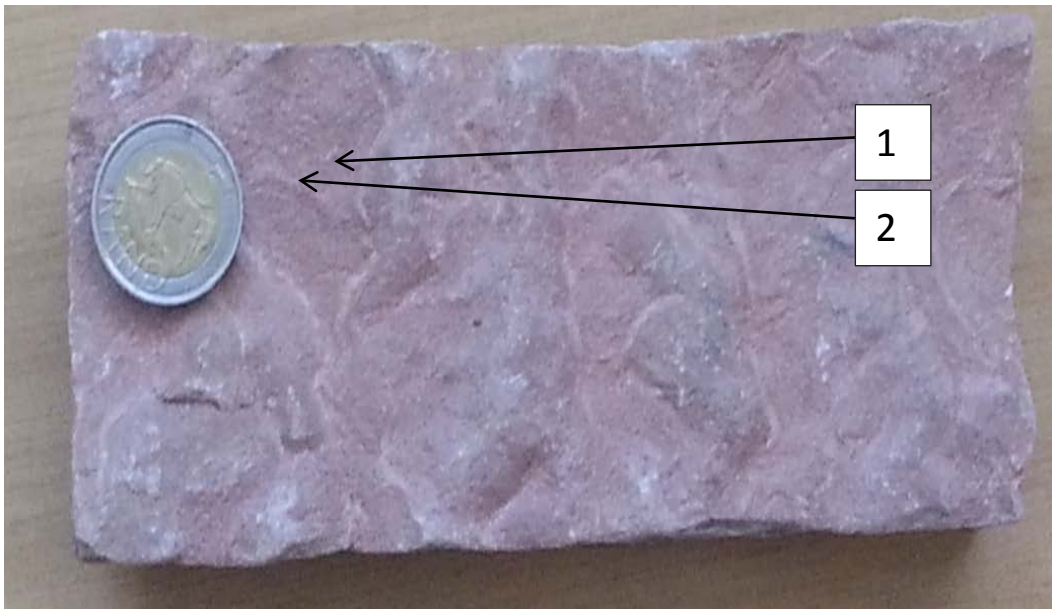

Figure 3.21: Sandstone upper bed surface marked by sinuous ripples with crest-line sympathetic cracks (shown by arrow 1) and another set of cracks (shown by arrow 2) intersecting the former at approximately 90°. (Coin for scale=2.6 cm in diameter)

Figure 3.22: Uncertain sedimentary feature on upper sandstone bed surface, that is possibly petee ridges (flattened due to later erosion?), or alternatively, flattened sinuous ripples; sand cracks (MISS) visible just to the right of the hammer handle (Hammer utilized for scale is 27.5 cm).

Figure 3.23: Sandstone bed (plan view) with numerous preserved largely angular fragments of reddish coloured mudstone; angular shapes (shown with arrow) of the latter support mat-binding to provide cohesion so that thin muddy fragments do not break up or immediately become rounded on transport. Some of the inferred mud-bearing mat fragments appear to have possibly not been widely separated at all following the onset of presumed mat breakup and transport of resultant fragments (Coin for scale is 2.2 cm in diameter).

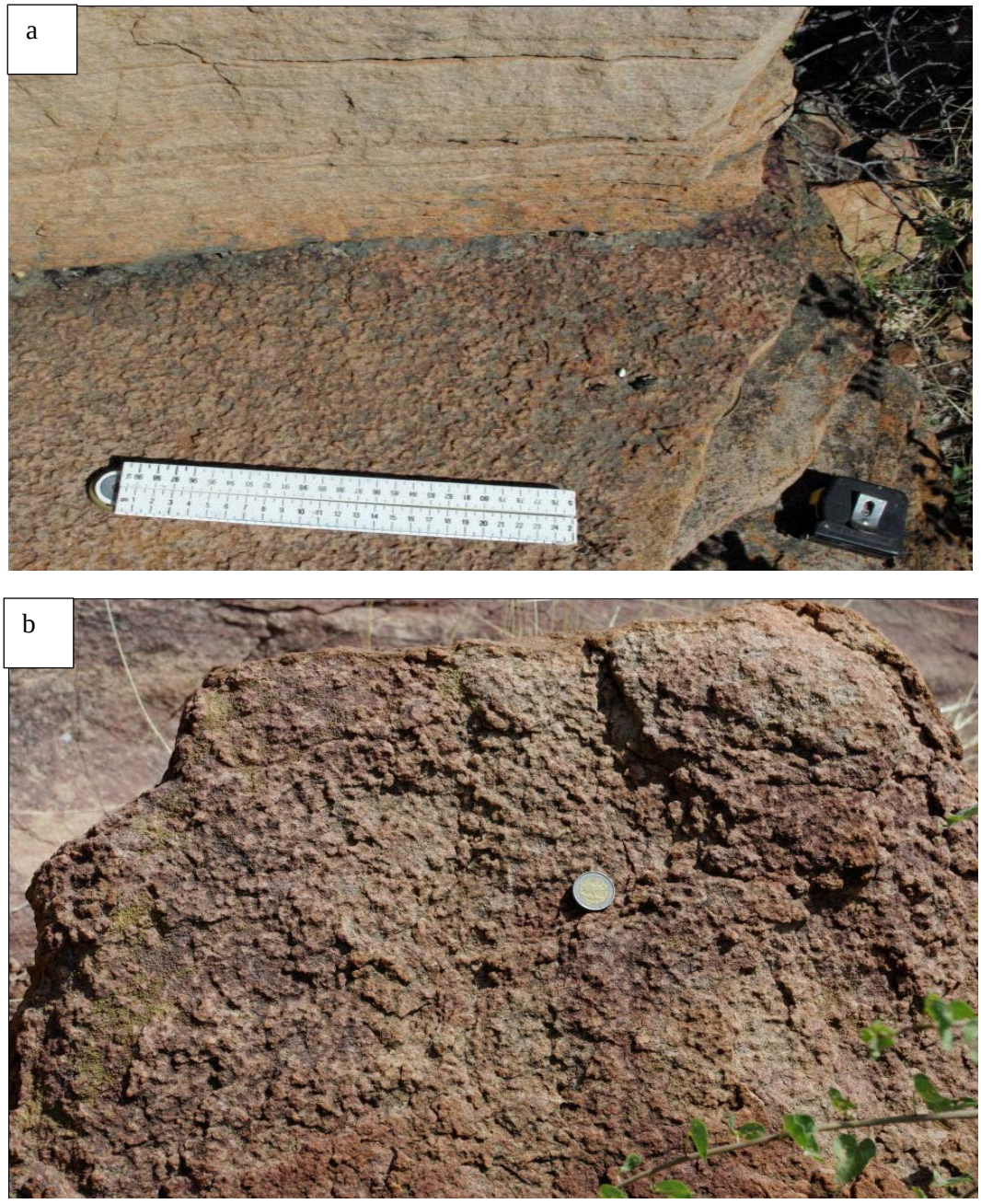

Figure 3.24: Crust-like morphology on sandstone upper bedding plane: (a) is an oblique picture and (b) is a plan view. Inferred possible MISS (pustular mat?) or adhesion ripples due to aeolian action on wet sand; sample not amenable for cross-section due to nature of outcrop and hard recrystallized silicified sandstone) (tape measure in (a) is centimetric in scale; coin for scale in (b) = 2.6cm in diameter).

The MISS catalogue for the Makgabeng Formation suggests that large angular mat fragments, petees and sand cracks (also filled sand cracks) are the most common features, with lesser rolled-up mats, and minor occurrences of possible domal sand build-ups and pustular mat fetaures. Mat destruction features thus predominate over mat growth MISS, as interpreted from the atlas of Schieber *et al.* (2007).

3.3 Associated sedimentary structures in the Magaliesberg Formation

Apart from the MISS features described and illustrated above in section 3.1, a set of commonly spatially associated and apparently not directly biologically-influenced sedimentary structures were found in this formation, as detailed briefly below.

Flat-crested slightly sinuous tidal ripples**:** all three examples of the slightly sinuous sand cracks (MISS) on ripple crests found in the study area are associated with straight- (**Figure 3.29**) to slightly sinuous-crested (**Figure 3.25**) ripple marks.
Bifurcating sinuous ripples (**Figure 3.26**).
Channel forms and planar bedding (**Figure 3.27**).
Planar bedding and palaeosol (**Figure 3.28**).

Figure 3.25: Flat-crested slightly sinuous current ripples: Note that the tops have been eroded by most probably current or tide. (Pen for scale =12.5cm). Note also associated MISS in the form of ripple crest sand cracks.

Figure 3.26: Bifurcating, sinuous ripples, surface wet for better illustration. (Coin for scale = 2.2 cm in diameter).

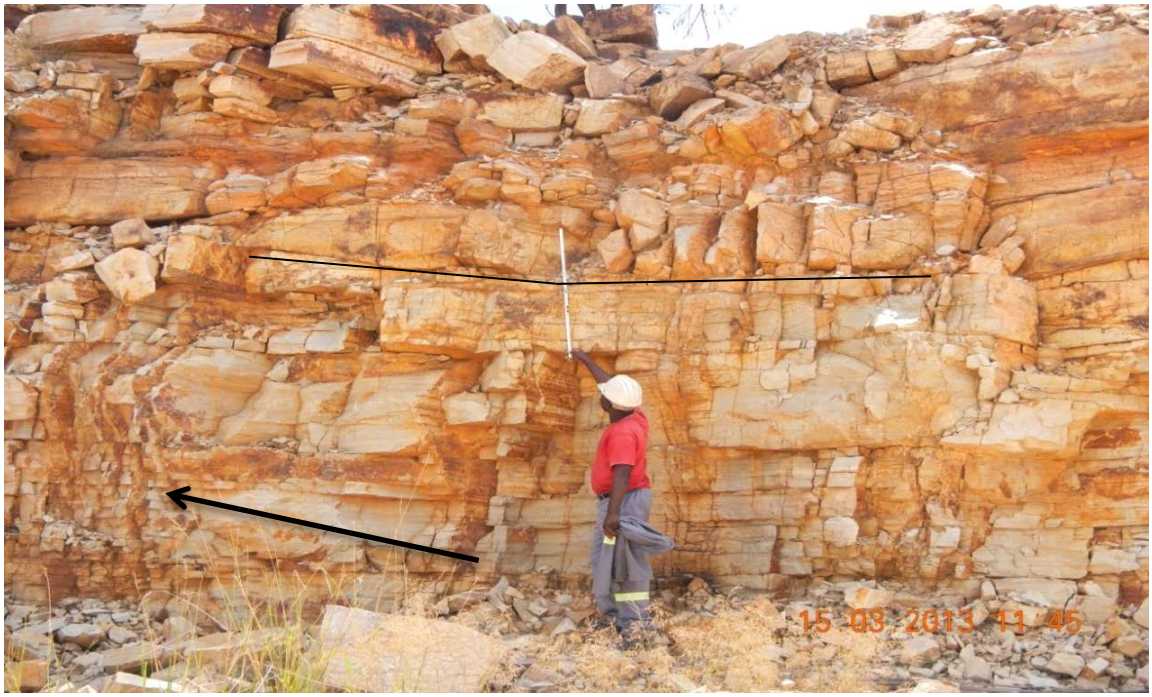

Figure 3.27: Channel forms and horizontal bedding. The man is indicating the edge of a channel form (channel shown with black line) with the white tape measure. The black arrow is pointed at the horizontal (cf. planar) bedding. (Scale is man with ruler: man = 1.68 m tall).

Figure 3.28: Planar bedding showing low angle regional dip of Magaliesberg Formation, northwards towards the Bushveld Complex. Inferred palaeosol shown with arrow (see Eriksson *et al*., 1995 for discussion thereof). Scale: quarry face = ~ 15 m in height.

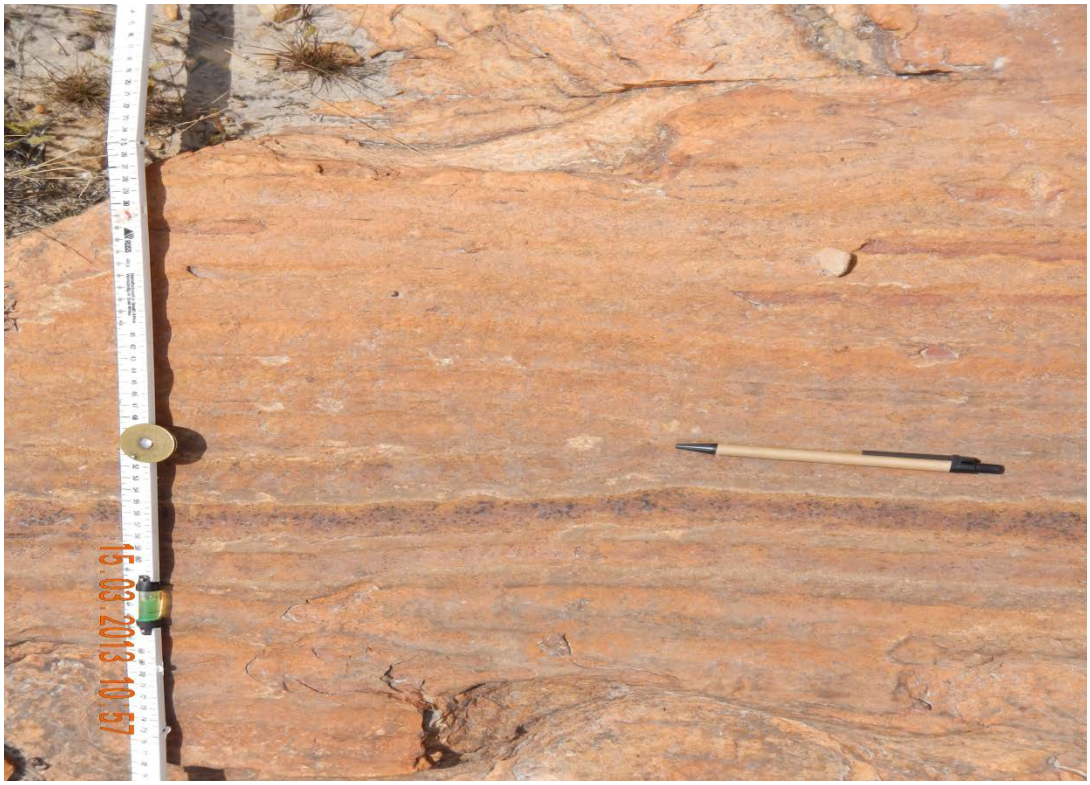

Figure 3.29: Bifurcating flat-crested ripples (tape measure for scale has centimetric divisions).

3.4. Associated sedimentary structures in the Makgabeng Formation

The following non-biogenic sedimentary structures are spatially associated with MISS in the Makgabeng Formation: Planar cross-bedding **(Figures 3.30 and 3.31) and** horizontally laminated sandstone **(Figure 3.32).**

Figure 3.30: Planar cross–bedding related to inferred barchanoid palaeo-dunes in the Makgabeng Formation study area (hammer for scale: 27.5 cm).

Figure 3.31: Planar cross stratification (arrow 2) normal to the plane of stratification (arrow 1). (Hammer for scale is 27.5 cm).

Figure 3.32: Horizontally laminated sandstone (person for scale =1.8 m).

Chapter 4

PHYSICAL SEDIMENTARY GRAIN ANALYSIS

This chapter presents studies made of some of the more prominent MISS features through cut and polished vertical (that is to bedding planes) sections of the sandstones containing them. It is particularly grain size that is pertinent and the relationship between grains and the surface MISS features observed on sandstone bedding planes. These granular studies are not mineral specific. Reflected light microscopy of cut-slabs of MISS-bearing samples is found to be very helpful to better understand evolution of these biogenic features. To a lesser extent thin sections were also utilised.

4.1 Magaliesberg Formation

4.1.1 MISS feature: pseudo petee ridges

Description

The uppermost surface of the slab section of the sample (characterized by positive ridges, petees) is draped by mudstone which underlies the petees (arrow (4) in Figure 4.1). Underlying the very thin mud veneer of the positive ridge is fine-grained sandstone; above the veneer fine-grained sandstone is rolled up into rounded forms that make up the inferred positive ridges. These rounded forms are locally characterized by an outer layer of coarser grained sandstone (Figure 4.1: arrows at 2 show the coarser grains forming outer layer of rounded grains). On its own this MISS can be termed a microscopic roll-up structure. The mudstone shown with arrow #4 overlay a distinctly uneven (and presumably thus, erosional) surface of coarser and finer grained sandstone (Figure 4.1). This lower mud drape thus post-dates the high energy erosional event and predates deposition of the sandy roll-up features. At arrow (3) two flattened mat chips, made up of relatively coarse sandstone can be seen below the right hand and largest roll-up feature comprising the ridge.

Interpretation

Megascopically, the MISS of the sample is that of petees or petee ridges as the sample displays polygonal and sinuous ridges (3 orders: a, b, c) on the uppermost bedding plane of the slab section, but the feature is quite clearly made up of microscopic sandy roll–ups when viewed in cut section under high lens power. Petees are defined as domes, buckles and folds

that are developed on flexible mat surfaces (e.g. Gavish et al., 1985; Reineck *et al.*, 1990); Gehling (1999, 2000) associates petees to sand cracks. Cracked sand layers are inferred to form from cracks that develop on a sandy bed surface because of the influence of overlying mats, which are themselves cracked after desiccation, on the upper sandy bed surface (see Eriksson, 2010 and references therein for further analogy). When these mats crack (due to dehydration or stretching), then the mat-bound sand immediately beneath, also become cracked. These cracks when filled up by the same sandy (same texture) material from the underlying bed forming positive polygonal structures on the upper bed surface are termed petees/petee ridges; they can also be filled from above by different and younger sandy material (e.g., Schieber *et al.*, 2007). The sample illustrated in section here(Figure 4.1) shows grain segregation which in this case is due to sandy roll-ups, most likely formed elsewhere and transported to their depositional site; possibly they became stuck there during transport due to the uneven and cohesive mud veneered sandy substrate. This particular feature, while resembling petees in plan view, clearly has a different origin to the norm, when seen in section. Hence the naming of this feature: **pseudo** petee ridges. The sandy sediments forming the micro – roll-ups must have been mat bound with mat enhanced cohesion to have being able to withstand erosion prior to their deposition to form the ridges.

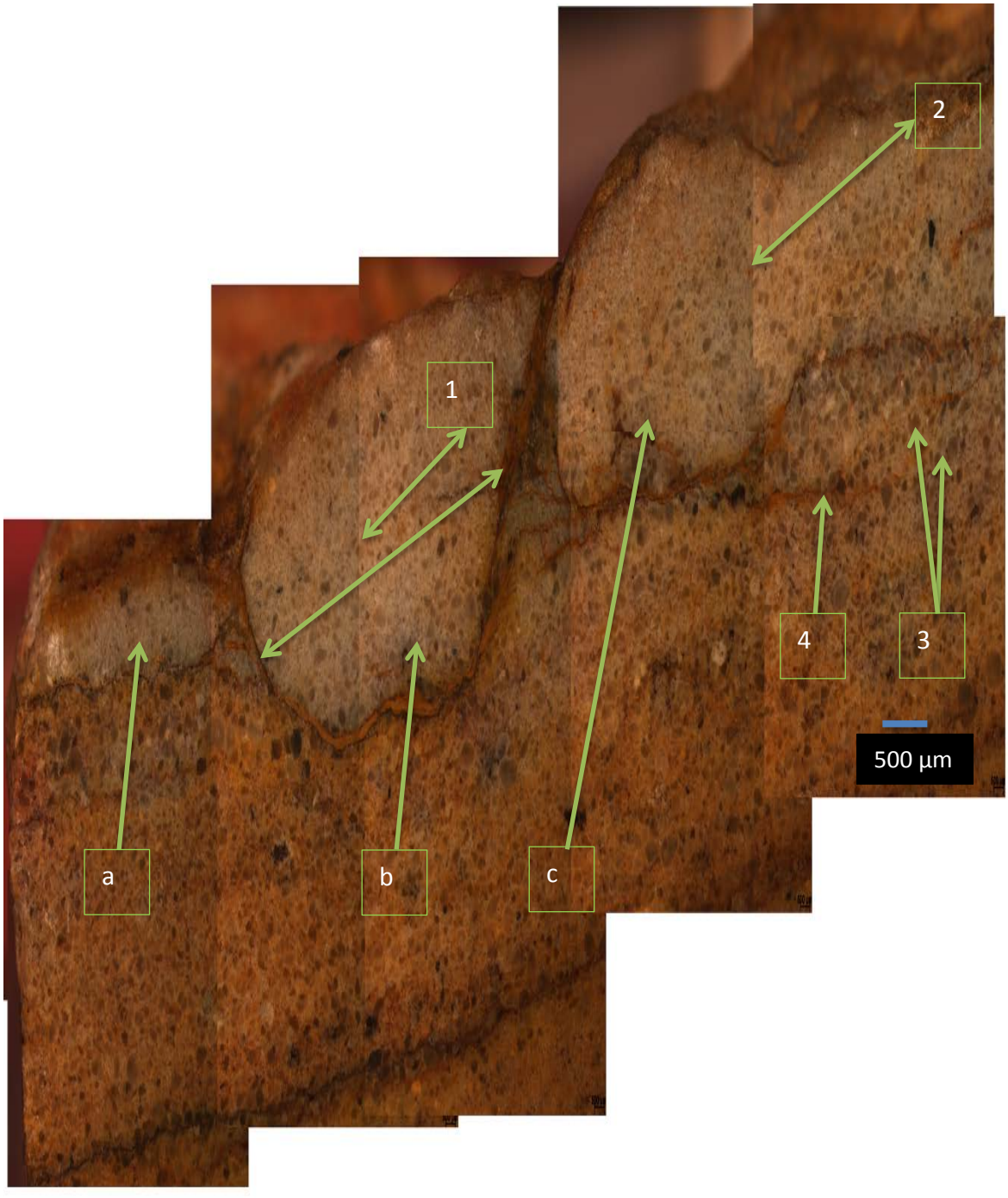

Figure 4.1: Pseudo petee ridges show finer grained sandy roll-ups; double arrows show three roll-ups, with double arrow at (1) indicating an internal smaller sandy roll surrounded by an outer roll shown by the wider arrow immediately underneath. A similar feature can be seen at arrow (2) where the boundary of the smaller internal roll is denoted by coarser grains. Flat mat chips are shown by arrow at (3). Arrow at (4) shows thin mudstone veneer below pseudo petees (roll-ups). The three orders of ridges in the MISS structure are shown with arrows as a, b, c. The figure comprises joined sectional micrographs of slab section taken on a non-transmitted light microscope. Scale bar at bottom right is 500µm

4.1.2 MISS feature: pseudo cross-lamination

Description

The uppermost surface of slab cross-section (Figure 4.2: shown with arrow (3) is draped by mud and immediately below the mud veneer, the sample has a sandy layer with good sorting and finer texture compared to the angular to sub-angular sand grains of the underlying section. The well sorted and finely textured quartz grains display inter-layered laminae, presumably resulting from microbial mats (cf., MISS features c and d in Fig. 2.1; Schieber, 2004). These inter-layered laminae are thrusted upwards (apparently from left to right in Fig. 4.2) forming a "pseudo cross-lamination" and helping to build a ridge on the right hand top surface of the sample.

Interpretation

The inferred genetic mechanism of this MISS structure is complex and thus segregated into two processes:

1. Fine sandy sediments deposited as biolaminites and accreted on the coarser sandy sandy substrate sedimentary surface were mediated by microbial communities (e.g., Burne and Moore, 1987). Siliciclastic biolaminites are produced by a process involving periods of non-deposition and sedimentation. During the period of non-deposition, the organisms are inferred to produce and establish mat layers (through biofilms and probable phototrophy) on a sediment surface, and during periods of subsequent sedimentation a thin layer of fine-grained sediments covers the mat. Motile bacteria later move upwards to the new sediment surface to establish a new mat. This process can be described by biostabilization (cf., Schieber *et al.*, 2007).
2. The mat-bound finer sandy sediments resist disintegration by currents, waves etc. and were being biostabilized and were amenable to being thrust upwards, with the individual biolaminae apparently stacked up on each other to form microscopic pseudo cross-lamination in section, and an apparent ridge in plan view. The cause of the thrusting remains speculative – possibly due to the biolaminated sand layers becoming partially loose at their base, and the action of a strong current or wave force to locally thrust them up against an immediately adjacent obstruction.

The laminated sandy sediments wouldn't have being able to resist disintegration without the cohesive influence of mats.

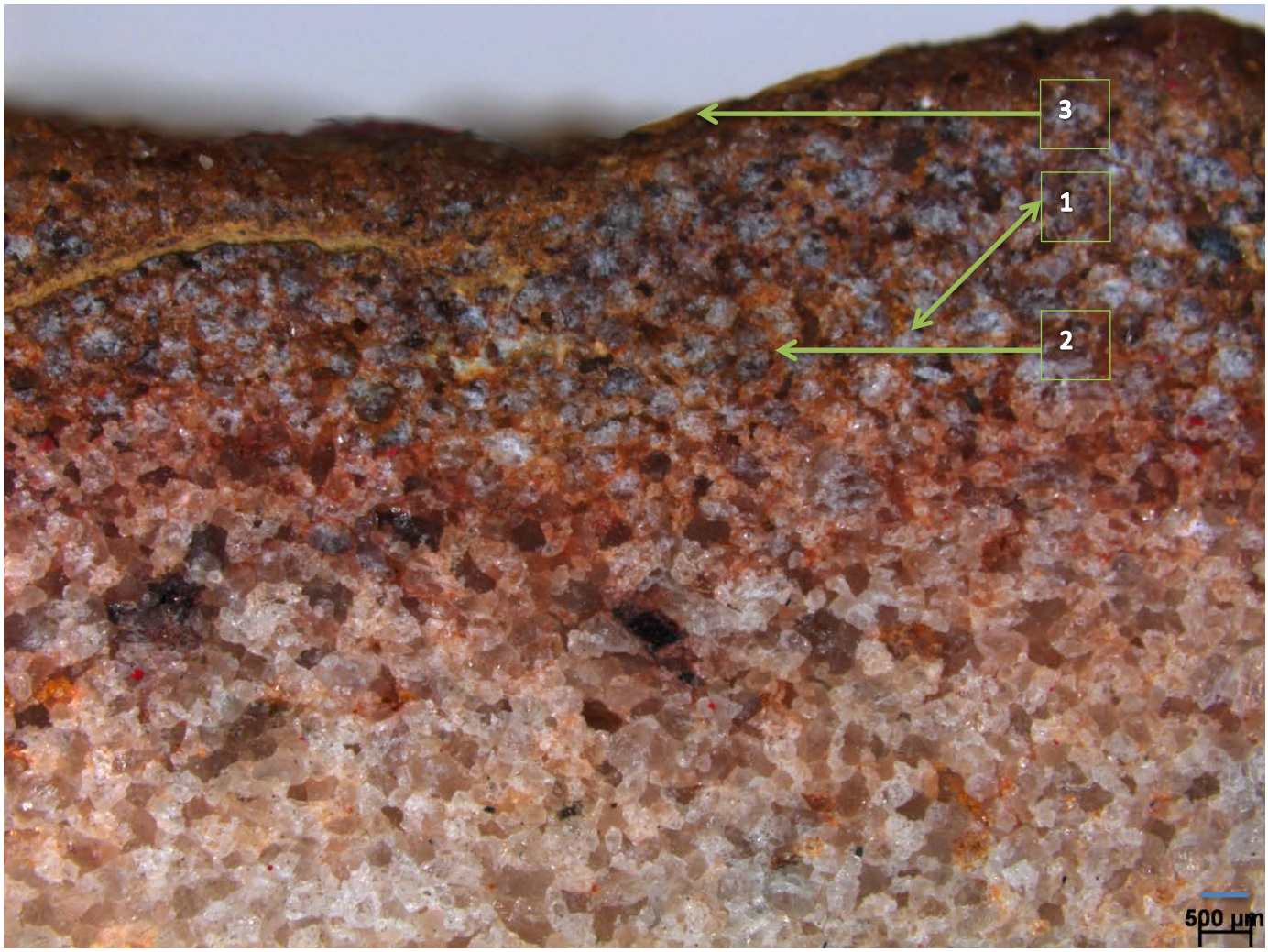

Figure 4.2: Pseudo cross-lamination (faintly visible and shown by the inclination of the double arrow at # 1) thought to have formed by microbiolaminites that were thrusted upwards from an original horizontal orientation as at position (2). Arrow 3 shows a very thin mudstone veneer covering the entire ridge-like feature (easily confused with a petee ridge). The micrograph is of a slab cut section and under non-transmitted light microscope. Scale at bottom right is 500 µm.

4.2 Makgabeng Formation

4.2.1 MISS feature: roll-up structure

Description

Ferruginous silty mud roll-ups are embedded in thinly-bedded well-developed millimetre scale planar laminated (lamination is mostly visible with differences in iron concentration), fine- to medium-grained sandstone (Fig. 4.3a). The roll-ups are of two, to two and a half full revolutions and these concentric layers (detail in Fig. 4.3b), due to syn- and post-diagenetic factors, are sometimes relatively flattened out and appear elliptical (2) in Fig. 4.3a).

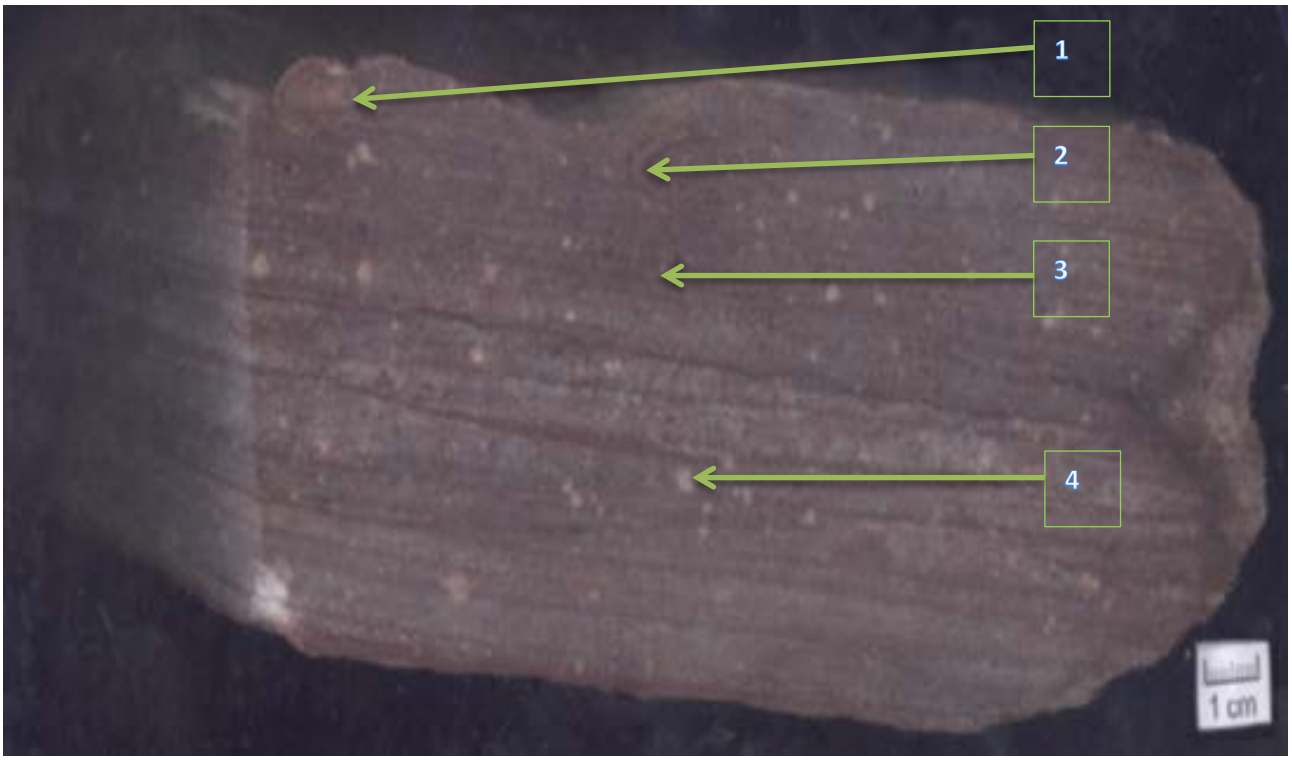

Figure 4.3a: Planar laminated (3) sandstone (mm scale lamina) within fine- to medium-grained sandstone. Roll-up structure (1 and 2) which is made up of ferruginous silty mud is embedded in the planar laminated sandstone. Of the two roll-ups shown, that at (1) is concentric and circular and that at (2) is concentric and ellipsoidal. Note that the white spots (4) are reduction spots that are inferred to be related to microbial activities. Picture is cross-sectional view of cut sandstone sample and scale is shown (1 cm).

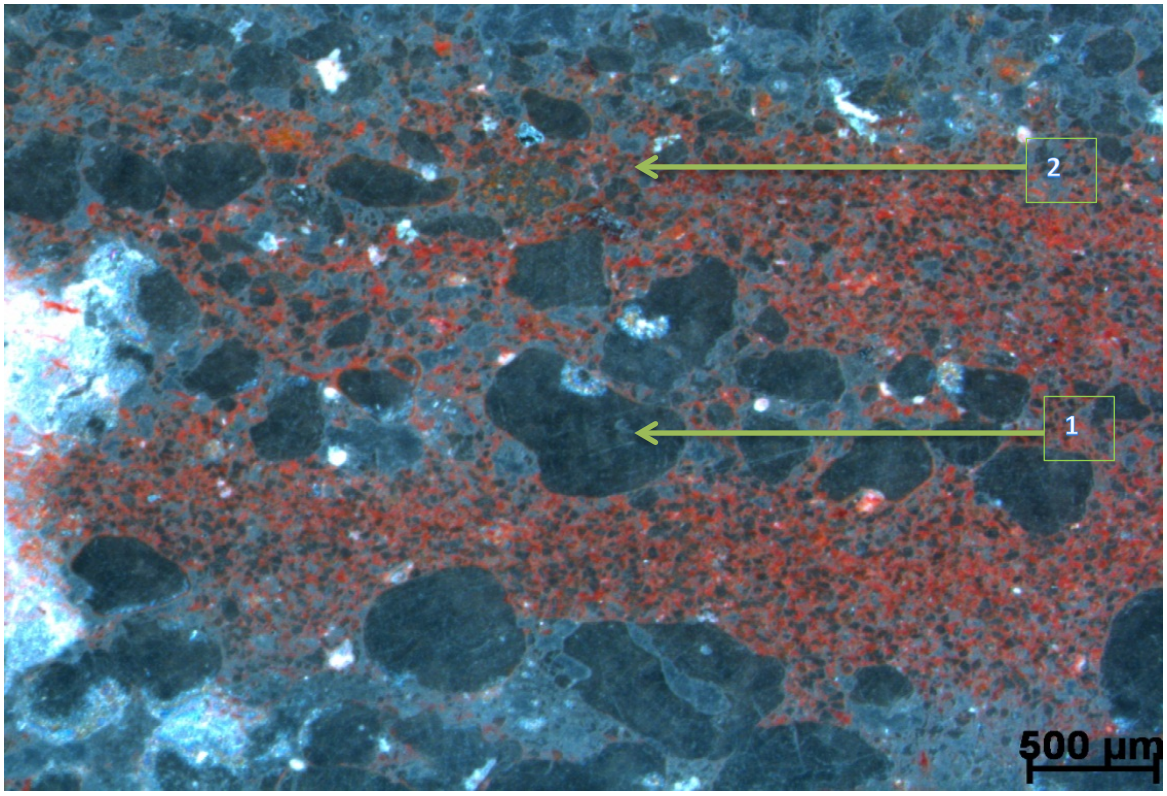

Figure 4.3b: Photograph of thin section of sandstone sample showing portion of two concentric layers within a single roll-up structure. Roll-up structure comprises layers of relatively large and sub-angular-subrounded grains (#1) encased and separated by thin mudstone layer (shown by arrow #2). Magnification is 2. 5x and microscope is using transmitted light; scale is 500 µm.

Interpretation

The laminated sandstone is inferred to reflect upper flow regime conditions and thus relatively high energy during formation and embedding of the roll-ups. Roll-ups are formed by the erosion and re-deposition of mat bound sediments, with the mats providing cohesion to thin mat-bound sandy or muddy sediment to enable the formation of several concentric rolls thereof (Figure 4.3a and b; Schieber *et al*., 2007 and references therein). The inter-dune flash floods inferred for the Makgabeng Formation palaeodesert (e.g., Simpson *et al*., 2002, 2013) would have eroded curled up mat-bound mud with microbial enhanced cohesion (not expected of ordinary mud which cannot curl beyond an approximate half circle) and deposited it on upper flow regime planar bed surfaces (see Eriksson *et al.*, 2007 for further illustration of roll-up structures and discussion of their origin in the Makgabeng Formation palaeoenvironment).

4.2.2 MISS feature: mat chips and composite mat chips

Description

These features consist of rounded and mostly oblate sandstone clasts, some of them have thin mudstone veneers. The latter feature makes their recognition in cut sandstone sections under the microscope much easier. Agglutinated inferred mat chips also occur quite frequently which reinforces the supposition of mat binding (Fig. 4.4).

Interpretation

Grains of sand lack the cohesion to form composite sandstone clasts unless bound by either mud or microbial mats; in the present case, the absence of a mudstone matrix between the sandstone grains supports mats as the binding medium (cf., Schieber *et al.*, 2007, and references therein). The survival of the sandstone clasts after high energy transport and deposition implies they were mat-bound at the time of their formation while the thin mudstone veneers are presumably picked up when being rolled over during transport. The presence of composite mat chips reinforces the inferred microbial binding further.

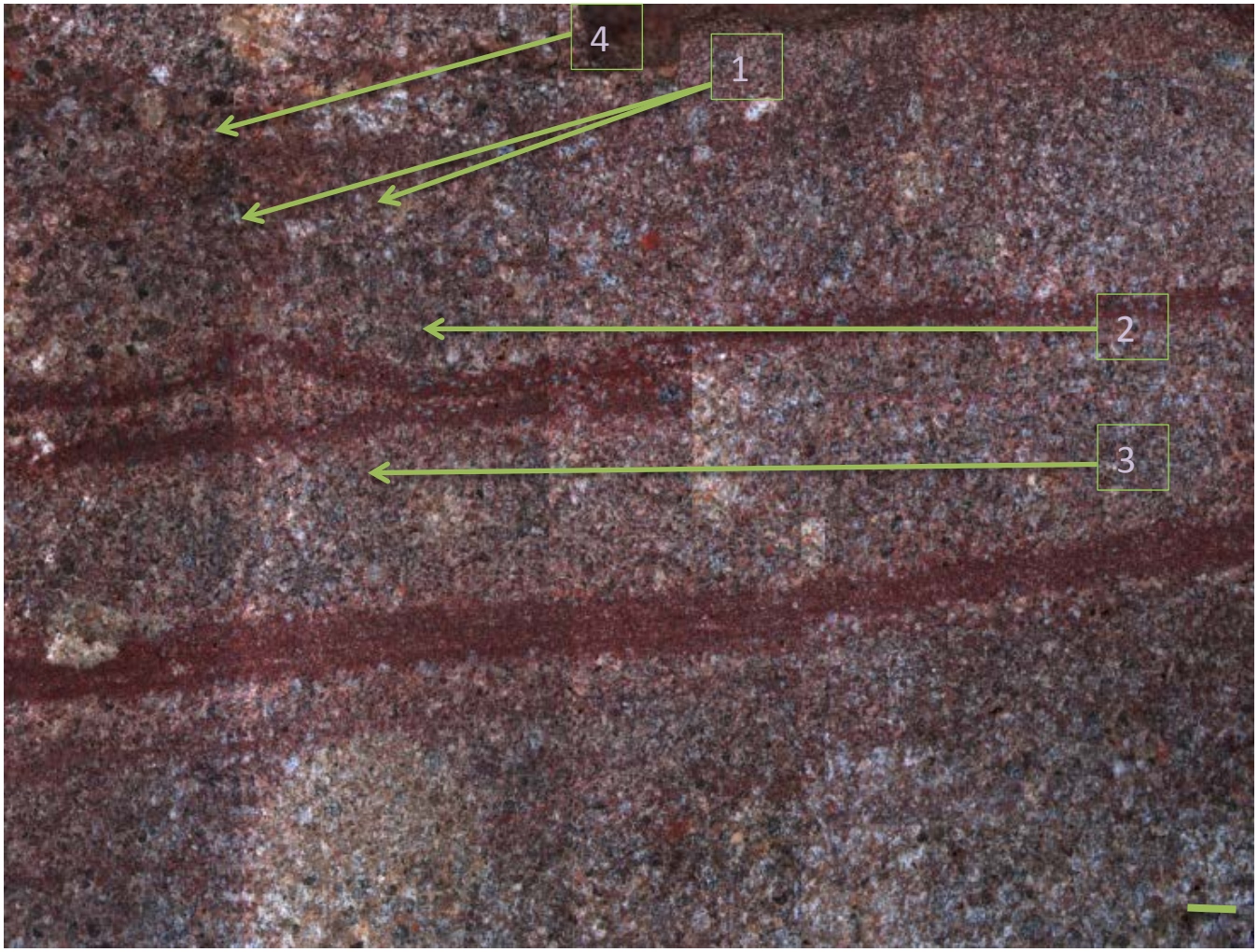

Figure 4.4: Mat chips (shown by two arrows at (1); chip defined by faintly visible flattened saucer-like shape), composite mat chips (shown by arrow at (2); note the grain agglutination of the two chips that is inferred to be microbially induced). Arrow at (3) shows two agglutinated mat chips or a composite mat chip that is difficult to see because the two chips lack any mudstone veneer (as is the case for #2 where the bases of the two chips is easily visible). Arrow at (4) shows a mat chip (just above arrow) where the rounded base of the chip clearly impinges into a thin sandstone bed. The microscopic picture of the sample is of adjoined micrographs of slab-cut section under non-transmitted light. Scale is 500 µm.

CHAPTER 5

GEOCHEMISTRY AND MINERALOGY

5.1 X-ray fluorescence spectrometry (XRF)

The results of the major element geochemical analyses of selected Magaliesberg Formation (MAG 101A and 101B, 102A and 102B, 103A and 103B) and Makgabeng Formation samples (MKG 101A and 101B, MAG 102A and 102B) in weight % are shown in table 5.1. The trace element geochemistry of these samples (ppm) is shown in table 5.2. It is important to note here, that for each of these five samples taken from inferred MISS features, the A sample is from sandy material directly from the MISS feature itself, while the B sample is from the underlying sandy substrate of the MISS feature. The intention is thus to compare the geochemistry of the sediment within which the MISS features is preserved, against its sedimentary substrate.

Table 5.1: XRF results of major element geochemistry in wt. %. (MAG = Magaliesberg Formation; MKG = Makgabeng Formation; SAM = sample). S.C.R. represents standard certified results.

SAM	MAG 101A	MAG 101B	MAG 102A	MAG1 02B	MAG 103A	MAG 103B	MKG1 01A	MKG 101B	MKG 102A	MKG 102B	S.C.R 2	S.C.R1
SiO_2	78.88	97.54	92.6	95.4	93.21	95.99	87.89	88.29	89.79	90.53	45.42	45.1
TiO_2	0.31	0	0.25	0.04	0.17	0.06	0.2	0.34	0.25	0.2	1.54	1.62
Al_2O_3	8.71	1.33	5.07	2.84	4.13	1.98	6.56	6.76	5.13	4.31	16.62	17.43
Fe_2O_3	8.54	0.82	0.78	0.63	0.86	1.09	2.09	0.94	2	2.47	9.73	10.16
MnO	0.003	0.007	0.006	0.005	0.005	0.005	0.027	0.024	0.029	0.031	0.18	0.177

MgO	<0.01	<0.01	<0.01	<0.01	<0.01	<0.01	0.33	0.39	0.17	0.2	8.15	7.91
CaO	0.05	<0.01	0.03	0.01	<0.01	<0.01	0.1	0.15	0.04	0.07	10.93	10.66
Na_2O	0.22	<0.01	0.05	<0.01	0.04	<0.01	0.07	0.07	0.05	0.06	3.65	3.64
K_2O	1.56	0.3	1.21	0.67	1.03	0.5	1.69	1.72	1.24	1	0.7	0.7
P_2O_5	0.077	0.009	0.022	0.012	0.019	0.015	0.085	0.149	0.259	0.204	0.259	0.266
Cr_2O_3	0.027	0.003	0.01	0.003	0.008	0.003	0.004	0.007	0.003	0.006	0.074	0.076
LOI	1.69	0.04	0.55	0.36	0.48	0.2	0.96	1.15	0.87	0.7	2.5	2.32

Table 5.2: XRF results of trace element geochemistry in ppm. (MAG = Magaliesberg Formation; MKG = Makgabeng Formation; SAM = sample). S.C.R. represents standard certified results.

SAM	MAG 101A	MAG 101B	MAG 102 A	MAG 102 B	MAG 103 A	MAG 103 B	MKG 101 A	MKG 101 B	MKG 102 A	MKG 102 B	S.C.R .1	S.C. R.2
As	<4	<4	4.1	<4	<4	<4	<4	5.3	5.2	<4	33.5	36
Ba	163	24	82	39	85	24	586	578	483	383	590	600
Bi	<3	<3	<3	<3	<3	<3	<3	<3	<3	<3	1.17	<3
Br	<2	<2	<2	<2	<2	<2	<2	<2	<2	<2	2.9	<2
Ce	32	20	69	29	38	17	28	281	41	44	70	70
Co	4	1.3	2	1.3	<1	1	3.3	4.7	3.3	4	14.2	15
Cr	159	29	62	28	48	18	27	44	27	32	62	62
Cs	<5	<5	<5	<5	<5	<5	<5	<5	<5	<5	9.0	9
Cu	7.5	6.6	8.2	8	8	8.4	7.2	6.3	8.7	8.4	21	23
Ga	13	1.7	6	2.3	5.1	1.5	7.3	6.4	5.4	5.4	19.3	20

Ge	1.2	1.8	1.3	1.6	1.5	1.3	1.3	<1	1.3	<1	1.3	1.7
Hf	7.1	<3	7.5	4.2	5.8	3.5	5.9	7.4	8.9	8.6	6.8	9.1
La	26	28	37	19	28	21	29	146	41	37	34	35
Mo	<2	<2	<2	<2	<2	<2	<2	<2	<2	<2	1.4	<2
Nb	7.6	3.5	7.7	4.5	6.1	4	6.3	9	6.1	6.3	16.6	17
Nd	16	11	21	<10	15	<10	16	116	24	24	28	29
Ni	15	3.5	4.1	4.7	3.5	3.4	6.4	8.8	7.1	7.2	20.4	21
Pb	8.3	4	6.8	2.2	5.7	2.4	7	3.7	5.1	6.2	98	95
Rb	55	9.9	43	24	33	17	53	55	42	34	140	141
Sc	17	<3	4.7	<3	<3	<3	<3	<3	<3	<3	11.2	10
Se	<1	<1	<1	<1	<1	<1	<1	<1	<1	<1	0.14	<1
Sm	<10	<10	<10	<10	<10	<10	<10	18	<10	<10	5.2	<10
Sr	111	18	36	17	33	11	17	17	14	15	155	157
Ta	<2	2.5	3.7	2.8	3.9	<2	<2	<2	<2	2.3	1.4	5.5
Th	10	<3	10	3.5	7.4	<3	6.3	8.9	5.5	7.1	11.6	11
Tl	<3	<3	<3	<3	<3	<3	<3	<3	<3	<3	1.0	<3
U	3.3	<2	3.4	<2	2.6	<2	<2	<2	<2	<2	3.3	4.1
V	54	9.7	68	19	53	16	19	24	17	19	86	88
W	<3	<3	<3	<3	<3	<3	<3	<3	<3	<3	3.1	5
Y	17	5.9	17	7.2	13	6.1	13	23	20	25	25	26
Yb	<3	<3	<3	<3	<3	<3	<3	3.4	<3	<3	2.66	<3
Zn	24	<3	7.7	4.9	12	8.1	8.7	11	5.7	7.2	680	687

Dissection of XRF data

These primary geochemical data are utilized for comprehension of higher concentration/lower concentration of a particular oxide/trace element in the MISS section of a sample compared to that of its underlying substrate, and for side-by-side comparison of the distribution of that element in all the samples of each of the two units (Magaliesberg Formation: tables 5.3.1-5.3.3; Makgabeng Formation: tables 5.3.4-5.3.5). The following

parameters are used as column headings on correlation tables and in this chapter: MAG 101, 102, 103 = Magaliesberg samples, MKG 101, 102 = Makgabeng samples, A = MISS-bearing sedimentary rock section, B = underlying sedimentary rock section; A-B = difference in concentration of A to B, A/B = factor of concentration of A to B, B/A = factor of concentration of B to A; (A-B/A)% = percentage of (A-B) over A; Mean = average, M.D. = mean deviation. The columnar heading (A-B) is of great statistical significance because values of concentration of elements (higher concentration/lower concentration) in A compared to B are easily decipherable (negative values of A-B are in red fonts for clarity) and are widely utilized in this treatise.

5.1.1 Major elements

It is noticeable from the primary analytical data tables that major elements are mostly of lower concentration in the MISS sedimentary rock section compared to the underlying sedimentary rock section of each of the Makgabeng samples (MKG 101, 102: manifold red fonts of A-B concentration values in tables 5.3.4- 5.3.5 showing negative values). In contrast, major elements are more concentrated in the MISS section of each of the analyzed Magaliesberg samples (MAG 101, 102, 103) compared to its underlying section (tables 5.3.1-5.3.3). However, for all five samples analysed there is homogeneity in the lower concentration of SiO_2 in all the MISS sections (MAG 101A, 102A, 103A; MKG 101A, 102A) compared to underlying sections (MAG 101B, 102B, 103B; MKG 101B, 102B) (see table 5.4). Comparatively, there is a larger difference in concentration of SiO_2 (shown in table 5.4) between underlying and MISS bearing sections of samples from the Magaliesberg Formation (MAG 101; 18.66, 102; 2.8, 103; 2.78) compared to difference in concentration of SiO_2 between underlying and MISS bearing sections of Makgabeng Formation samples (MKG 101; 0.4, 102; 0.74).

Table 5.3.1: Primary analytical data table of MAG 101

MAG 101	A	B	A-B	A/B	B/A	(A-B/A)%	MEAN	M.D
SiO_2	78.88	97.54	-18.66	0.809	1.237	-23.656	88.21	9.33
Al_2O_3	8.71	1.33	7.38	6.549	0.153	84.73	5.02	3.69
TiO_2	0.31	0	0.31	0	0	100	0.155	0.155
Fe_2O_3	8.54	0.82	7.72	10.415	0.096	90.4	4.68	3.86
MnO	0.003	0.007	-0.004	0.429	2.333	-133.333	0.005	0.002
MgO	0.01	0.01	0	1	1	0	0.01	0
CaO	0.05	0.01	0.04	5	0.2	80	0.03	0.02
Na_2O	0.22	0.01	0.21	22	0.0455	95.455	0.115	0.105
K_2O	1.56	0.3	1.26	5.2	0.192	80.769	0.93	0.63
P_2O_5	0.077	0.009	0.068	8.556	0.117	88.311	0.043	0.034
Cr_2O_3	0.027	0.003	0.024	9	0.111	88.889	0.015	0.012

Table 5.3.2: Primary analytical data table of MAG 102

MAG 102	A	B	A-B	A/B	B/A	(A-B/A)%	MEAN	M.D
SiO_2	92.6	95.4	-2.8	0.971	1.03	-3.023	94	1.4
TiO_2	0.25	0.04	0.21	6.25	0.16	84	0.145	0.105
Al_2O_3	5.07	2.84	2.23	1.785	0.56	43.984	3.955	1.115
Fe_2O_3	0.78	0.63	0.15	1.238	0.808	19.23	0.705	0.075
MnO	0.006	0.005	0.001	1.2	0.833	16.667	0.006	0.006
MgO	0.01	0.01	0	1	1	0	0.01	0
CaO	0.03	0.01	0.02	3	0.333	66.667	0.02	0.01
Na_2O	0.05	0.01	0.04	5	0.2	80	0.03	0.02
K_2O	1.21	0.67	0.54	1.806	0.554	44.628	0.94	0.27
P_2O_5	0.022	0.012	0.01	1.833	0.545	45.455	0.017	0.005
Cr_2O_3	0.01	0.003	0.007	3.333	0.03	70	0.007	0.004

Table 5.3.3: Primary analytical data table of MAG 103

MAG 103	A	B	A-B	A/B	B/A	(A-B/A)%	MEAN	M.D
SiO_2	93.21	95.99	-2.78	0.971	1.03	-2.983	94.6	1.39
TiO_2	0.17	0.06	0.11	2.833	0.353	64.706	0.115	0.055
Al_2O_3	4.13	1.98	2.15	2.086	0.479	52.058	3.055	1.075
Fe_2O_3	0.86	1.09	-0.23	0.789	1.267	26.744	0.975	0.115
MnO	0.005	0.005	0	1	1	0	0.005	0
MgO	0.01	0.01	0	1	1	0	0.01	0
CaO	0.01	0.01	0	1	1	0	0.01	0
Na_2O	0.04	0.01	0.03	4	0.25	75	0.025	0.015
K_2O	1.03	0.5	0.53	2.06	0.485	51.456	0.765	0.265
P_2O_5	0.019	0.015	0.004	1.267	0.789	21.053	0.017	0.002
Cr_2O_3	0.008	0.003	0.005	2.667	0.375	62.5	0.006	0.002

Table 5.3.4: Primary analytical data table of MKG 101

MKG 102	A	B	A-B	A/B	B/A	(A-B/A)%	MEAN	M.D
SiO_2	89.79	90.53	-0.74	0.992	1.008	0.824	90.16	0.37
TiO_2	0.25	0.2	0.05	1.25	0.8	20	0.225	0.025
Al_2O_3	5.13	4.31	0.82	1.19	0.84	15.984	4.72	0.41
Fe_2O_3	2	2.47	-0.47	0.81	1.235	-23.5	2.235	0.235
MnO	0.029	0.031	-0.002	0.935	1.069	-6.897	0.03	0.001
MgO	0.17	0.2	-0.03	0.85	1.177	-17.647	0.185	0.015
CaO	0.04	0.7	-0.03	0.571	1.75	-75	0.055	0.015
Na_2O	0.05	0.06	-0.01	0.833	1.2	-20	0.055	0.005
K_2O	1.24	1	0.24	1.24	0.806	19.355	1.12	0.12
P_2O_5	0.259	0.204	0.055	1.27	0.788	21.236	0.232	0.028
Cr_2O_3	0.003	0.006	-0.003	0.5	2	-100	0.005	0.002

Table 5.3.5: Primary analytical data table of MKG 102

MKG 102	A	B	A-B	A/B	B/A	(A-B/A)%	MEAN	M.D
SiO_2	89.79	90.53	-0.74	0.992	1.008	0.824	90.16	0.37
TiO_2	0.25	0.2	0.05	1.25	0.8	20	0.225	0.025
Al_2O_3	5.13	4.31	0.82	1.19	0.84	15.984	4.72	0.41
Fe_2O_3	2	2.47	-0.47	0.81	1.235	-23.5	2.235	0.235
MnO	0.029	0.031	-0.002	0.935	1.069	-6.897	0.03	0.001
MgO	0.17	0.2	-0.03	0.85	1.177	-17.647	0.185	0.015
CaO	0.04	0.7	-0.03	0.571	1.75	-75	0.055	0.015
Na_2O	0.05	0.06	-0.01	0.833	1.2	-20	0.055	0.005
K_2O	1.24	1	0.24	1.24	0.806	19.355	1.12	0.12
P_2O_5	0.259	0.204	0.055	1.27	0.788	21.236	0.232	0.028
Cr_2O_3	0.003	0.006	-0.003	0.5	2	-100	0.005	0.002

Table 5.4: Negative relationship between SiO_2 and Al_2O_3 is common to samples MAG 101A and 101B, 102A and 102B, 103A and 103B (table is based on A-B concentration value). It is significant to note that in each case the MISS section has lower SiO_2 (A-B: negative value) and higher Al_2O3 (A-B: positive value) concentrations compared to the underlying section. A negative statistical relationship between SiO_2 and Al_2O_3 is shown by MKG 102; lower SiO_2 (A-B: negative value) and higher Al_2O_3 (A-B: positive value) concentrations in the MISS section, and higher SiO_2 (A-B: positive value) and lower Al_2O_3 (A-B: negative value) in the underlying section. MKG 101 has lower concentrations of both SiO_2 and Al_2O_3 in the MISS section (A-B: negative value) compared to the underlying section. Red fonts represent negative difference in concentration of A-B

SAMPLE	MAG101	MAG 102	MAG 103	MKG 101	MKG 102
SiO_2	-18.66	-2.8	-2.78	-0.4	-0.74
Al_2O_3	7.38	2.23	2.15	-0.2	0.82

The three analysed samples from the Magaliesberg Formation (MAG 101, 102, 103) and MKG 102 (Makgabeng Formation) have higher Al_2O_3 concentration in the MISS section compared to the underlying section (shown in table 5.4: A-B = positive value). Comparatively, there is a higher Al_2O_3 concentration difference between the underlying section and the MISS section (B-A) of each of the Magaliesberg samples (MAG 101, 102, 103) compared to the concentration difference of Al_2O_3 (B-A) between the underlying section and MISS section of MKG 102 (see table 5.4 for comparison). MKG 101 has lower concentrations of Al_2O_3 and SiO_2 in the MISS section compared to the underlying section (both are shown in red fonts in table 5.4).

Figure 5.1 (plotted with A-B values; table 5.4) shows that SiO_2 and Al_2O_3 have a negative statistical correlative relationship in four samples: MAG 101, 102, 103; MKG 102 which translates in the A-B concentrations of Al_2O_3 and SiO_2 plotting on the positive and negative segments of the graph respectively ($Al_2O_{3:}$ above zero line of the x- axis; $SiO_{2:}$ below zero line of the x- axis). A-B concentration values of both SiO_2 and Al_2O_3 of MKG 101 both plot on the negative segment of the graph (SiO_2 and $Al_2O_{3:}$ below zero line of the x- axis).

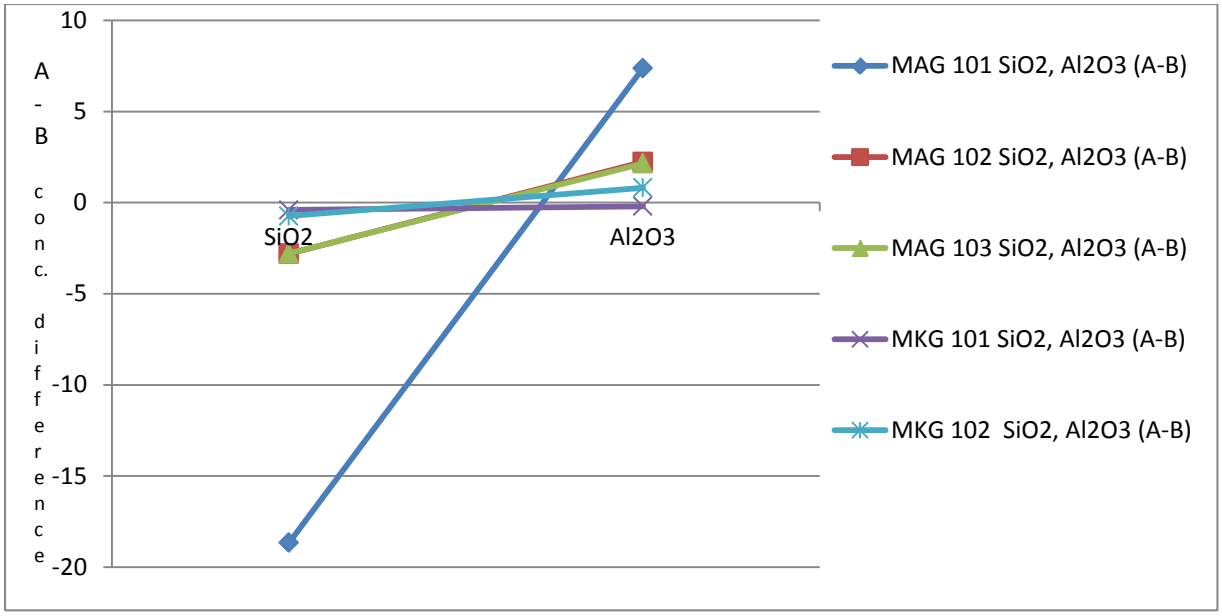

Figure 5.1: Homogeneous negative statistical correlative relationship in SiO_2 and Al_2O_3 concentrations of the Magaliesberg samples (MAG 101, 102, 103), and heterogeneous statistical correlative relationship of the Makgabeng samples (MKG 101, 102) in SiO_2 and Al_2O_3 concentrations. It is significant to note that MAG 101, 102, 103 have SiO_2 and Al_2O_3 plotting on the negative and positive segments of the graph respectively (A-B concentration value: SiO_2, below zero line of the x-axis; Al_2O_3, above zero line of the x-axis). MKG 102 also has SiO_2 and Al_2O_3 plotting on the negative and positive segments of the graph respectively (SiO_2, below zero line of the x-axis; Al_2O_3, above zero line of the x-axis). MKG 101 has both SiO_2 and Al_2O_3 plotting on the negative segment of the graph (below zero line of the x-axis). Graph is based on difference in concentration between MISS-bearing sedimentary rock section and underlying sedimentary rock section (A-B). Conc. represents concentration on plot.

Figure 5.2 (plotted with both A and B concentrations of MAG 101, 102, 103; MKG 101, 102) illustrates the homogeneity of the negative statistical correlative relationship of SiO_2 and Al_2O_3 in MAG 101, 102, 103. Each sample (MAG 101, 102, 103) has point divergence of SiO_2 and Al_2O_3 (shown with 2 orange double arrow shapes for one example, MAG 101) in the MISS (A), and underlying section (B). This statistical negative correlative behaviour between SiO_2 and Al_2O_3 is also exhibited by MKG 102 (note the point divergence of SiO_2 and Al_2O_3 in MKG 102A and MKG 102B; shown with purple double arrow shape). It is significant to note the near-horizontality of the SiO_2 and Al_2O_3 trend between the MISS (A) and underlying section (B) of MKG 101 (shown with dark double arrow shapes in figure 5.2).

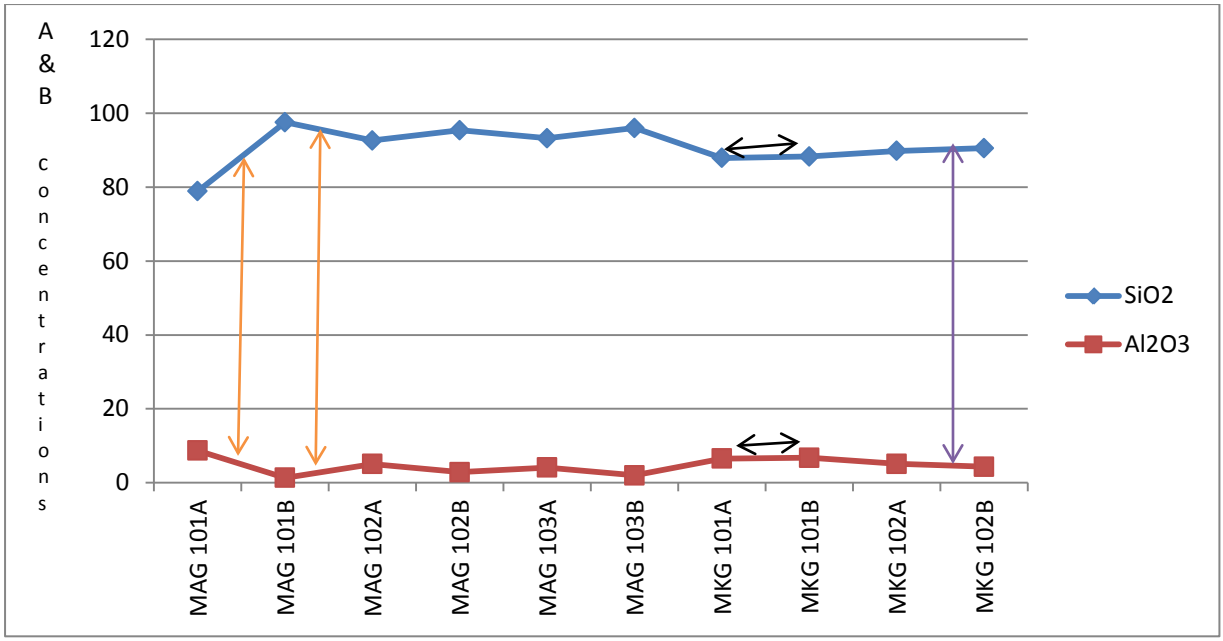

Figure 5.2: Plot of the concentration of SiO_2 and Al_2O_3 of samples MAG 101, 102, 103; MKG 101, 102 (both MISS-bearing sedimentary rock section (A) and underlying sedimentary rock section (B). It is significant to note that MAG 101, 102, 103, and MKG 102 have point divergence of SiO_2 and Al_2O_3 in each section of the sample (MISS/underlying). The Magaliesberg example is shown with 2 orange double arrows and MKG 102 is shown with a purple double arrow. Note the near-horizontality of SiO_2 and Al_2O_3 trend lines between MKG 101A and MKG 101B (shown with 2 dark double arrow shapes).

MAG 101, 102, and 103 show higher concentrations of Al_2O_3, TiO_2, K_2O, and P_2O_5 in the MISS section compared to the underlying section (shown in table 5.5.1). MKG 102 also shows higher concentrations of Al_2O_3, TiO_2, K_2O, and P_2O_5 in the MISS section compared to the underlying section (shown in table 5.5.2). There is a lower concentration of Al_2O_3, TiO_2, K_2O, and P_2O_5 in the MISS section of MKG 101 compared to the underlying section (table 5.5.2). Figure 5.3 illustrates the homogeneity of MAG 101, 102, and 103 in the higher concentration of Al_2O_3, TiO_2, K_2O, and P_2O_5 in each of the MISS sections compared to the underlying section of a particular sample. It is significant to note that the analyzed Magaliesberg samples (MAG 101, 102, 103) show relatively identical trends in the A-B concentration graph of Al_2O_3, TiO_2, K_2O, and P_2O_5, with all plotting in the positive segment of the graph (above zero line of the X-axis). Higher concentration of Al_2O_3, TiO_2, K_2O, and P_2O_5 in the MISS section compared to the underlying section is also shown by MKG 102 (note that the A-B value plots on the positive segment of the graph and that the trend is relatively identical to the trend of MAG 101, 102 and 103). MKG 101 has lower concentrations of Al_2O_3, TiO_2, K_2O, and P_2O_5 in the MISS section compared to the

underlying section (A-B = negative value) and has these oxides plotting on the negative segment of the same graph.

There is thus heterogeneity in concentration relationship between SiO_2 and Al_2O_3, TiO_2, K_2O, P_2O_5 between MKG 101 and MKG 102. MKG 102 is clearly congruous to the negative correlative relationship between SiO_2 and the major element oxide quartet of Al_2O_3, TiO_2, K_2O, P_2O_5 that is shown by MAG 101, 102, 103: lower SiO_2 in the MISS section (compared to the underlying section) is aligned with higher Al_2O_3, TiO_2, K_2O, and P_2O_5 (compared to the underlying section), and higher SiO_2 in the underlying section (compared to the MISS section) is aligned with lower Al_2O_3, TiO_2, K_2O, and P_2O_5 (compared to the MISS section).

Table 5.5.1: The MISS-bearing section of MAG 101, 102 and 103 each has higher concentration of Al_2O_3, TiO_2, K_2O and P_2O_5 compared to the underlying section. Note that the negative correlative relationship between these major oxides (Al_2O_3, TiO_2, K_2O and P_2O_5) and SiO_2 is homogeneously obtained with all three Magaliesberg samples (Negative SiO_2 A-B values are shown in red fonts). Negative SiO_2 values (A-B) shown in the table to espouse the negative correlative relationship with the quartet: Al_2O_3, TiO_2, K_2O and P_2O_5. SAM represents sample.

SAM	MAG 101A	MAG 101B	A-B	MAG 102A	MAG 102B	A-B	MAG 103A	MAG 103B	A-B
SiO_2	78.88	97.54	-18.66	92.6	95.4	-2.8	93.21	95.99	-2.78
Al_2O_3	8.71	1.33	7.38	5.07	2.84	2.23	4.13	1.98	2.15
TiO_2	0.31	0	0.31	0.25	0.04	0.21	0.17	0.06	0.11
K_2O	1.56	0.3	1.26	1.21	0.67	0.54	1.03	0.5	0.53
P_2O_5	0.077	0.009	0.068	0.022	0.012	0.01	0.019	0.015	0.004

It is significant to note that MKG 101 has a lower concentration of SiO_2 aligned with lower concentrations of the quartet of the oxides of the major elements (Al_2O_3, TiO_2, K_2O, and P_2O_5) in the MISS section compared to the underlying section (table 5.5).

Table 5.5.2: MKG 102 has a higher concentration of Al_2O_3, TiO_2, K_2O and P_2O_5 in the MISS section compared to the underlying section. Note that the negative correlative relationship between the quartet of the oxides of the major elements (Al_2O_3, TiO_3, K_2O and P_2O_5) and SiO_2 seen in MKG 102 is what also applies to MAG 101, 102, 103 (shown in table 5.5.1). MKG 101 has lower concentrations of SiO_2, Al_2O_3, TiO_2, K_2O and P_2O_5 in the MISS section compared to the underlying section (row completely of red fonts; negative A-B). This table is illustrational of the heterogeneity of MKG 101 and MKG 102 in correlation between SiO_2 and the quartet of Al_2O_3, TiO_2, K_2O, and P_2O_5.

SAMPLE	MKG 101A	MKG 101B	A-B	MKG 102A	MKG 102B	A-B
SiO_2	87.89	88.29	-0.4	89.79	90.53	-0.74
Al_2O_3	6.56	6.76	-0.2	5.13	4.31	0.82
TiO_2	0.2	0.34	-0.14	0.25	0.2	0.05
K_2O	1.69	1.72	-0.03	1.24	1	0.204
P_2O_5	0.085	0.149	-0.064	0.259	0.204	0.055

There are lower concentrations of CaO, Na_2O and Cr_2O_3 in the MISS-bearing sedimentary rock section of samples MKG 101 and MKG 102, when compared to the underlying sedimentary rock section (table 5.6: shown in red), with the exception of Na_2O in MKG 101 which has similar values of concentration in the MISS and underlying sections.

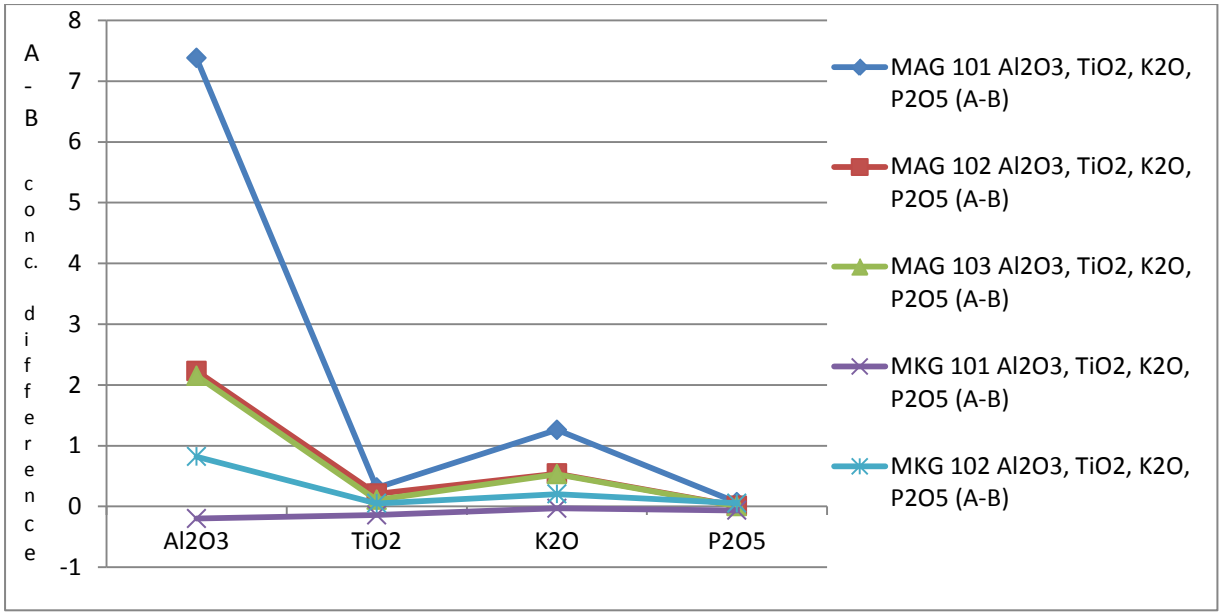

Figure 5.3: Plot presentation of data in tables 5.4 and 5.5 The analyzed Magaliesberg Formation samples (MAG 101, 102, 103) and sample MKG 102 from the Makgabeng Formation have the A-B difference in concentration of the quartet of the oxides (Al_2O_3, TiO_2, K_2O and P_2O_5) plotting on the positive segment of the graph and with a relatively identical trend. Note that the A-B concentration difference of the quartet oxides (Al_2O_3, TiO_2, K_2O and P_2O_5) plots on the negative segment of the graph for Makgabeng Formation sample MKG 101.

Table 5.6: The MISS section of Makgabeng Formation samples MKG 101 and 102 has lower concentrations of CaO, Na_2O and Cr_2O_3 compared to the underlying section of each of the samples (shown in red). The exception to this is Na_2O in MKG 101 which has the same values of concentration in the MISS and underlying sedimentary rock sections. SAM represents sample.

SAM	MKG 101A	MKG 101B	A-B	MKG 102A	MKG 102B	A-B
CaO	0.1	0.15	-0.05	0.04	0.07	-0.03
Na_2O	0.07	0.07	0	0.05	0.06	-0.01
Cr_2O_3	0.004	0.007	-0.003	0.003	0.006	-0.003

The MISS sections of each of MAG 101, 102, 103 have higher concentrations of CaO, Na_2O, and Cr_2O_3 compared to the underlying sections of the respective samples (table 5.7; figure 5.4). The only exception is CaO in MAG 103 which has the same values of concentration in the MISS and underlying sections.

Table 5.7: There are higher concentrations of CaO, Na_2O and Cr_2O_3 in the MISS sections of Magaliesberg Formation samples MAG 101, 102 and 103 compared to the underlying sections (the exception being CaO in MAG 103 which has equal concentration values in the MISS and underlying sections). SAM represents sample.

SAM	MAG 101A	MAG 101B	A-B	MAG 102A	MAG 102B	A-B	MAG 103A	MAG 103B	A-B
CaO	0.05	0.01	0.04	0.03	0.01	0.02	0.01	0.01	0
Na_2O	0.22	0.01	0.21	0.05	0.01	0.04	0.04	0.01	0.03
Cr_2O_3	0.027	0.003	0.024	0.01	0.003	0.007	0.008	0.003	0.005

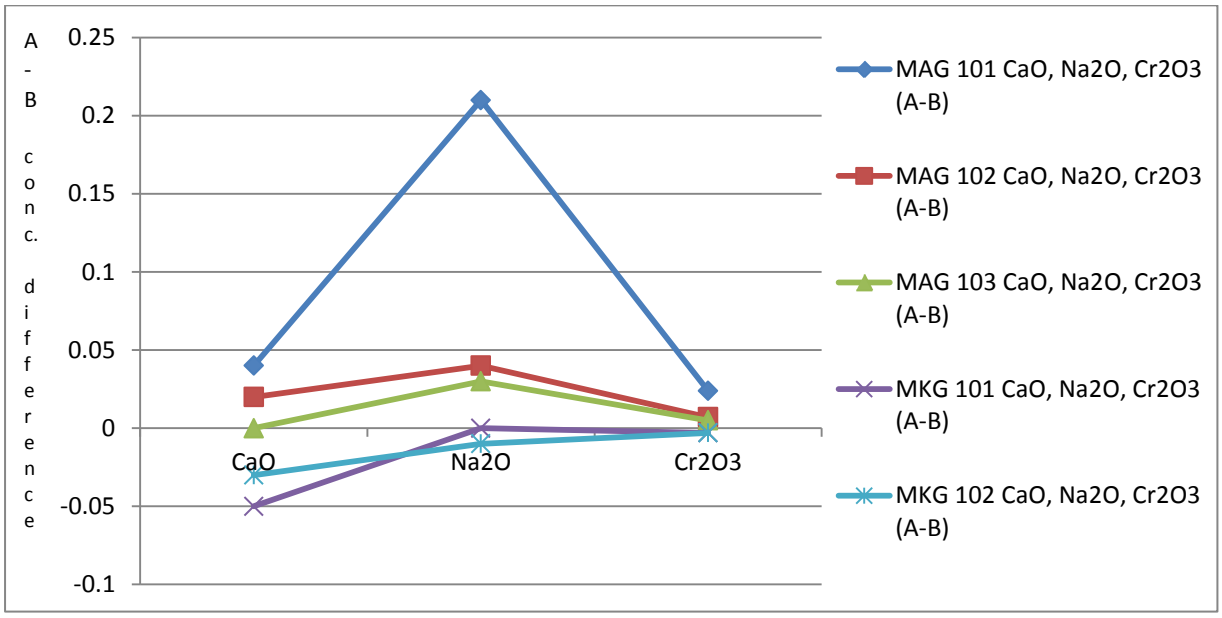

Figure 5.4: Plot of data from tables 5.6 and 5.7. It is significant to note that CaO, Na_2O and Cr_2O_3 point values of MAG 101, 102, and 103 plot on the positive segment of the graph (above zero line of the Y-axis). The exception is CaO concentration difference in MAG 103 which is zero (equal concentrations in MISS and underlying sections) with the point value plotting precisely on the zero line of the x-axis. MKG 101 and 102 have CaO, Na_2O and Cr_2O_3 plotting on the negative segments of the graph (below the zero line of the Y-axis) with the exception of Na_2O in MKG 101 which has equal concentrations in the MISS and underlying sections and is zero in concentration difference (A-B). Graph is based on A-B difference.

The concentration of MgO is homogeneous (>0.01) in samples MAG 101, 102, 103, irrespective of whether the MISS-bearing section or the underlying sedimentary rock section

are evaluated (table 5.8; figure 5.5). There are lower concentrations of MgO in the MISS section of MKG 101 and 102, compared to the underlying section (table 5.8; figure 5.5). Figure 5.5 (plotted with A-B values of table 5.8) shows MAG 101, 102, 103 plotting on the zero line of the Y-axis and MKG 101 and 102 plotting on the negative segment of the graph (below the zero line of the x-axis). Fe_2O_3 values and those for TiO_2 are discussed analogously below through use of table 5.9 and plotted on figure 5.6 showing A-B differences; similarly, table 5.10 and figure 5.7 show A-B trends for MnO and TiO_2.

Table 5.8: MKG 101 and 102 have lower concentrations of MgO in the MISS section compared to the underlying section (seen in red figures), and MAG 101, 102 and 103 have equal concentrations of MgO (<0.01) in all the samples (MISS and underlying sections).

Sample	MgO	Sample	MgO
MAG 101A	0.01	**MKG 101A**	0.33
MAG 101B	0.01	**MKG 101B**	0.39
A-B	0.00	A-B	-0.06
MAG 102A	0.01	**MKG 102A**	0.17
MAG 102B	0.01	**MKG 102B**	0.20
A-B	0.00	A-B	-0.03
MAG 103A	0.01		
MAG 103B	0.01		
A-B	0.00		

Figure 5.5: Plot of the data in table 5.8. Note that samples MAG 101, 102 and 103 are of equal concentration of MgO (<0.01) in both MISS and underlying sections, and that MKG 101 and 102 have lower concentrations of MgO in the MISS section compared to the underlying section.

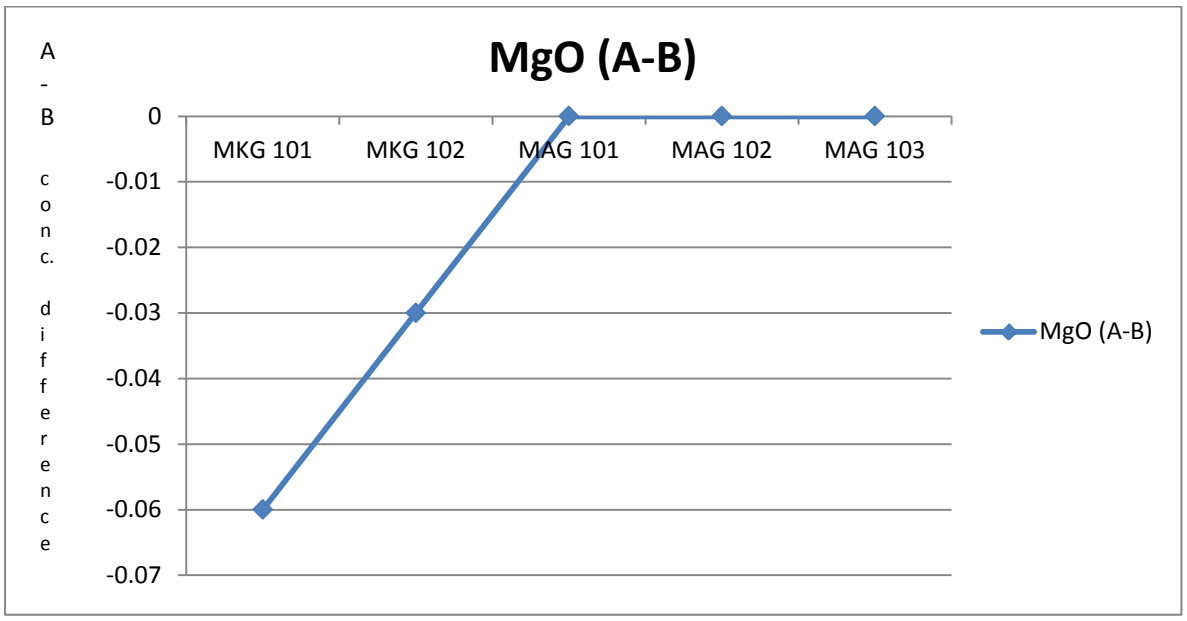

Table 5.9: Samples MAG 101 and 102 have higher concentrations of Fe_2O_3 in the MISS section compared to the underlying section. In contrast, MAG 103 has lower concentration of Fe_2O_3 in the MISS section compared to the underlying section. MKG 101 has higher concentration of Fe_2O_3 in the MISS section compared to the underlying section, and in contrast MKG 102 has lower concentration of Fe_2O_3 in the MISS section compared to the underlying section. Note that TiO_2 is added to foster illustrational relativity with the quartet of major elements (Al_2O_3, TiO_2, K_2O and P_2O_5)

SAMPLE	MAG 101 (A-B)	MAG 102 (A-B)	MAG 103 (A-B)	MKG 101 (A-B)	MKG 102 (A-B)
TiO_2	0.31	0.21	0.11	-0.14	0.05
Fe_2O_3	7.72	0.15	-0.23	1.15	-0.47

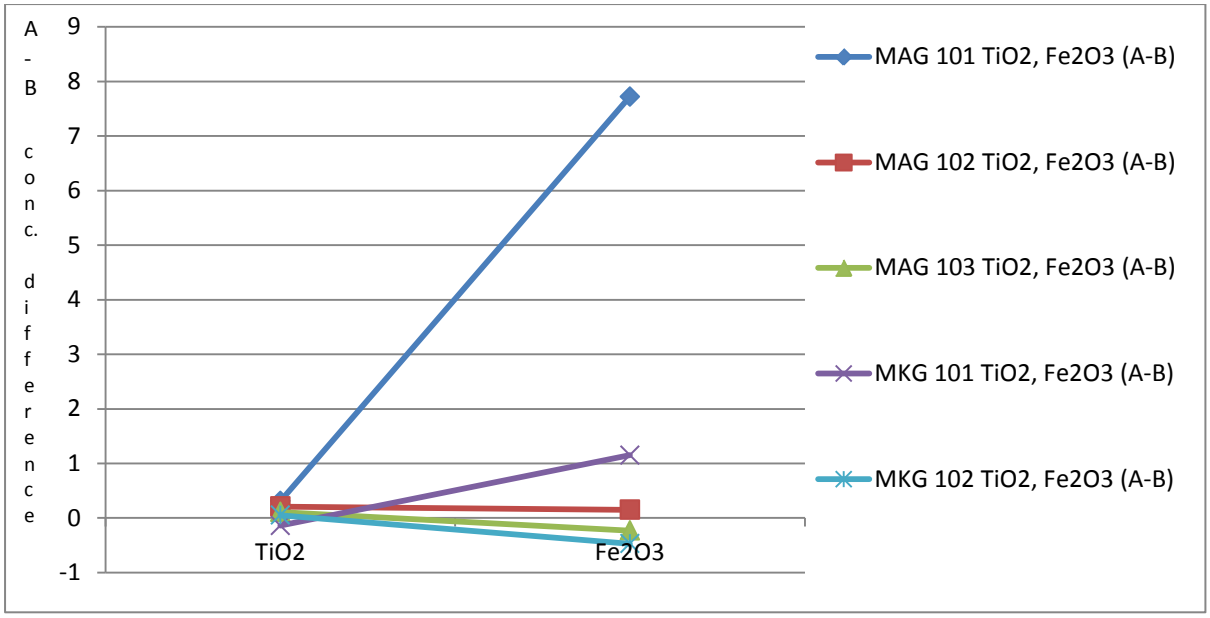

Figure 5.6: Plot showing that MAG 101 and 102 have higher concentrations of Fe_2O_3 in the MISS section compared to the underlying section and MAG 103 has lower concentration of Fe_2O_3 in the MISS section compared to the underlying section. MKG 101 has higher concentration of Fe_2O_3 in the MISS section compared to the underlying section and MKG 102 has lower concentration of Fe_2O_3 in the MISS section compared to the underlying section. Plot is based on A-B concentration difference.

Table 5.10: MAG 101 has lower concentration of MnO in the MISS section compared to the underlying section; MAG 102 has higher concentration of MnO in the MISS section compared to the underlying section and MAG 103 has MnO of equal concentration in the two sections (A and B).

Sample	**MAG 101 (A-B)**	**MAG 102 (A-B)**	**MAG 103 (A-B)**	**MKG 101 (A-B)**	**MKG 102 (A-B)**
TiO_2	0.31	0.21	0.11	-0.14	0.05
MnO	-0.004	0.001	0	0.003	-0.002

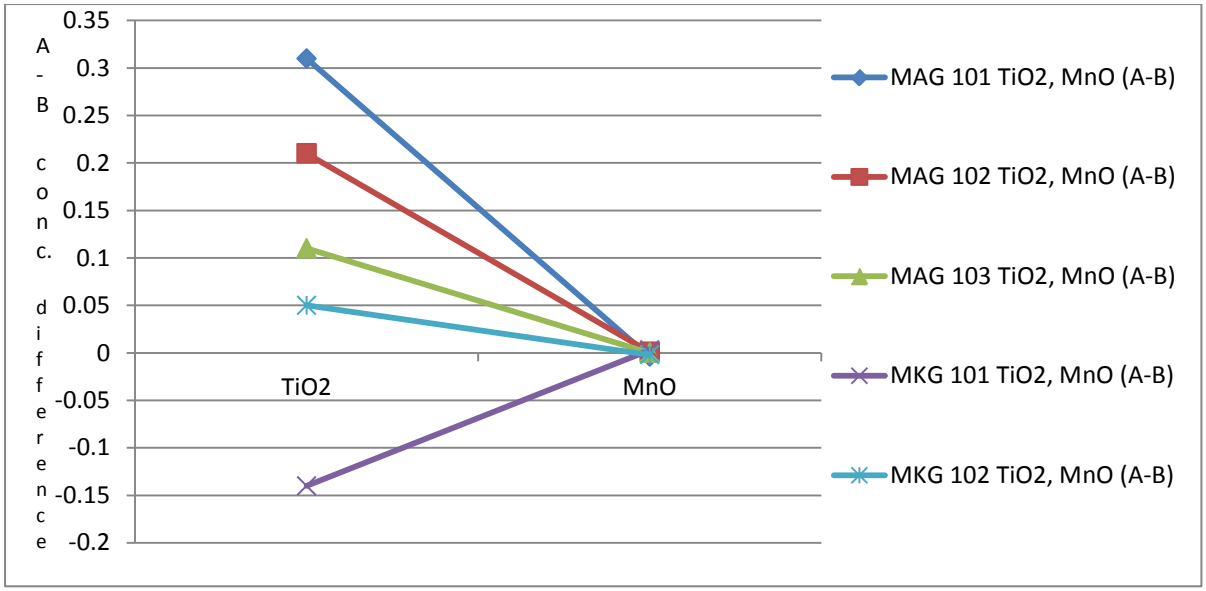

Figure 5.7: Plot of TiO_2 and MnO concentrations of the five samples. Note the relatively homogeneous trends of MAG 101, 102, and 103; it seems that the higher the concentration of TiO2, the lower the concentration of MnO. Also, MAG 102 is of correlative trend. It is significant to note that the opposite pertains to MKG 101 as low TiO_2 is aligned with higher MnO.

5.1.2 Trace elements

Primary data treatment was effected by cleaning of the trace element results (trace elements results are shown in table 5.2) before the preparation of a primary analytical data table for each individual sample (these data shown in tables 5.11.1 – 5.11.5). This cleaning of the results was done with the set objective of comparison of the MISS-bearing section of a particular sample to the underlying sedimentary rock section and consequently to compare the geochemistry of the samples (MISS sections; A, and underlying sections; B) from the two Formations. Some trace elements (Bi, Br, Mo, Se, Ti, W, Cs) were removed because they show uniform concentrations in both Magaliesberg Formation (MAG 101, 102, 103) and Makgabeng Formation samples (MKG 101, 102) irrespective of A or B. Samples with > (greater than) preceding a numeral in tables 5.11.1 – 5.11.5 were confined to the basic numerical value.

Table 5.11.1: Primary trace element analytical data table of sample MAG 101 (Magaliesberg Formation)

MAG 101	A	B	A-B	A/B	B/A	(A-B/A)%	MEAN	M.D
As	4	4	0	1	1	0	4	0
Ba	163	24	139	6.792	0.147	85.276	93.5	69.5
Ce	32	20	12	1.6	0.625	37.5	26	6
Co	4	1.3	2.7	3.077	0.325	67.5	2.65	1.35
Cr	159	29	130	5.483	0.182	81.761	94	65
Cu	7.5	6.6	0.9	1.136	0.88	12	7.05	0.45
Ga	13	1.7	11.3	7.647	0.131	86.923	7.35	5.65
Ge	1.2	1.8	-0.6	0.667	1.5	-50	1.5	0.3
Hf	7.1	3	4.1	2.367	0.423	57.746	5.05	2.05
La	26	28	-2	0.929	1.077	-7.692	27	1
Nb	7.6	3.5	4.1	2.171	0.461	53.947	5.55	2.05
Nd	16	11	5	1.455	0.688	31.25	13.5	2.5
Ni	15	3.5	11.5	4.286	0.233	76.667	9.25	5.75
Pb	8.3	4	4.3	2.075	0.482	51.807	6.15	2.15
Rb	55	9.9	45.1	5.556	0.18	82	32.45	22.55
Sc	17	3	14	5.667	0.176	82.353	10	7
Sm	10	10	0	1	1	0	10	0
Sr	111	18	93	6.167	0.162	83.784	64.5	46.5
Ta	2	2.5	-0.5	0.8	1.25	-25	2.25	0.25
Th	10	3	7	3.333	0.3	70	6.5	3.5
U	3.3	2	1.3	1.65	0.606	39.394	2.65	0.65
V	54	9.7	44.3	5.567	0.18	82.037	31.85	22.15
Y	17	5.9	11.1	2.881	0.347	65.294	11.45	5.55
Yb	3	3	0	1	1	0	3	0
Zn	24	3	21	8	0.125	87.5	13.5	10.5
Zr	190	51	139	3.725	0.268	73.158	120.5	69.5

Table 5.11.2: Primary trace element analytical data table of sample MAG 102 (Magaliesberg Formation)

MAG 102	A	B	A-B	A/B	B/A	(A-B/A)%	MEAN	M.D
As	4.1	4	0.1	1.025	0.976	2.439	4.05	0.05
Ba	82	39	43	2.103	0.476	52.439	60.5	21.5
Ce	69	29	40	2.379	0.42	57.971	49	20
Co	2	1.3	0.7	1.538	0.65	35	1.65	0.35
Cr	62	28	34	2.214	0.452	54.839	45	17
Cu	8.2	8	0.2	1.025	0.976	2.439	8.1	0.1
Ga	6	2.3	3.7	2.609	0.383	61.667	4.15	1.85
Ge	1.3	1.6	-0.3	0.813	1.231	-23.077	1.45	0.15
Hf	7.5	4.2	3.3	1.786	0.56	44	5.85	1.65
La	37	19	18	1.947	0.514	48.649	28	9
Nb	7.7	4.5	3.2	1.711	0.584	41.558	6.1	1.6
Nd	21	10	11	2.1	0.476	52.381	15.5	5.5
Ni	4.1	4.7	-0.6	0.872	1.146	-14.634	4.4	0.3
Pb	6.8	2.2	4.6	3.091	0.324	67.647	4.5	2.3
Rb	43	24	19	1.792	0.558	44.186	33.5	9.5
Sc	4.3	3	1.7	1.567	0.638	36.17	3.85	0.85
Sm	10	10	0	1	1	0	10	0
Sr	36	17	19	2.118	0.472	52.778	26.5	9.5
Ta	3.7	2.8	0.9	1.321	0.757	24.324	3.25	0.757
Th	10	3.5	6.5	2.857	0.35	65	6.75	3.25
U	3.4	2	1.4	1.7	0.588	41.176	2.7	0.7
V	68	19	49	3.579	0.279	72.059	43.5	24.5
Y	17	7.2	9.8	2.361	0.424	57.647	12.1	4.9
Yb	3	3	0	1	1	0	0	10
Zn	7.7	4.9	2.8	1.571	0.636	36.364	6.3	1.4
Zr	233	107	126	2.178	0.459	54.077	170	63

Table 5.11.3: Primary trace element analytical data table of sample MAG 103 (Makgabeng Formation)

MAG 103	A	B	(A-B)	(A/B)	B/A	(A-B/A)%	MEAN	M.D
As	4	4	0	1	1	0	4	0
Ba	85	24	61	3.542	0.282	71.765	54.5	30.5
Ce	38	17	21	2.235	0.447	55.263	27.5	10.5
Co	1	1	0	1.000	1,000	0.000	1	0
Cr	48	18	30	2.667	0.375	62.500	33	15
Cu	8	8.4	-0,4	0.952	1,050	-5,000	8,2	0,2
Ga	5.1	1.5	3.6	3.400	0.294	70.588	3,3	1,8
Ge	1.5	1.3	0.2	1.154	0.867	13.333	1,4	0,1
Hf	5.8	3.5	2.3	1.657	0,603	39,655	4,65	1,15
La	28	21	7	1.333	0.750	25.000	24.5	3.5
Nb	6.1	4	2.1	1,525	0,656	34,426	5,05	1,05
Nd	15	10	5	1.500	0.667	33.333	12.5	2.5
Ni	3.5	3.4	0.1	1.029	0.971	2.857	3.45	0.05
Pb	5.7	2.4	3.3	2.375	0.421	57.895	4.05	1.65
Rb	33	17	16	1.941	0.515	48.485	25	8
Sc	3	3	0	1.000	1.000	0.000	3	0
Sm	10	10	0	1.000	1.000	0.000	10	0
Sr	33	11	22	3.000	0.333	66.667	22	11
Ta	3.9	2	1,9	1.950	0.513	48.718	2.95	0.95
Th	7.4	3	4,4	2.467	0.405	59.459	5.2	2.2
U	2.6	2	0.6	1.300	0.769	23.077	2.3	0,3
V	53	16	37	3.313	0.302	69.811	34.5	18.5
Y	13	6.1	6.9	2.131	0.469	53.077	9.55	3.45
Yb	3	3	0	1.000	1.000	0.000	3	0
Zn	12	8.1	3.9	1.481	0.675	32.500	10.05	1.95
Zr	167	72	95	2.319	0.431	56.886	119.5	47.5

Table 5.11.4: Primary trace element analytical data table of sample MKG 101 (Makgabeng Formation)

MKG 101	A	B	A-B	A/B	B/A	(A-B/A)%	MEAN	M.D
As	4	5.3	-1.3	0.755	1.325	32.5	4.65	0.65
Ba	586	578	8	1.014	0.986	1.365	582	4
Ce	28	281	-253	0.1	10.036	-903.571	154.4	126.5
Co	3.3	4.7	-1.4	0.702	1.424	-42.424	4	0.7
Cr	27	44	-17	0.614	1.63	-62.963	35.5	8.5
Cu	7.2	6.3	0.9	1.143	0.875	12.5	6.75	0.45
Ga	7.3	6.4	0.9	1.141	0.877	12.329	6.85	0.45
Ge	1.3	1	0.3	1.3	0.769	23.077	1.15	0.15
Hf	5.9	7.4	-1.5	0.797	1.254	-25.424	6.65	0.75
La	29	146	-117	0.199	5.034	-403.448	87.5	58.5
Nb	6.3	9	-2.7	0.7	1.429	-42.857	7.65	1.35
Nd	16	116	-100	0.138	7.25	-625	66	50
Ni	6.4	8.8	-2.4	0.727	1.375	-37.5	7.6	1.375
Pb	7	3.7	3.3	1.892	0.529	47.143	5.35	1.65
Rb	53	55	-2	0.964	1.038	-3.774	54	1
Sc	3	3	0	1	1	0	3	0
Sm	10	18	-8	0.556	1.8	-80	14	4
Sr	17	17	0	1	1	0	17	0
Ta	2	2	0	1	1	0	2	0
Th	6.3	8.9	-2.6	0.708	1.413	-41.27	7.6	1.3
U	2	2	0	1	1	0	2	0
V	19	24	-5	0.792	1.263	-26.316	21.5	2.5
Y	13	23	-10	0.565	1.769	-76.923	18	5
Yb	3	3.4	-0.4	0.882	1.133	-13.333	3.2	0.2
Zn	8.7	11	-2.3	0.791	1.264	-26.437	9.85	1.15
Zr	157	234	-77	0.671	1.49	-49.045	195.5	38.5

Table 5.11.5: Primary trace element analytical data table of sample MKG 102 (Magaliesberg Formation)

MKG 102	A	B	A-B	A/B	B/A	(A-B/A)%	MEAN	M.D
As	5.2	4	1.2	1.3	0.769	23.077	4.6	0.6
Ba	483	383	100	1.261	0.793	20.704	433	50
Ce	41	44	-3	0.932	1.073	-7.317	42.5	1.5
Co	3.3	4	-0.7	0.825	1.212	-21.212	3.65	0.35
Cr	27	32	-5	0.844	1.185	-18.519	29.5	2.5
Cu	8.7	8.4	0.3	1.036	0.966	3.448	8.55	0.15
Ga	5.4	5.4	0	1	1	0	5.4	0
Ge	1.3	1	0.3	1.3	0.769	23.077	1.15	0.15
Hf	8.9	8.6	0.3	1.035	0.966	3.371	8.75	0.15
La	41	37	4	1.108	0.902	9.756	39	2
Nb	6.1	6.3	-0.2	0.968	1.033	-3.279	6.2	0.1
Nd	24	24	0	1	1	0	24	0
Ni	7.1	7.2	-0.1	0.986	1.014	-1.408	7.15	0.05
Pb	5.1	6.2	-1.1	0.823	1.216	-21.569	5.65	0.55
Rb	42	34	8	1.235	0.81	19.048	38	4
Sc	3	3	0	1	1	0	3	0
Sm	10	10	0	1	1	0	10	0
Sr	14	15	-1	0.933	1.071	-7.143	14.5	0.5
Ta	2	2.3	-0.3	0.87	1.15	-15	2.15	0.15
Th	5.5	7.1	-1.6	0.775	1.291	-29.091	6.3	0.8
U	2	2	0	1	1	0	2	0
V	17	19	-2	0.895	1.118	-11.765	18	1
Y	20	25	-5	0.8	1.25	-25	22.5	2.5
Yb	3	3	0	1	1	0	3	0
Zn	5.7	7.2	-1.5	0.792	1.263	-26.316	6.45	0.75
Zr	146	220	-74	0.664	1.507	-50.685	183	37

In all the samples of the two studied formations (MAG 101, 102, 103; MKG 101, 102), the concentration of Ba is higher in the MISS section compared to the underlying section. Overall (MISS-bearing and underlying sedimentary rock sections), there are higher concentrations of Ba in the Makgabeng Formation samples compared to the Magaliesberg Formation samples. As shown in red colour in table 5.12, the MISS section of the Makgabeng Formation samples (MKG 101A, 102A) have lower concentrations in most trace elements compared to the underlying section. The MISS sections of Magaliesberg Formation samples (MAG 101, 102, 103) have higher concentration of most trace elements compared to the underlying section (see table 5.12). A-B difference in concentration of trace elements for samples MAG 101, MAG 102, MAG 103; MKG 101, MKG 102, is shown side by side in table 5.12 (note the manifold red colour in the MKG 101 and 102 columns, denoting lower concentration of most trace elements in the MISS section compared to the underlying substrate sediment section).

Table 5.13, based on A-B difference in concentration, shows trace elements Ce, Cr, Nb, Th, V, Y, Zn, Zr that are uniformly of higher concentration in the MISS-bearing sedimentary rock section of each of the analysed samples from the Magaliesberg Formation (MAG 101, 102, and 103) compared to its underlying sedimentary rock section. The exact same trace elements are, conversely, of lower concentration in the MISS section of each of the Makgabeng Formation samples (MKG 101, 102) compared to the underlying section of each of those two particular sample (table 5.13). Figure 5.8 is a plot of data from table 5.13. Note that Ce, Cr, Nb, Th, V, Y, Zn, Zr all plot on the positive segment of the graph for the analysed Magaliesberg Formation samples (MAG 101, 102, 103) and that Makgabeng Formation samples (MKG 101 and 102) have these trace elements plotting on the negative segment of the graph. It is significant to note that the A-B concentration difference of MKG 101 is quite a bit lower in Ce, Cr, Nb, Th, V, Y, Zn, Zr compared to the A-B concentration difference of MKG 102 in Ce, Cr, Nb, Th, V, Y, Zn, Zr (possibly reflecting enrichment of the quartet of major elements - Al_2O_3, TiO_2, K_2O and P_2O_5 - in the MISS section?).

There is a need for grouping of these trace elements in batches of confined range as there is extreme range in the low and high A-B differences in concentrations, which blurred the clarity of the plot in figure 5.8. The trace elements Ce, Cr, V, Y, and Zr have especially high A-B differences in the Magaliesberg Formation analyzed samples and very low A-B differences in the Makgabeng Formation analyzed samples. These are shown in table 5.14

and plotted in figure 5.9. The results show Ce: MAG 101 = 12, MAG 102 = 40, MAG 103 = 21, and MKG 101 = -253, MKG 102 = -3 (Cr, V, Y, and Zr are also shown in the same table to understand the extremity of the A-B difference in concentration). Table 5.15 shows Nb, Th and Zn (based on A-B difference in concentration) and this is further illustrated in figure 5.10 where the plot is based on the relatively confined A-B difference in concentration of these trace elements.

Table 5.12: A-B parameter is of geochemical-statistical significance and is thus utilized as being effective in side-by-side comparison of the difference in trace element concentration of the MISS section compared to the underlying section of each sample, and for all the analyzed samples. Note the manifold red fonts and manifold zero values in the two columns on the right (MKG 101, 102) and the lack of fonts in red and the few zero values on the three columns on the left (MAG 101, 102, 103). The MISS section (A) of each of the Magaliesberg Formation samples has higher concentration of most trace elements compared to its underlying section (B). The MISS section (A) of the Makgabeng Formation samples has lower concentrations of most trace elements compared to the underlying section (B). (Note that Bi, Br, Mo, Se, Ti, W, are not included).

SAMPLE	MAG 101 (A-B)	MAG 102 (A-B)	MAG 103 (A-B)	MKG 101 (A-B)	MKG 102 (A-B)
As	0	0.1	0	-1.3	1.2
Ba	139	43	61	8	100
Ce	12	40	21	-253	-3
Co	2.7	0.7	0	-1.4	-0.7
Cr	130	34	30	-17	-5
Cu	0.9	0.2	-0.4	0.9	0.3
Ga	11.3	3.7	3.6	0.9	0
Ge	-0.6	-0.3	0.2	0.3	0.3
Hf	4.1	3.3	2.3	-1.5	0.3
La	-2	18	7	-117	4
Nb	4.1	3.2	2.1	-2.7	-0.2
Nd	5	11	5	-100	0
Ni	11.5	-0.6	0.1	-2.4	-0.1
Pb	4.3	4.6	3.3	3.3	-1.1
Rb	45.1	19	16	-2	8
Sc	14	1.7	0	0	0
Sm	0	0	0	-8	0
Sr	93	19	22	0	-1
Ta	-0.5	0.9	1.9	0	-0.3
Th	7	6.5	4.4	-2.6	-1.6
U	1.3	1.4	0.6	0	0
V	44.3	49	37	-5	-2
Y	11.1	9.8	6.9	-10	-5
Yb	0	0	0	-0.4	0
Zn	21	2.8	3.9	-2.3	-1.5
Zr	139	126	95	-77	-74

Table 5.13: MAG 101, 102, 103 each have higher concentrations of Ce, Cr, Nb, Th, V, Y, Zn, Zr (A-B) in the MISS section compared to the underlying section of each of the samples. MKG 101, 102 have lower concentrations of Ce, Cr, Nb, Th, V, Y, Zn, and Zr in the MISS section compared to the underlying section. It is important to note that MKG 101 has lower concentration differences (A-B) of these elements compared to the concentration differences (A-B) of MKG 102. Table is based on A-B concentration difference.

SAMPLE	MAG 101	MAG 102	MAG 103	MKG101	MKG 102
Ce	12	40	21	-253	-3
Cr	130	34	30	-17	-5
Nb	4.1	3.2	2.1	-2.7	-0.2
Th	7	6.5	4.4	-2.6	-1.6
V	44.3	49	37	-5	-2
Y	11.1	9.8	6.9	-10	-5
Zn	21	2.8	3.9	-2.3	-1.5
Zr	139	126	95	-77	-74

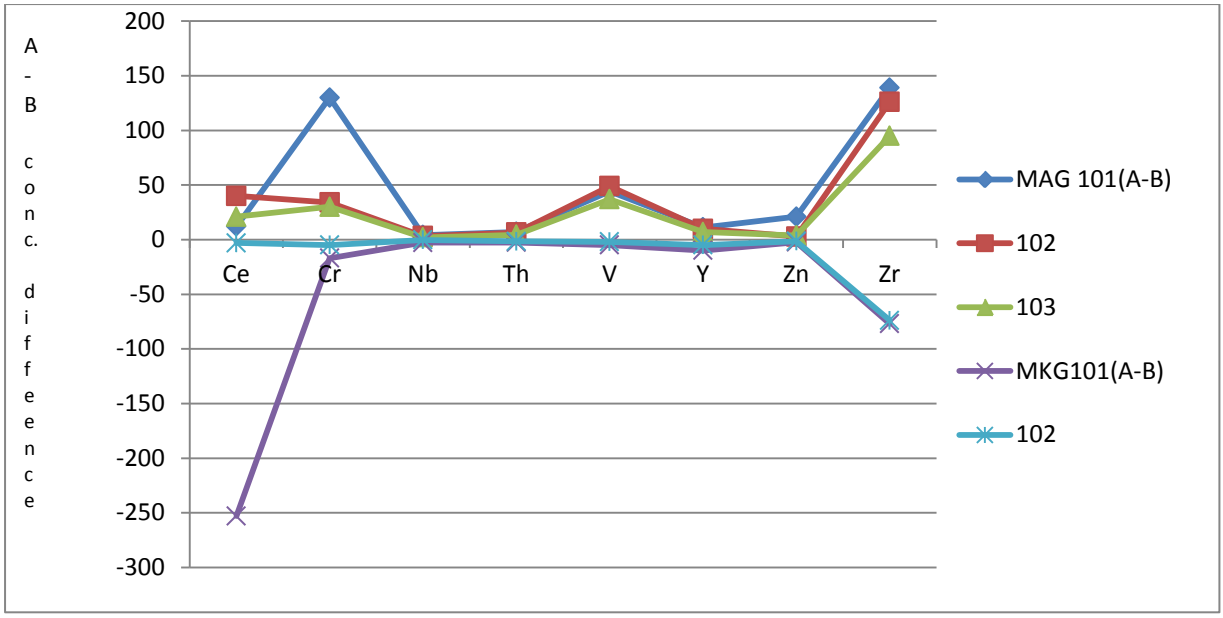

Figure 5.8: Plot showing the higher concentration of the MISS-bearing section of each of the Magaliesberg Formation samples (MAG 101, 102 and 103) in Ce, Cr, Nb, Th, V, Y, Zn, Zr compared to the underlying sediment section (Note that MAG 101, 102 and 103 have the points of these elements plotting in the positive segment of the graph, above the zero line of the Y-axis). The lower concentration of Ce, Cr, Nb, Th , V, Y, Zn, Zr in the MISS sections of samples MKG 101, 102 compared to the underlying section is also shown in the same graph. Note that the points of these trace elements plot on the negative segment of the graph for MKG 101 and 102. Comparatively, MKG 101 has lower difference in concentration (A-B) of these elements compared to difference in concentration (A-B) of MKG 102.

Table 5.14: Ce, Cr, V, Y, and Zr concentration difference (A-B) of each of samples MAG 101, 102 and 103 is very high (positive value) compared to the A-B concentration difference of each of samples MKG 101, and 102 (negative value). It is significant to note that MKG 101 has lower concentration difference (A-B) in these trace elements compared to that (A-B) of MKG 102. Table is based on A-B concentration difference.

SAMPLE	MAG 101	MAG 102	MAG 103	MKG 101	MKG 102
Ce	12	40	21	-253	-3
Cr	130	34	30	-17	-5
V	44.3	49	37	-5	-2
Y	11.1	9.8	6.9	-10	-5
Zr	139	126	95	-77	-74

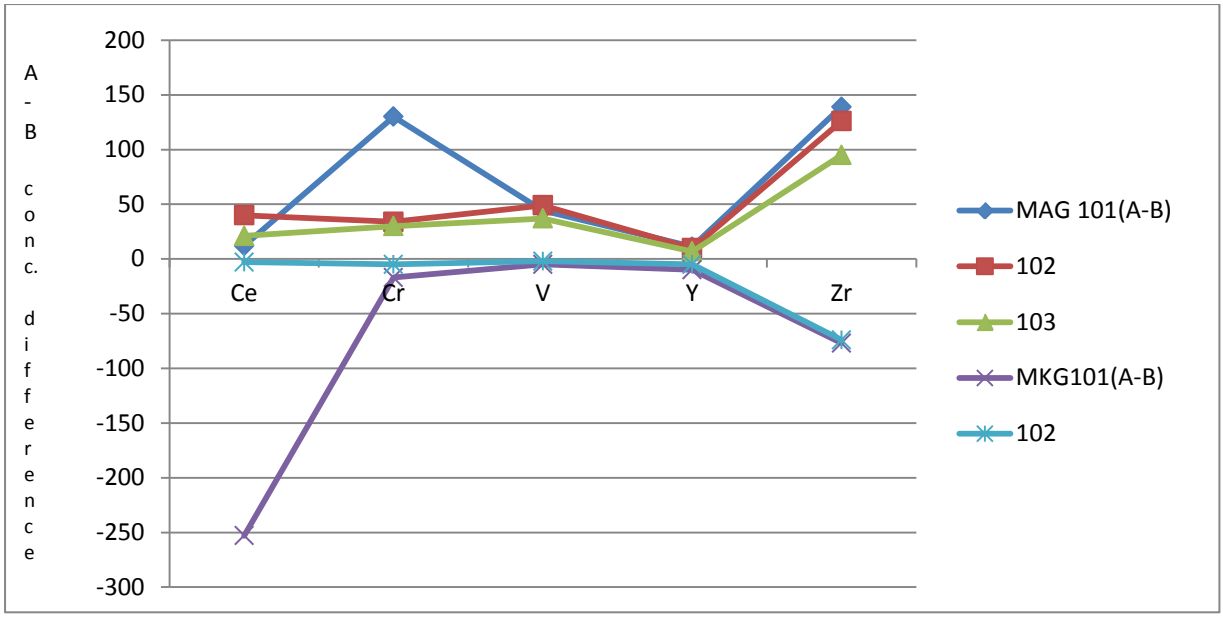

Figure 5.9: There is higher concentration of Ce, Cr, V, Y and Zr in the MISS section of each of MAG 101, 102 and 103 compared to the underlying section, and lower concentration of these elements in the MISS section compared to the underlying section of MKG 101 and 102. Comparatively, MKG 101 has lower concentration differences (A-B) in Ce, Cr, V, Y and Zr compared to A-B of MKG 102. Plot is based on A-B concentration difference.

Table 5.15: Magaliesberg Formation samples show analogous higher concentration of the MISS-bearing section in Nb, Th, and Zn compared to the underlying sediment section. Makgabeng Formation samples show homogeneous lower concentration of Nb, Th and Zn in the MISS-bearing section of the sample compared to the underlying sediment section.

SAMPLE	MAG 101	MAG 102	MAG 103	MKG 101	MKG 102
Nb	4.1	3.2	2.1	-2.7	-0.2
Th	7	6.5	4.4	-2.6	-1.6
Zn	21	2.8	3.9	-2.3	-1.5

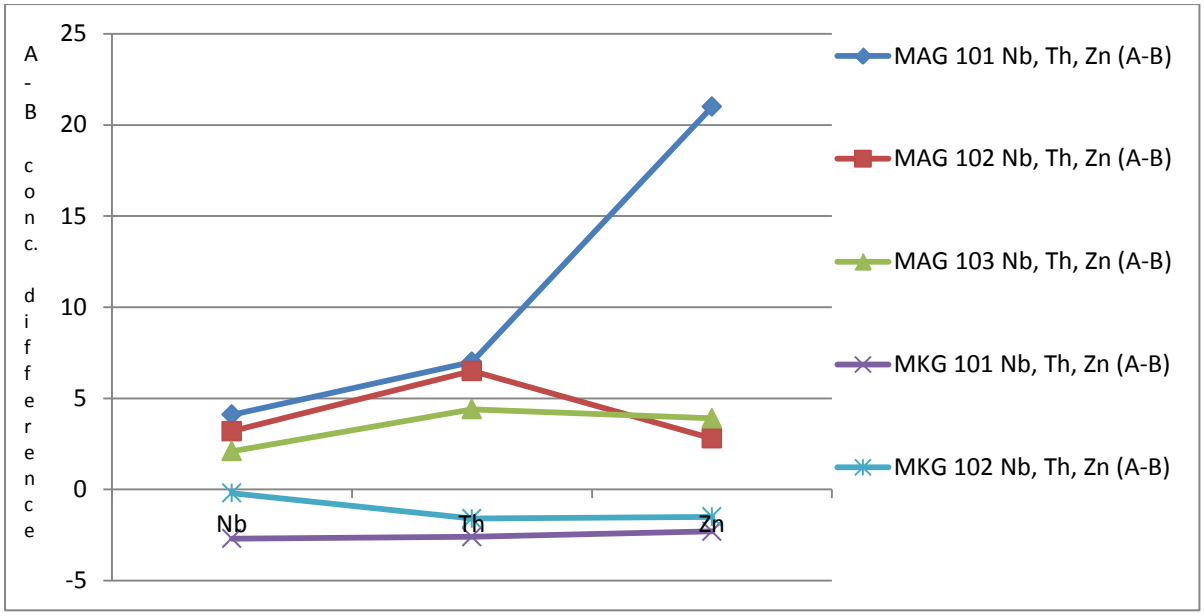

Figure 5.10: Plot of data shown in table 5.15. MAG 101, 102, and 103 each has higher A-B concentration difference in Nb, Th, Zn, compared to A-B concentration difference of samples MKG 101 and 102. Comparatively, MKG 101 has lower concentration difference (A-B) of these trace elements compared to A-B of MKG 102.

The relationship between Nd, Sr, and U for all the samples is shown in table 5.16 and figure 5.11**.** The MISS bearing section of Makgabeng Formation sample MKG 101 is of lower concentration of Nd compared to the underlying sediment section, and the MISS bearing section and the underlying sediment section of MKG 102 are of equal concentration of Nd. Sr is of equal concentration in the MISS bearing section of MKG 101 compared to the underlying section, while MKG 102 has lower concentration of Sr in the MISS bearing section of the sample compared to the underlying sediment section. MKG 101 and MKG 102 have U of equal concentration in their respective MISS bearing sections compared to the underlying sediment sections. |For the Magaliesberg Formation, samples MAG 101, 102 and 103 homogeneously show higher concentrations of Nd, Sr, and U in each of the MISS-bearing sections compared to their respective underlying sections.

Table 5.16: MAG 101, 102 and 103 homogeneously show higher concentrations of Nd, Sr, and U in each of the MISS-bearing sections compared to their respective underlying sections. MKG 101 has very low A-B difference in concentration compared to MKG 102. MKG 102 has lower concentration of Sr in the MISS section compared to the underlying section and MKG 101 has equal concentration of Sr in the MISS and underlying sections. Both MKG 101 and 102 have equal concentrations of U in the MISS and underlying sections.

SAMPLE	MAG 101	MAG 102	MAG 103	MKG 101	MKG 102
Nd	5	11	5	-100	0
Sr	93	19	22	0	-1
U	1.3	1.4	0.6	0	0

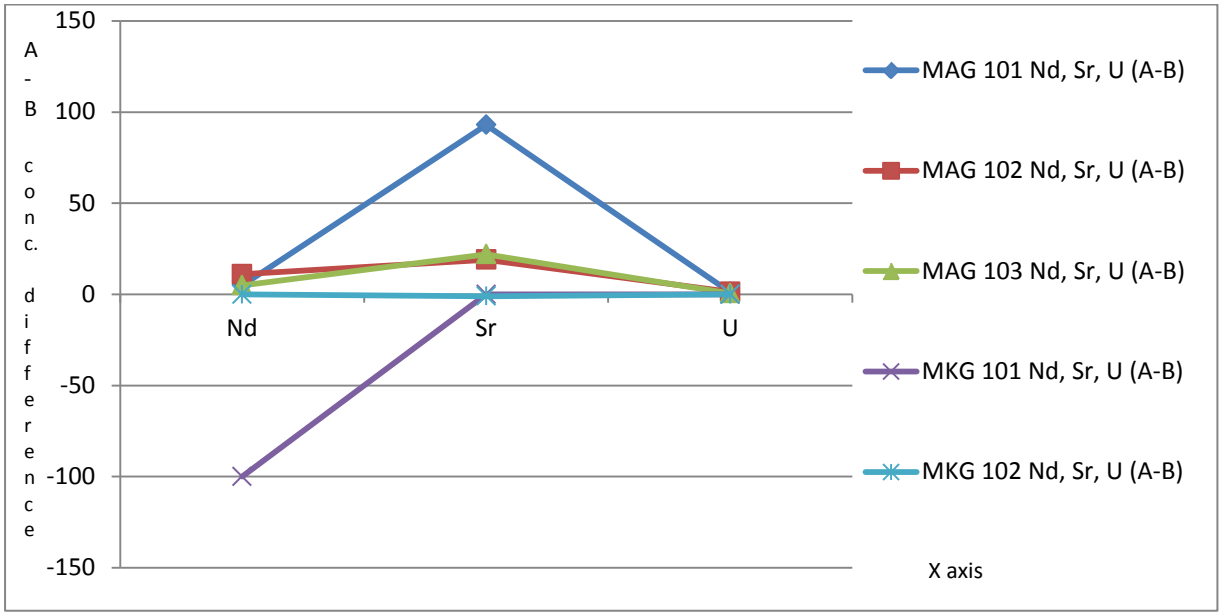

Figure 5.11: Magaliesberg Formation samples MAG 101, 102, and 103 each has higher concentration difference (A-B) of Nd, Sr and U compared to Makgabeng Formation samples MKG 101 and 102.

The MISS sections of each of MAG 101, 102, 103 have higher concentrations of Co, Ga and Pb, compared to the MISS sections of each of MKG 101 and 102; the exception is Pb which has the same concentrations in MAG 103 and MKG 101 (shown in table 5.17 and illustrated by figure 5.12).

Table 5.17: The MISS sections of each of MAG 101, 102, 103 have higher concentrations of Co, Ga and Pb, compared to the MISS sections of each of MKG 101 and 102. The exception is Pb which has the same concentrations in MAG 103 and MKG 101.

SAMPLE	MAG 101	MAG 102	MAG 103	MKG 101	MKG 102
Co	2.7	0.7	0	-1.4	-0.7
Ga	11.3	3.7	3.6	0.9	0
Pb	4.3	4.6	3.3	3.3	-1.1

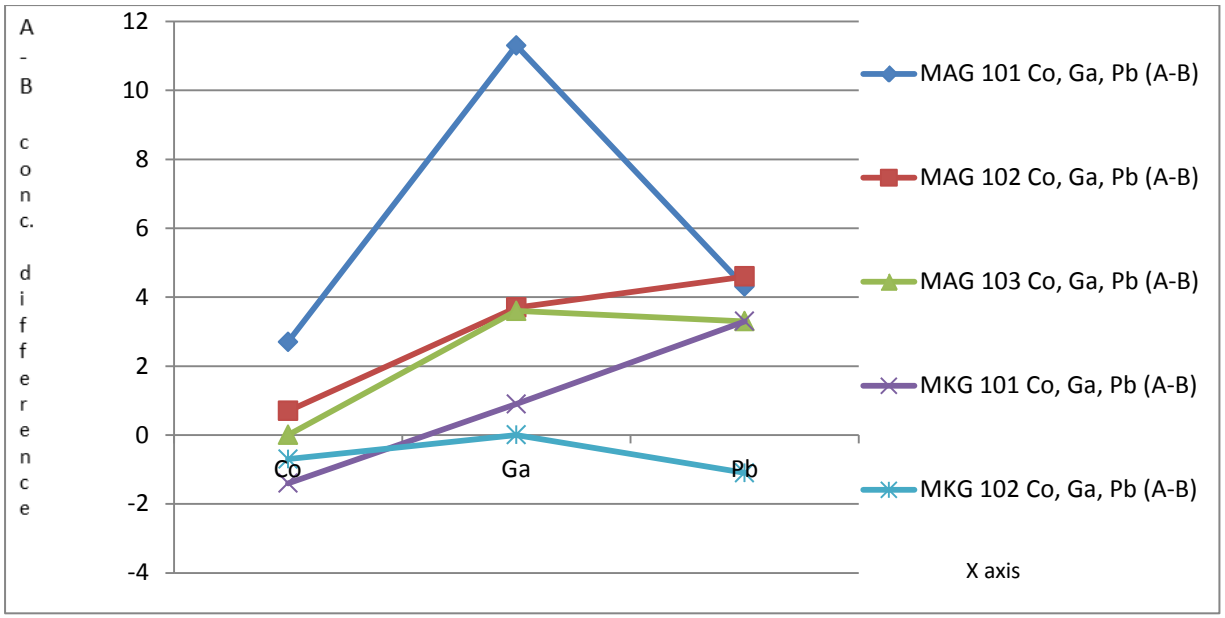

Figure 5.12: Plot showing that Magaliesberg Formation samples MAG 101, 102, and 103 have higher concentration differences (A-B) of Co, Ga and Pb compared to the concentration differences (A-B) of Makgabeng Formation samples MKG 101 and 102.

There is higher concentration of Hf and Rb in the MISS section of each of the analyzed Magaliesberg Formation samples and MKG 102 (Makgabeng Formation) compared to the underlying section (reflecting the behaviour of the quartet oxides?), while MKG 101 (Makgabeng Formation) has lower concentration of Hf and Rb in the MISS bearing section compared to the underlying sediment section (table 5.18; illustrated by a plot in figure 5.13).

Table 5.18: MAG 101, 102 and 103 and MKG 102 have high concentrations of Hf and Rb in the MISS-bearing section compared to the underlying section. MKG 101 has lower concentration of Hf and Rb in the MISS-bearing section compared to the underlying section. Table is based on A-B concentration difference.

SAMPLE	MAG 101	MAG 102	MAG 103	MKG 101	MKG 102
Hf	4.1	3.3	2.3	-1.5	0.3
Rb	45.1	19	16	-2	8

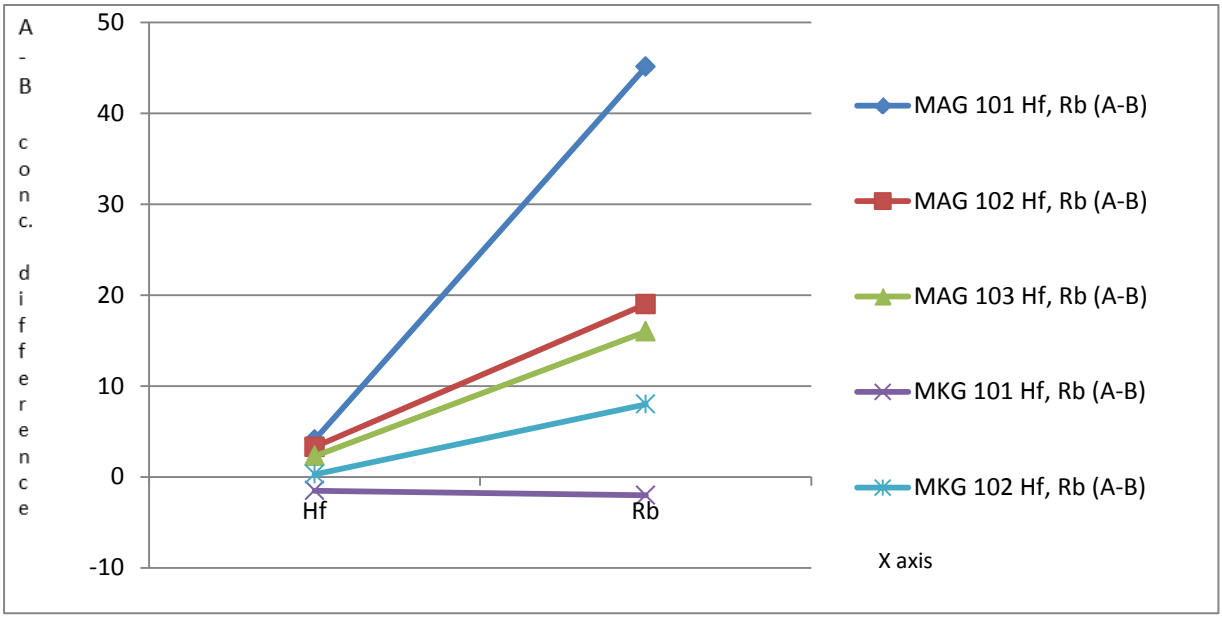

Figure 5.13: The MISS section of each of Magaliesberg Formation samples MAG 101, 102, and 103 has higher concentration of Hf and Rb compared to its underlying section. Makgabeng Formation sample MKG 102 also has higher concentration of Hf and Rb in the MISS section compared to the underlying section. MKG 101 has lower concentrations of Hf and Rb in the MISS section compared to the underlying section.

5.3 XRD RESULTS

All the samples show high quartz content compared to average sandstone.

Table 5.19: XRD Quantitative results for samples from the Magaliesberg (MAG 101, 102, 103) and Makgabeng (MKG 101 and 102) Formations, in each case for MISS-bearing (A) and substrate (B) sedimentary sections.

MAG 101A	**weight %**	**3 σ error**	**MAG 101B**	**weight %**	**3 σ error**	**MAG 102B**	**weight %**	**3 σ error**
Kaolinite	3.93	0.66	**Muscovite**	2.25	0.33	**Muscovite**	2.84	0.36
Muscovite	12.66	0.57	**Quartz**	97.75	0.33	**Quartz**	97.16	0.36
Quartz	81.69	0.78						
Rutile	1.72	0.22						
MAG 102A	**weight %**	**3 σ error**	**MAG 103A**	**weight %**	**3 σ error**	**MAG 103B**	**weight %**	**3 σ error**
Muscovite	7.06	0.3	**Muscovite**	7.44	0.33	**Hematite**	0.65	0.18
Quartz	92.94	0.3	**Quartz**	92.56	0.33	**Muscovite**	2.02	0.33
						Quartz	97.33	0.39
MKG 101A	**weight %**	**3 σ error**	**MKG 101B**	**weight %**	**3 σ error**	**MKG 102A**	**weight %**	**3 σ error**
Hematite	1.71	0.14	**Muscovite**	9.24	0.42	**Hematite**	1.58	0.13
Muscovite	7.21	0.42	**Quartz**	90.76	0.42	**Muscovite**	5.19	0.39
Quartz	91.08	0.45				**Quartz**	93.23	0.42
MKG 102B	**weight %**	**3 σ error**						
Hematite	1.85	0.17						
Muscovite	4.85	0.36						
Quartz	93.3	0.39						

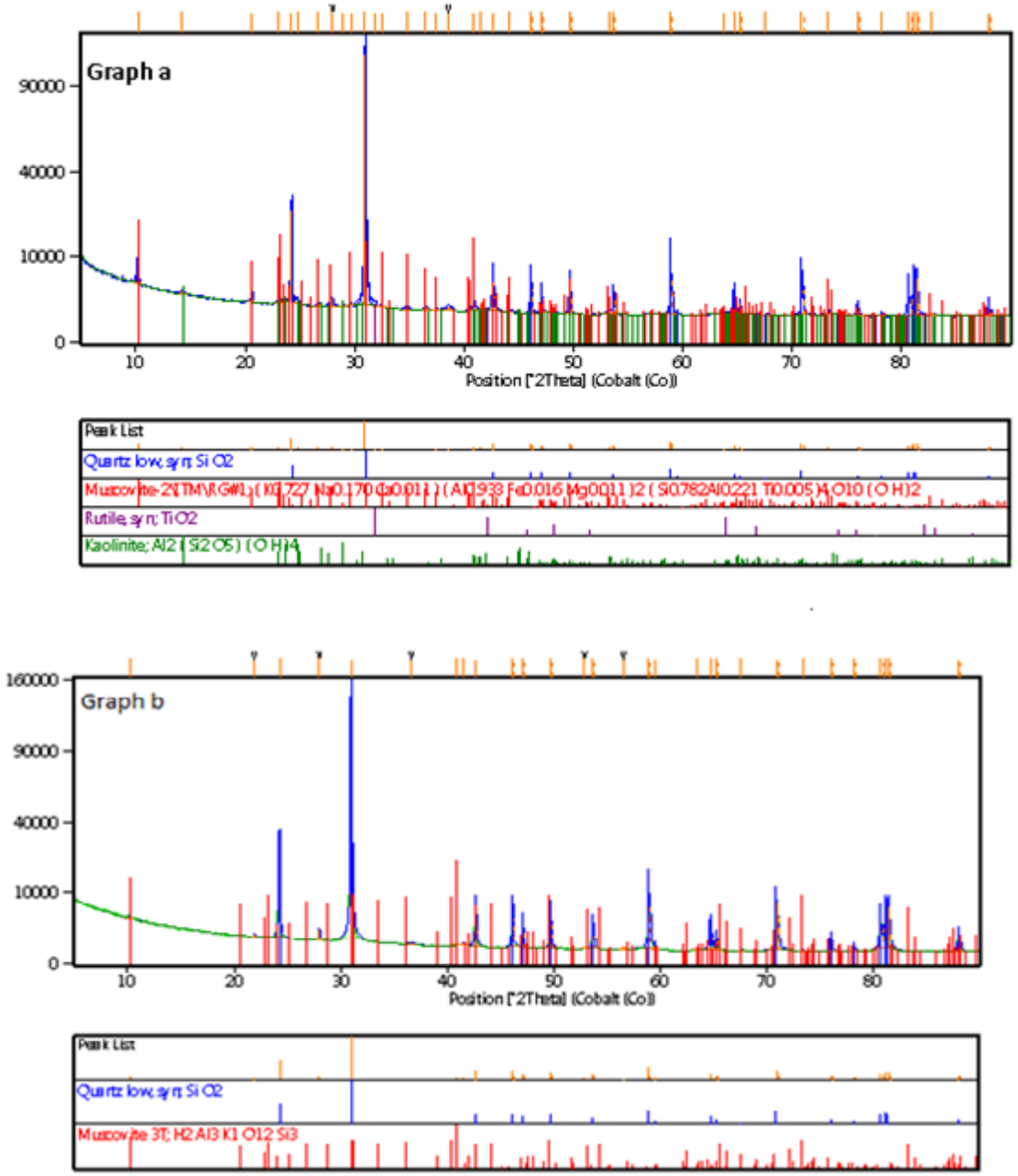

Figure 5.14: Graphical representations of the XRD qualitative results of MAG 101. MAG 101A is shown as graph (a) and MAG 101B as graph (b).

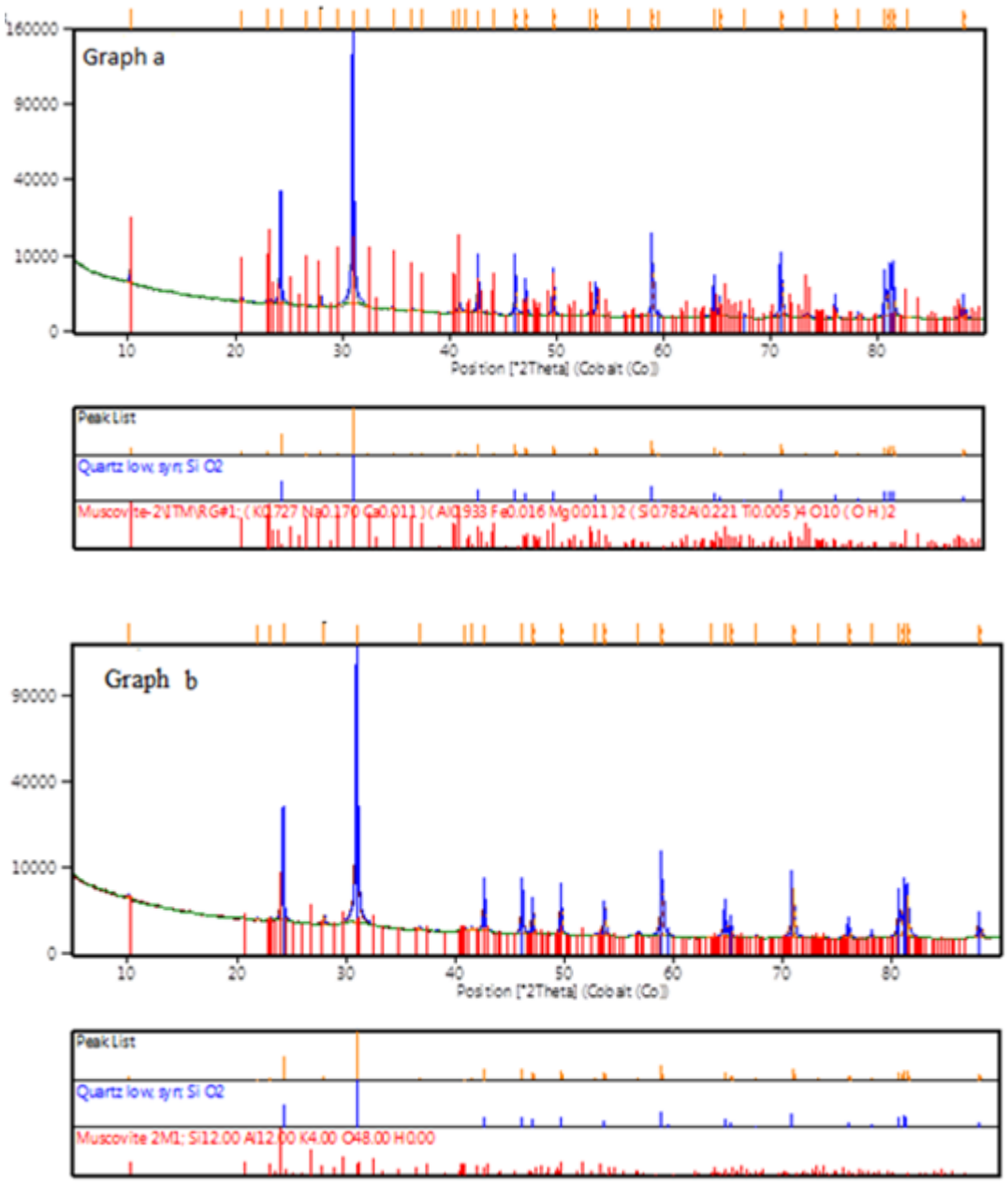

Figure 5.15: Graphical representations of the qualitative results of MAG 102. MAG 102A is shown as graph (a) and MAG 102B is shown as graph (b).

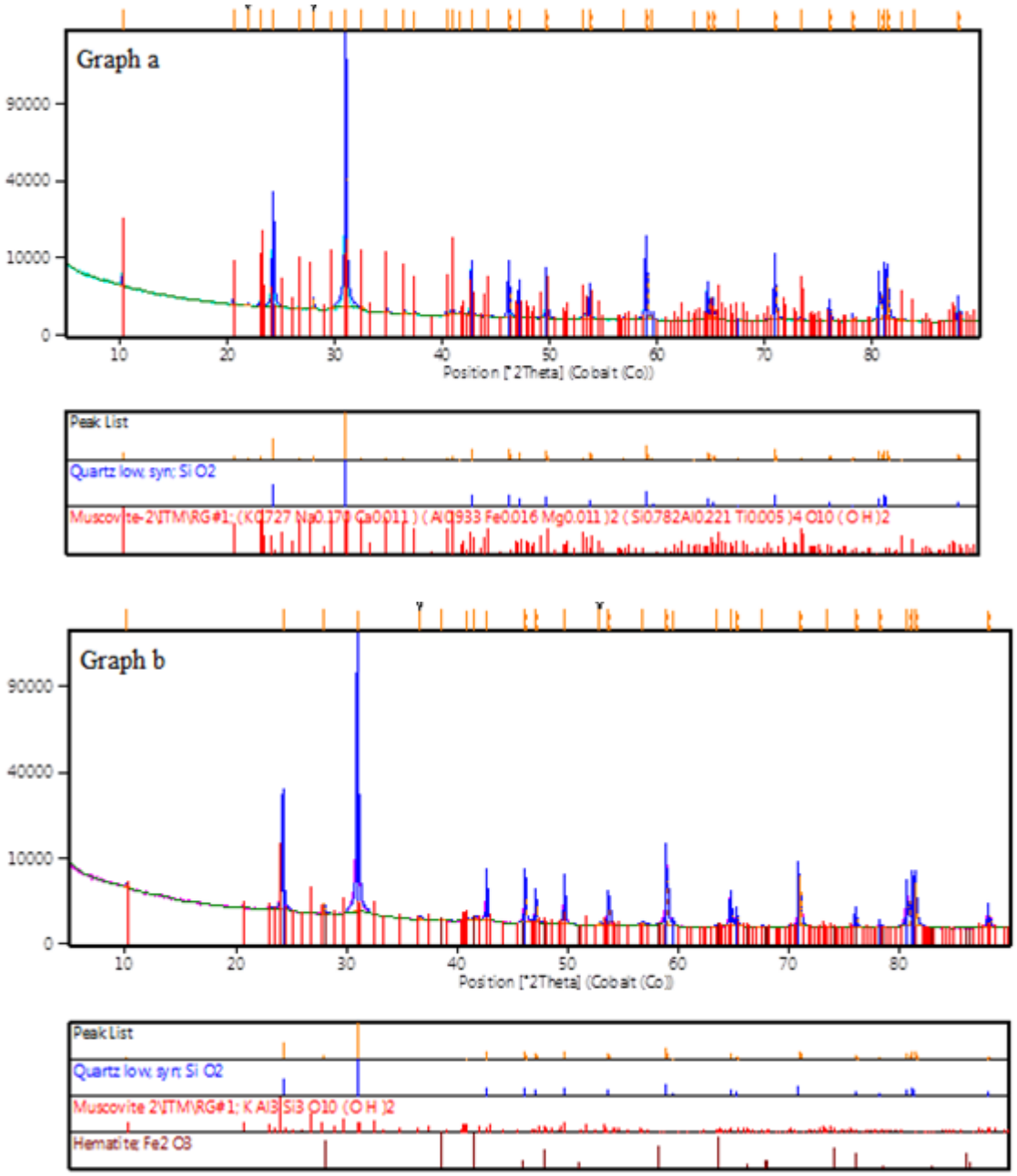

Figure 5.16: Graphical representations of the qualitative results of MAG 103. MAG 103A is shown as graph (a) and 103B as graph (b).

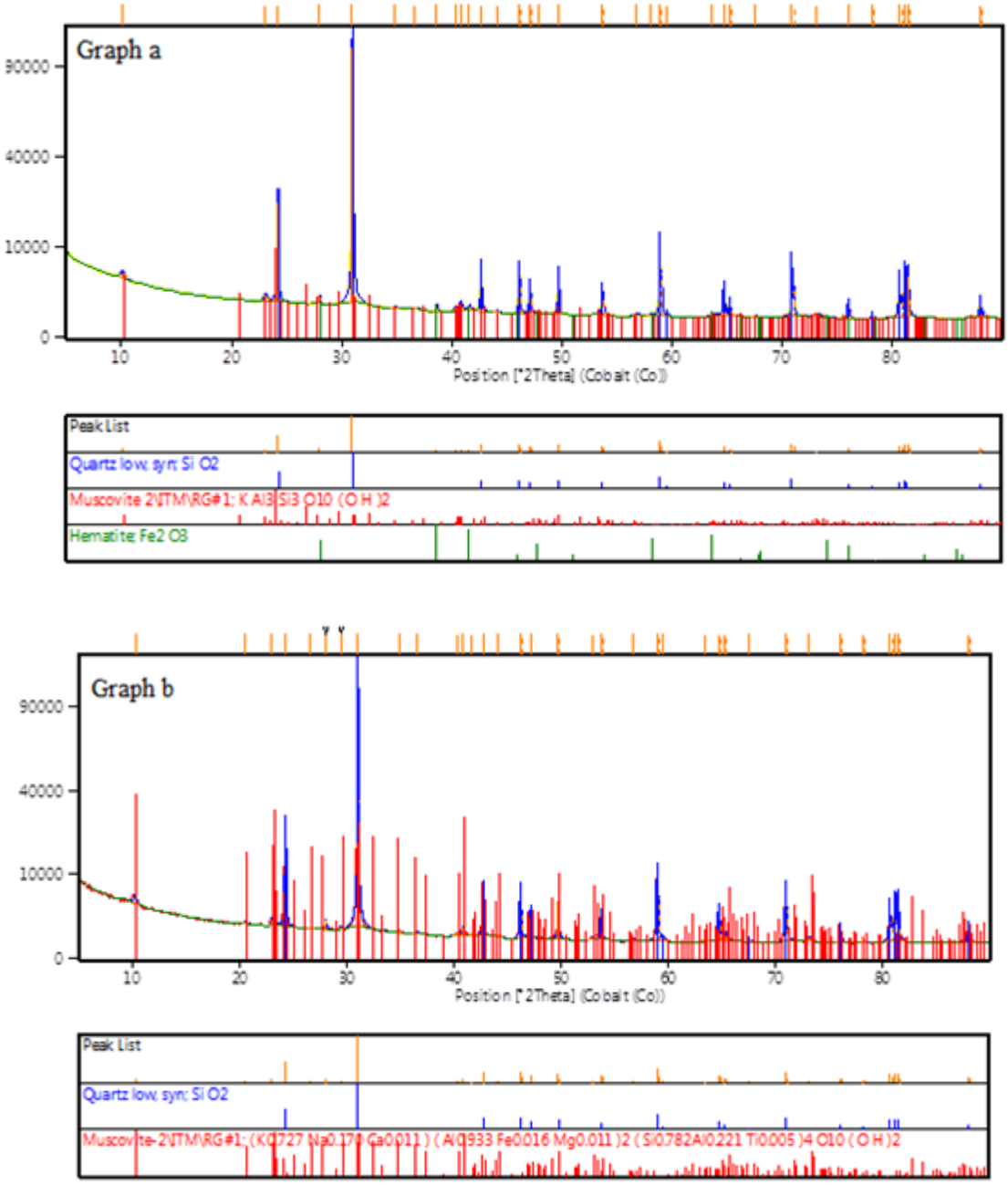

Figure 5.17: Graphical representations of the qualitative results of MKG 101. MKG 101A is shown as graph (a) and MKG 101B is shown as graph (b).

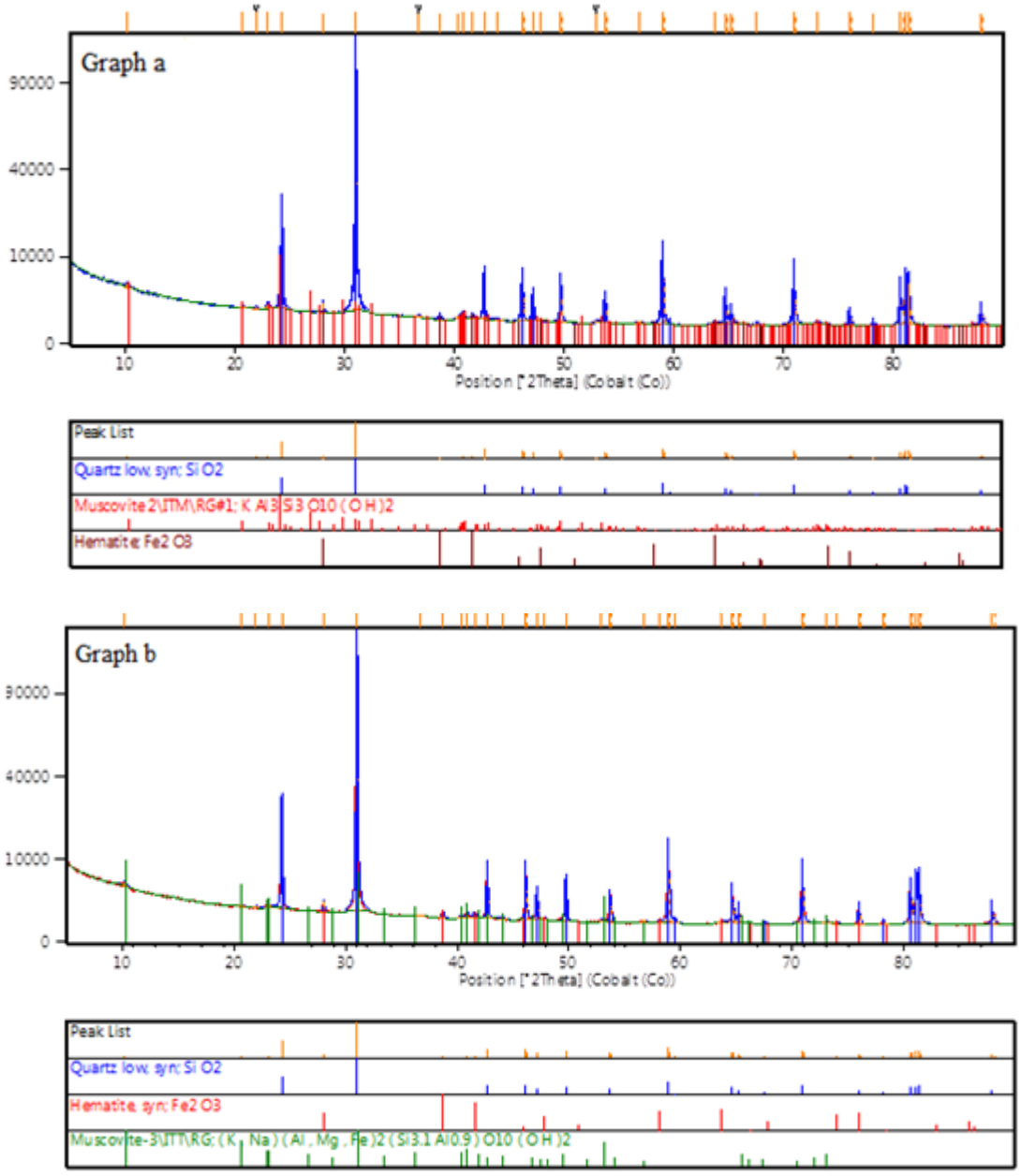

Figure 5.18: Graphical representations of the qualitative results of MKG 102. MKG 102A is shown as graph (a) and MKG 102B is shown as graph (b).

The XRD results show that the MISS -bearing sections of all three Magaliesberg samples have lower quartz and higher muscovite concentrations compared to the underlying substrate sediment sections (shown in table 5.20). Sample The MKG 102 from the Makgabeng Formation has this same established mineralogical relationship between the primary minerals - muscovite and quartz - as the Magaliesberg samples: lower quartz and higher muscovite content in the MISS bearing section compared to the underlying sediment section (shown in Table 5.21). Sample MKG 101 has the reverse relationship between quartz and muscovite.

Table 5.20: Established negative correlative mineralogical relationship between quartz and muscovite in the Magaliesberg Formation samples: higher concentration of muscovite and lower concentration of quartz in the MISS-bearing section of the Magaliesberg samples compared to the underlying sediment sections. Red colour shows comparative lower values.

MAG 101	**Wt. %**	**MAG 101B wt%**	**Wt. %**
Quartz	81.69	**Quartz**	97.75
Muscovite	12.66	**Muscovite**	2.25
Kaolinite	3.93		
Rutile	1.72		
MAG 102A	**Wt. %**	**MAG 102B**	**Wt. %**
Quartz	92.94	**Quartz**	97.16
Muscovite	7.06	**Muscovite**	2.84
MAG 103A	**Wt. %**	**MAG 103B**	**Wt. %**
Quartz	92.56	**Quartz**	97.33
Muscovite	7.44	**Muscovite**	2.02
		Hematite	0.65

Table 5.21: Established negative correlative mineralogical relationship between muscovite and quartz in MKG 102 (and reverse relationship for MKG 101). Table is based on A-B concentration value. Red colour shows comparative lower values.

MKG 101A	**Wt. %**	**MKG 101B**	**Wt. %**
Quartz	91.08	**Quartz**	90.76
Muscovite	7.21	**Muscovite**	9.24
Hematite	1.71		
MKG 102A	**Wt. %**	**MKG 102B**	**Wt. %**
Quartz	93.23	**Quartz**	93.3
Muscovite	5.19	**Muscovite**	4.85
Hematite	1.58	**Hematite**	1.85

The integration of the geochemical and mineralogical results show that the Magaliesberg Formation MISS bearing samples have higher Al_2O_3 and muscovite concentrations, and lower quartz and SiO_2, when compared to the underlying substrate sandstone of each of the analyzed samples (figure 5.19). This same character is shown by MKG 102, but in contrast, MKG 101 deviates from this characteristic (table 5.22; figure 5.19).

Table 5.22: Table showing concordance between geochemistry and mineralogy of Magaliesberg Formation samples (MAG 101, 102, and 102), and sample MKG 102 of the Makgabeng Formation: lower Quartz and SiO_2 in the MISS-bearing section compared to the underlying sediment section and higher Muscovite and Al_2O_3 in the MISS-bearing section compared to the underlying sediment section.

MAG 101	**Element**	**A-B Value**	**Mineral**	**A-B Value**
	SiO_2	-18.66	**Quartz**	-16.06
	Al_2O_3	7.38	**Muscovite**	10.41
MAG 102	**Element**	**A-B**	**Mineral**	**A-B Value**
	SiO_2	-2.8	**Quartz**	-4.22
	Al_2O_3	2.23	**Muscovite**	4.22
MAG 103	**Element**	**A-B**	**Mineral**	**A-B Value**
	SiO_2	-2.78	**Quartz**	-4.77
	Al_2O_3	2.15	**Muscovite**	5.42
MKG 101	Element	A-B	Mineral	A-B Value

	SiO_2	-0.4	**Quartz**	0.32
	Al_2O_3	-0.2	**Muscovite**	-2.03
MKG 102	**Element**	**A-B**	**Mineral**	A-B Value
	SiO_2	-0.74	**Quartz**	-0.07
	Al_2O_3	0.82	**Muscovite**	0.34

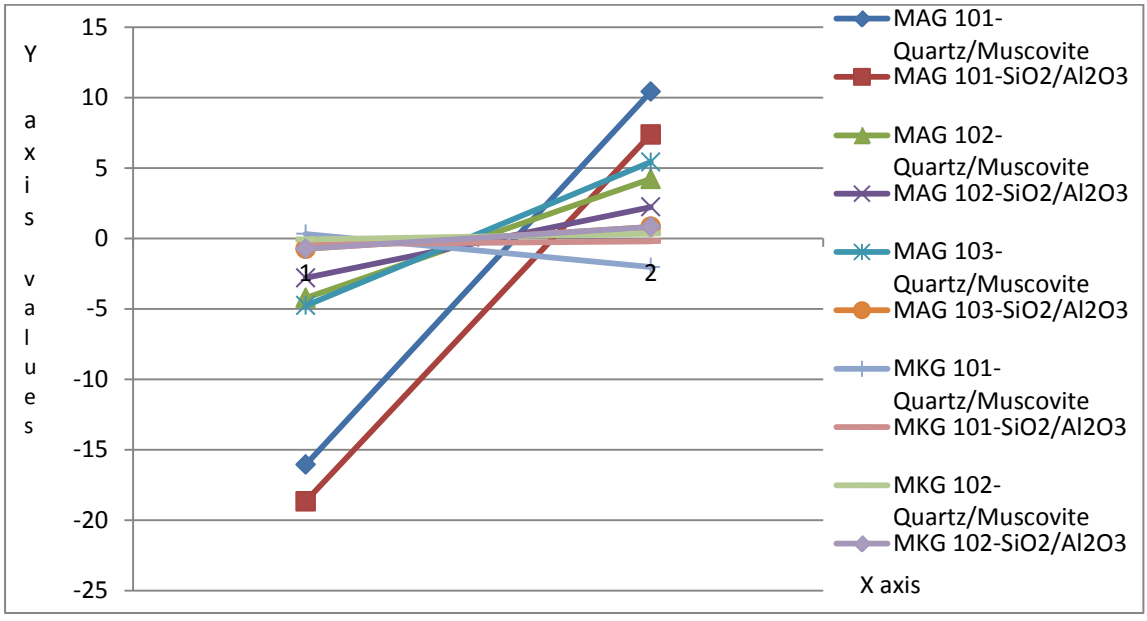

Figure 5.19: Concordance between the Magaliesberg Formation XRF and XRD results and that of the Makgabeng Formation sample MKG 102; quartz and SiO_2 is negatively correlated with muscovite and Al_2O_3 in MAG 101, 102, 103, and MKG 102. Note that MAG 101, 102, 103, and MKG 102 have the same trend direction and that of MKG 101 is quite different. Graph is based on A-B concentration value.

Chapter 6

Discussion

Research aimed at the discrimination of a direct relationship between different microbially-induced sedimentary structures (MISS, Noffke *et al.*, 2001a; cf. microbial related structures of Eriksson *et al.*, 2010) that are preserved in clastic sedimentary records, and a precise palaeoenvironmental model or to parts of identified depositional settings, is limited (e.g. Schieber *et al.*, 2007c; see Eriksson *et al.*, 2012 for recent discussion). The catalogue of inferred MISS formed by organo-physico-chemical processes and found in the Makgabeng and Magaliesberg Formations is shown in chapter 3. Emphasis must be laid on the fact that analogous sedimentary structures can also form through means that are completely physical and without biological influence (see Eriksson *et al.*, 2012 and references therein, for further explanation). The fundamental interest in the study of MISS is that they serve as a link between physically formed sedimentary features in clastic sediments and biological processes.

The comparison of the MISS of the two Formations through the catalogue (chapter 3), their unusual textural attributes (chapter 4), and geochemical and mineralogical data (chapter 5) can contribute to improved comprehension of the environmental parameters of different types of MISS. A comparative basis for the work in this thesis is proffered by the published literature on MISS research, MISS palaeoenvironmental research on the two studied Formations, and palaeoenvironmental interpretation of physical sedimentary structures recorded in the field from the two Formations (shown in chapter 3). The approach taken here is the integration of similarities and differences of the MISS-bearing section of a particular sample to the underlying sediment section, and to compare the MISS-bearing section of the samples from the Magaliesberg Formation to the MISS-bearing section of the samples from the Makgabeng Formation. Finally, the results are compared to literature.

6.1 Catalogue of the two Formations

The MISS catalogue of the two Formations shows that there is more phylogenetic and morphological diversity in the MISS of the Makgabeng Formation compared to that of Magaliesberg Formation (see chapter 3 for comparison). Eriksson *et al.*, 2010 noted the

reverse, namely more diversity in the Magaliesberg Formation MISS compared to that of the Makgabeng Formation. Further discoveries of more MISS features in the Makgabeng Formation and much more detailed palaeoenvironmental work (Simpson *et al.*, 2013; Hennes *et al.*, 2014) indicate a much more complex inferred setting for the Makgabeng Formation deposits, in line with this thesis. This could also have been related to the harsh desert palaeoenvironment inferred for the Makgabeng Formation (e.g., Simpson *et al.*, 2013) which positively influenced phenotypic diversity in the adaptation of extremophiles in time and space, as compared to the inferred Magaliesberg epeiric marine coastal palaeoenvironment (e.g., Bosch and Eriksson, 2008) which would have been less subject to palaeoclimatic changes and more homogeneous in chemical character.

6.2 Relative Proportions of MISS features in the Magaliesberg and Makgabeng Formations

Based on field work and the catalogue created, the MISS of the Magaliesberg Formation encompass positive (<3mm above upper sandstone bed surfaces) and some minor negative structures with different geometries on sandstone upper bedding surfaces (sand cracks, petees and petee ridges and wrinkle structures), palimpset ripples, and multi-directional ripples (arranged in descending order of predominance). The MISS of the Makgabeng Formation are sand cracks and wrinkle structures, mat fragments, roll-ups, and petees and petee ridges arranged in descending order of predominance.

6.3 Similarities between the MISS of the two Formations

The basic similarity amongst the MISS features of the two Formations is the occurrence of sand cracks, petees, petee ridges and wrinkle marks which are relatively common in both of the Formations. Although their inferred palaeoenvironments are quite different in many respects, the epeiric marine coastline of the Magaliesberg sea compares favourably with the postulated playa lakes of the Makgabeng palaeodesert in the sense that MISS in both formations would have flourished in an essentially analogous saline and shallow water setting subject to episodic sedimentation. This similarity at the larger scale, in terms of overall depositional settings, is contrasted against distinct differences at a smaller scale as discussed in the next section.

6.4 Differences between the MISS of the two Formations

The basic difference between the two Formations is that the Magaliesberg Formation MISS are mostly surface ornamentation features and the Makgabeng Formation MISS are mostly mat destruction features. Differences recorded in the comparison of the MISS of the two Formations are inferred to be related to differences in palaeoenvironmental characters of the two Formations; Makgabeng Formation MISS reflect the effect of high energy transportation of desiccated mat remains, while for the Magaliesberg Formation, the MISS mostly reflect the effects of biostabilization. While desiccation features are also common in the Magaliesberg Formation they mostly were succeeded by further mat growth and biostabilization, and not by mat destruction as for the Makgabeng Formation. Microbes affect the sedimentary environment through the moderation of the sediment continuity equation by streamlining bio-physico-chemical factors that range from sediment cohesion and tensility, water pH and residence time, to rate of sediment erosion, transportation and deposition (cf. Noffke 2010 and references therein).

The aforementioned factors are relatively interwoven and are inferred to have produced specific MISS ecological and taphonomic factors (see Noffke, 2010 for elaboration on MISS ecological and taphonomic factors) which would have produced specific MISS features in the two Formations. Cyanobacteria are widely adapted and are renowned as the most prominent mat builders, and environmental variation can result in diverse conditions and invariably impact on the establishment of different groups of mat-builders; this is supported by the disparity observed in the comparison of the catalogue of the MISS of the two Formations.

6.5 Textural characterization

In all the samples (both Magaliesberg and Makgabeng Formations), the MISS bearing section is of smaller grain size compared to the underlying sediment section. This homogeneity in the smaller grain size of the MISS-bearing section compared to the underlying section implies sympathy of microbes to fine- to medium-grained sediments as compared to larger grains, regardless of sedimentary environment, as also found by Noffke (2010, for example).

The pseudo petee ridges (Figure 4.1) found in the Magaliesberg Formation are a new feature amongst known MISS (none reported in literature consulted for this thesis) and reflect finer-grained cigar-like roll-ups inside the ridge structure. Pseudo petee ridges of the Magaliesberg Formation megascopically resemble petee ridges because of their positive polygonal ridges

on sandstone uppermost bedding planes, but are microscopically seen to be roll-ups of smaller scale compared to those of the Makgabeng Formation. Roll-ups are formed by the process continuum of mat destruction and transport of mat fragments (mat desiccation, mat curling, erosion, transportation and re-deposition); while they are inferred to have been transported in the Makgabeng Formation palaeoenvironment by the high energy inter-dune flash floods (cf. Eriksson *et al*., 2000), in the Magaliesberg Formation setting they were probably transported by high energy tidal currents. However, in the latter palaeoenvironment, the roll-ups interacted with predominant petee ridge-forming events and became incorporated into those forms, hence showing detailed differences for the palaeoenvironments of the two studied Formations.

Pseudo cross-lamination (Figure 4.2), another apparently new MISS from the Magaliesberg Formation (not reported in literature consulted here) denotes transportation and accretion of biostabilized sediments and consequent resistance to re-working. Pseudo cross-lamination has features resembling cross-stratification on a smaller (microscopic) scale and this feature forms low ridges that are inferred to have been formed by thrusting of several biostabilized sediment layers (thrusting shown with inclination of double arrow in figure 4.2) because of the resistance of the mat-bound sediments to erosion and reworking. The thrusting to form the low ridges was a local and small scale result of re-working, but after that the MISS feature remained stable and in place. The biostabilization encompasses binding, trapping and baffling caused by biofilms that are constituted by intermingled sand grains and microbial filaments which enhance cohesion and tensile strength of the sandstones (e.g., Eriksson *et al.*, 2012 and references therein). The resistance to extreme re-working of the biolaminite through microbial binding to enable subsequent thrusting and deformation of the said lamina wouldn't have been possible without microbial enhanced cohesion of silt and sand grains through the influence of microbes. Microbes enhance the response of originally granular sand surfaces to stress, by making sand behave like mud and forming a host of features that are normally not expected of sand, as similarly found by most previous workers (e.g. Parizot *et al*., 2005; Shieber *et al.*, 2007; Eriksson et al., 2010 and references therein). While the findings of this thesis in this respect align completely with previous work, the feature itself, pseudo cross-lamination has not been reported previously and an original contribution to MISS research is thus made.

Mat chips and composite mat chips are found in the Makgabeng Formation. Mat chips (Figure 4.4; shown with two arrows at #1) are formed by the erosion of mat bound sediment and consequent reworking and rounding before deposition. Composite mat chips (Figure 4.4; shown with arrow at #3) involve the mutual alignment of two or more mat chips that appear to have been transported together as a single composite chip. Mat chips are formed by high energy events (e.g. Eriksson *et al.*, 2007b), presumably related to inter-dune flash floods in the case of the Makgabeng Formation palaeoenvironment (Simpson *et al.*, 2002, 2013). Roll-up structures (figure 4.3a; 4.3b) set within planar laminated sandstone that is interpreted as upper flow regime beds (cf., Eriksson *et al.*, 2000) is associated with high energy erosive events which wouldn't favour the preservation of ordinary sedimentary structures. The roll-ups and mat chips are preserved due to the enhanced cohesion caused by mats, thus protecting them during high energy sandy clastic sedimentation events. The microscopic roll-ups of the Magaliesberg Formation are of lower scale compared to the megascopic roll-ups of the Makgabeng Formation. The lower resolution of the Magaliesberg Formation roll-ups compared to that of the Makgabeng Formation show the lower energy level of the Magalieberg Formation inter-tidal coastline palaeoenvironment compared to that of the Makgabeng Formation. The thesis thus contributes here to enhanced detailed palaeoenvironmental interpretation of such delicate features and argues against simple assignments of specific MISS features to particular environmental settings, as is the case for most sedimentary structures, biologically influenced or not.

The basic difference between the two Formations in textural characters is the higher energy of the inferred inter-dune flash flood setting of the Makgabeng Formation palaeoenvironment, which positively influenced complete erosion, transportation and re-deposition of the mat chips and composite mat chips. The Magaliesberg samples show that biostabilization prevailed over shear stress, thereby mostly leading to the *in situ* construction of MISS rather than erosion and re-deposition. Makgabeng Formation samples show that shear stress prevailed over biostabilization leading to the complete erosion and re-deposition of the microbially bound sediments by the inter-dune flash floods. The high energy inter-dune flash flood setting of the Makgabeng Formation is shown by evidence of tearing prevailing over the tensile strength of biostabilized sediments; in comparison, in the Magaliesberg Formation palaeoenvironment resistance of biostabilised sediments to being re-worked prevailed.

6.6 Relationship between different MISS features of the Formations

6.6.1 Magaliesberg Formation

The MISS of the Magaliesberg Formation are mostly bedding surface ornamentation features that are related to each other by the prevailing factors of biostabilization. Water residence time, intermittent sedimentation (i.e. periods without active sedimentation, essential to forming MISS), and resistance to total re-working of sediments are some of the interwoven factors that moderated the construction of the MISS of the Magaliesberg Formation. Water residence time in this context is described by the relationship between emergence and inundation of sediments which is a very important factor in the formation of surface ornamentation-type MISS. The intermittent inundation and exposure of sediments positively influence the growth of benthic microbes, and benthic microbes are renowned mat builders (e.g. Shieber *et al.*, 2007 and references therein). In this context, inundation involves the covering of sediments by rise in water level during high tide, and emergence describes the shrinking of the sediments due to desiccation caused by ebb tide/low tide. Where the desiccation inferred for the tidal setting of the Magaliesberg Formation was short-lived and regularly alternated with inundation, desiccation in the Makgabeng Formation palaeodesert was long-term and often terminal for the microbial mats.

6.6.2 Makgabeng Formation

The basic relationship inferred here is the process continuum of deposition, erosion, transportation and re-deposition of microbially bound sediments. The mat chips are inferred to have been a feature resulting from longer transportation distance, as compared to the less robust roll-ups. The physical process continuum is inferred as:

1. Curling up of microbial mat (and mat-bound thin sediment layer) due to desiccation.
2. Shear stress and erosion prevail, and consequent transportation and deposition of mat bound sediments.
3. Roll-ups are deposited in more proximal sites compared to mat chips and mat chips are deposited in more distal sites compared to the roll-ups.

6.7 Geochemistry

Geochemical (XRF) results and analysis thereof (detailed in chapter 5) and briefly summarized here, show disparity between the MISS-bearing section (A) of each of the samples compared to the underlying sediment section (B) of the exact same samples (both Magaliesberg and Makgabeng Formations). This established relationship of redox fluxes provides support for the position of Farmer (1999) that concentration of elements above background noise (background in this context is the underlying substrate arenite) may be utilized as a biomarker when there is low preservation or non-preservation of live carbon. Organisms can affect the larger-scale geochemical cycles of both major elements (Si, Al, Fe, Ca, K, Na) and trace (Ge, Ga, P, REE, etc) in minerals because elemental uptake, redox reactions and microbial products can actuate control on mineral weathering rate (Welsh *et al*., 2003).

The significant major element oxide similarity between all the samples (both Magaliesberg and Makgabeng Formations) is that SiO_2 is of lower concentration in the MISS-bearing section of all the samples compared to the underlying sediment section. The uniform enrichment of Ba in the MISS bearing section of all the samples (both Makgabeng and Magaliesberg Formations) compared to the underlying section, is significant for both the Formations.

The oxides of the major element (Al_2O_3, TiO_2, K_2O, and P_2O_5) geochemistry of the MISS-bearing section of the samples from the Magaliesberg Formation are relatively uniform: all samples show higher concentrations in the MISS-bearing section (A) compared to the underlying sediment section (B). In contrast, the same major element (Al_2O_3, TiO_2, K_2O, and P_2O_5) of the Makgabeng Formation samples is non-uniform, in the sense that there are higher concentrations in A compared to B in sample MKG 102, and lower concentration in A of MKG 101 compared to B. Also, there are uniform higher concentrations of Hf and Rb in the MISS section (A) of each of the analyzed Magaliesberg Formation samples compared to the underlying sediment section (B). The Makgabeng Formation samples are non-uniform in the concentration of Hf and Rb; MKG 101 has lower concentration of Hf and Rb in the MISS bearing section compared to the underlying sediment section, and that of MKG 102 is the reverse (shows the concentration trend of the Magaliesberg Formation samples). This observed homogeneous geochemical character of the Magaliesberg Formation samples is inferred to reflect the high rate of mixing of sediments by tides, waves, wind and the

homogeneous marine chemistry of the coastline of the inferred epeiric marine coastline setting. The observed heterogeneous geochemical characteristic of the Makgabeng Formation samples is interpreted to reflect the much less regular physical dynamics of the high energy inter-dune flash flood setting, with sample MKG 101 (characteristic MISS is mat chips) having been transported further than sample MKG 101 (roll-ups characterize the MISS).

The MISS bearing sections of Makgabeng Formation samples MKG 101 and 102 exhibit lower concentrations of CaO, Na_2O and Cr_2O_3 compared to the underlying sediment sections (the exception is Na_2O which has the same concentration in the MISS bearing and underlying sediment sections of MKG 101). The MISS bearing sections of the Magaliesberg Formation samples all have higher concentrations of CaO, Na_2O and Cr_2O_3 compared to the underlying sediment section. The MISS bearing section of all the analyzed Magaliesberg samples have higher concentrations of most trace elements compared to the underlying sediment section; in contrast, the MISS bearing sections of the Makgabeng samples have lower concentrations of most trace elements compared to the underlying sediment section (table 5.13). The MISS sections of each of the Magaliesberg samples are more enriched in trace elements Ce, Cr, Nb, Th, V, Y, Zn, and Zr compared to the underlying section, and the MISS bearing sections of the Makgabeng samples are of lower concentration in Ce, Cr, Nb, Th, V, Y, Zn, and Zr compared to the underlying sediment section. This comparative incongruity of the two Formations is inferred to reflect differences in the character of the two shallow marine environments.

The MISS bearing sections of each of the Magaliesberg Formation samples are uniformly of higher concentration in Nd, Sr and U (Table 5.16) compared to the underlying sediment section. The MISS bearing section of MKG 101 is of lower concentration of Nd compared to the underlying sediment section, and the MISS bearing section and the underlying sediment section of MKG 102 are of equal concentration of Nd. Sr is of equal concentration in the MISS bearing section of MKG 101 compared to the underlying section, while MKG 102 has lower concentration of Sr in the MISS bearing section of the sample compared to the underlying sediment section. MKG 101 and MKG 102 have U of equal concentration in their respective MISS bearing sections compared to the underlying sediment sections.

Overall, thus, the geochemistry shows that for both major and trace elements, there is a uniform geochemical relationship (between upper MISS bearing and underlying sediment substrate sub-samples) in the Magaliesberg Formation samples and that the Makgabeng

Formation samples are heterogeneous (non-uniform major elements, and relatively uniform minor element concentrations between subsamples A and B).

6.7.1 Interpretation of geochemical contrast between the samples from the two Formations

The basic reason for the geochemical contrast between the two Formations is postulated to be the difference in palaeoenvironment. Sedimentary environments affect the ecological and taxonomic factors of MISS preservation by positively influencing the proliferation of particular morphotypes of epibentic and endobenthic bacteria; this results in the observed differences in geochemistry (figure 6.1). MISS are formed by mats and mat types are chemically, physically and biologically controlled adaptations of microbial communities to a particular locally prevailing condition (e.g. Eriksson *et al.*, 2010).

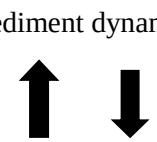

Figure 6.1: Sediment dynamics and sediment biogeochemistry are cyclic (cf. Noffke 2010)

The relative homogeneity of the geochemistry of the MISS bearing section (A) of the Magaliesberg Formation samples when compared to the underlying sediment section (B) is probably related to the homogeneous geochemistry of the mass of the ocean and the enhanced mixing of sediments by wind, small waves and tides inherent in the coastal palaeoenvironment postulated for the Formation (e.g., Eriksson *et al.*, 2006). The geochemical heterogeneity/variation of the Makgabeng Formation A and B samples is thought to be because of the ephemeral nature of the shallow water playa lakes and concomitant significant influence of groundwater in that setting, with intermittent high energy flood/erosive events inferred for the palaeoenvironment of the Makgabeng Formation deposits (e.g., Simpson *et al.*, 2004, 2013; Hennes *et al.*, 2014). Clastic sediments from the episodic braided rivers debouching into the epeiric coastline of the Magaliesberg Formation (Eriksson *et al.*, 2006) would have intermittently covered the shallow marine mats; the mats grew through them and survived or died off and with the elapse of time (on the geological scale), the geochemistry would have remained uniform because of the influence of the homogeneous marine water chemistry (e.g., Eriksson *et al.*, 2002 and references therein). The

high energy inter-dune flash floods of the Makgabeng Formation would have actuated highly variable chemistry of mat bound sediments and substrate sediments and the two could have become rapidly mixed up during intermittent floods which would have eroded both mat bound sediment and its substrate. Also, the ephemerally high energy of the Makgabeng Formation palaeoenvironment would have destroyed mats and also the covering of the mats would have being temporally irregular when compared to that of the more cyclical and regular sedimentation patterns inferred for the Magaliesberg Formation. The geochemical uniformity of the Magaliesberg samples might also be related to higher water residence time compared to the geochemically variable samples from the Makgabeng Formation; playa lakes by definition imply long desiccation periods.

6.7.2 Interpretation of major element geochemical similarity between Magaliesberg Formation samples (MAG 101, 102, 103) and Makgabeng Formation sample MKG 102, and interpretation of deviation of sample MKG 101 from this geochemical character

The similarity in major element geochemistry of MAG 101, 102, 103 and MKG 102 might be related to the shared character of overall relatively shallow depth of the water bodies postulated in both Magaliesberg and Makgabeng Formation palaeoenvironments, and also the relatively similar provenance of ephemeral braided fluvial sediment feeding both saline shallow water settings (Kaapvaal craton basement rocks). The observed disparity in major element oxide concentrations between samples MKG 101 and MKG 102 is inferred to have been caused by the dynamics of the inter-dune process; Makgabeng Formation sample MKG 102 is typified by roll-up MISS and Makgabeng Formation sample MKG 101 by mat fragment MISS. It is a convention that mat fragments are eroded MISS that have generally been transported farther than roll ups (e.g., Eriksson *et al.*, 2007b and references therein) so the sedimentary dynamics of the inter-dune processes might have played a role, with the mat and substrate of the more proximal MISS (MKG 102) not becoming so mixed up compared to the more distal mat fragments (MKG 101) with better mixing of mat and substrate particles (but still with the two Makgabeng Formation samples having mostly trace element homogeneity).

6.8 Mineralogy

The high quartz content of all the samples reflects sediments derived from cratonic basement rocks. Additionally, it is now generally accepted that intense chemical weathering promoted by microbial activity during the Proterozoic, left behind a quartzose-rich remnant that was reworked into quartz arenites (e.g. Dott, 2003). The high quartz content of all the samples

(both A and B subsamples of the two Formations) when compared to average sandstones is in agreement with the suggestion that microbes have an affinity for quartz rich sediments mainly because of the deeper conduction of light by the translucence quartz grains which is important for phototrophic-photoautotrophic reactions (see Noffke, 2010 for further elaboration). Cynobacteria are inferred to be the most important mat builder and are mostly phototrophic (e.g. Stal, 2000; Noffke 2010).

The lower quartz content and higher muscovite content of the MISS bearing section of the samples (MAG 101, 102, 103, and MKG 102) compared to the underlying sediment section might be due to bio-mediated and/or physico-chemical weathering rearrangement of phylosilicates. Dissolution of silicate minerals is based on pH; decrease in pH and increase in dissolution rate is the mineralogical dissolution norm (cf. Welsh and Ullman, 1993). Metabolic byproducts, chelates, extracellular enzymes, simple and complex organic acids produced by microbes (e.g. Bennet and Cassey, 1994) decrease pH, catalyze silicate dissolution rates through the formation of framework destabilizing surface complexes, or through the complexation of metals in solution (e.g. Bennet and Cassey, 1994; Blake and Walter, 1996; Drever and Vance, 1994). The sediment provenance of the two Formations is Kaapvaal craton basement rocks with K-feldspar and muscovite as important constituents of the detrital sediment liberated from the source rock; the K-feldspar can also weather when pH is lowered, forming muscovite. This is shown by the higher muscovite content of the MISS bearing sediment section compared to the underlying sediment section, which is expected as MISS is a surface phenomenon (cf. Schieber, 2007).

The equation showing the formation of muscovite from K-feldspar encompasses the lowering of pH by the increasing of acidity through the addition of hydrogen ions is given by –

$$3\ KAlSi_3O_8 + 2\ H^+ \rightarrow\leftarrow K\ Al_2SiAlO\ (OH)_2 + 2K + 6\ SiO_2\ (aq)$$

Even at the same pH, it has been shown experimentally by Welch and Ullman (1993) that the rates of plagioclase dissolution are more than ten times greater in solutions containing organic acid compared to solutions containing inorganic acid.

The phylosilicate mineral kaolinite recorded in one of the MISS-bearing Magaliesberg Formation sections might have been a product of biogenically-induced reactions, as microbes increases the acidity of their immediate environment; this concordantly increases Al solubility and mobility leading to the formation of secondary minerals, as dissolution of

aluminosilicates and increase in acidity are interwoven (cf. Welsh and Ullman, 1993). In sedimentary rocks, kaolinite is mostly a product of early diagenetic alteration of parent minerals – detrital feldspars and muscovite, which are favourable parent phases for kaolinite formation. Sandstones favour the formation of secondary diagenetic minerals like kaolinite because of their high permeability and porosity (cf. Ruiz Cruz, 2007):

$$2\ KAlSi_3O_8 + 3\ H_2O \rightarrow Al_2Si_2O_5\ (OH)_4 + 4\ SiO2 + 2\ K\ (OH)$$

The basic causative factor for the similarity in mineralogy of the two Formations is the mutual sediment derivation from the same cratonic basement rocks. Post-diagenetic alteration of the sedimentary rocks of both the Magaliesberg and Makgabeng Formations is thought to have been relatively insignificant. For the Magaliesberg Formation, sedimentation in the Pretoria Group basin persisted after deposition of that unit, with five further formations laid down above it, and exhibiting a stratigraphic trend of increasing arkosic components upwards in the stratigraphy (Eriksson *et al.*, 2006). Geochemical analysis of over 1500 samples from the Pretoria Group (Reczko, 1994) indicated an essentially homogeneous geochemistry for the sandstone-dominated formations, with significant geochemical contrasts only seen for thick mudrock units, such as the Silverton Formation (below the Magaliesberg Formation). Post-diagenetic alteration of the Makgabeng Formation deposits, which again form part of a thick pile of sedimentary rocks, filling the Main Waterberg Basin, would have been constrained by the dry desert setting persisting during formation of this unit (Bumby, 2000).

6.9 Comparison of the MISS catalogue of the two Formations and relation to sedimentary processes

The sedimentary processes that streamlined the genetic formational mechanism of the MISS of the Makgabeng Formation were mostly allochthonous (mat destruction features; mat desiccation, mat curling, erosion, transportation and consequent re-deposition) and the genetic factors forming the MISS of the Magaliesberg Formation were mostly autochthonous (formed *in situ*; emergence and inundation, distortion of mat growth and mat metabolism, and high quartz content favouring conduction of light by translucence; cf. Noffke, 2010). The surface ornamentation features of the MISS of the Magaliesberg Formation show shallow water palaeoenvironmental affinities and the MISS of the Makgabeng Formation are mostly of the mat destructive types that support the high energy desert palaeoenvironment of the Makgabeng Formation.

The channel-fills, wave ripples and minor flat-topped ripples, planar cross-bedding (shown in chapter 3) recorded in the Magaliesberg Formation at outcrop scale, combined together, are emblematic of the influence of a shallow marine environment during sedimentation, with concomitant gaps in sedimentation (Eriksson *et al*., 2006) whose impact is the *in situ* construction of MISS. The surface ornamentation features as seen in the Magaliesberrg Formation show resistance to re-working due to enhanced biostabilization of sediments due to regular inundation; emergence and concomitant gaps in sedimentation processes which allowed desiccation features to be common, yet not lead to mat destruction. This resistance to sediment reworking in the Magaliesberg Formation due to microbially enhanced biostabilization in a shallow water environment (e.g. Eriksson *et al.*, 2007b, and references therein) is further attested to by the multi-directional/palimpsest ripples with previous ripples resisting reworking as new ripples are formed. Parizot *et al.* (2005) utilized the wave ripple parameters to apply the formulae of Tanner (1971) and obtained estimated water depths of ≤40m confirming the shallow water Magaliesberg Formation environment. Biolamination (as seen in figure 4.2) is formed due to growth induced by sedimentation processes (e.g. Gerdes, 2010), and is emblematic of modern tidal flat deposits and reflects regular gaps in the sedimentation processes and microbes gliding upwards with the re-establishment of a new mat after each sedimentation event. This MISS morphology is mostly caused by motile, filamentous cyanobacteria (renowned prominent architects of biostabilization; M. *Chthonoplastes*, *Lyngbya* sp., and *Oscillatoria* sp.).

The physical sedimentary structures of the Makgabeng Formation that are together interpreted as having formed in a palaeodesert setting with episodic flashfloods, when aligned with the mat destruction MISS features observed in this thesis (process continuum of mat desiccation, mat curling, erosion, transportation and re-deposition), provide detailed amplification of physical and biological processes not discerned from the study of physically formed sedimentary structures alone. Desiccation and curling during time of aridity positively influencing erosion, transportation and re-deposition during episodes of high energy inter-dune flash flood.

6.10 Comparison with literature

The physical sedimentary and MISS structures studied here from the Magaliesberg and Makgabeng Formations show that MISS and sedimentary structures observed on outcrop scale in the field and through microscopic examination, when aligned with literature, provide

an important tool for overall palaeoenvironmental modeling. MISS can be utilized in palaeoenvironmental modeling and can be aligned with physically formed sedimentary structures and careful microscopic examination to enhance the resolution of results. Typically, in most sedimentological studies in the literature, recourse is to either physical or biological (MISS) features and few studies combine the two approaches for detailed palaeoenvironmental analysis. This thesis has attempted to bridge this gap, and the results obtained here for the Makgabeng Formation support the findings of Hennes *et al*. (2014) and earlier work (e.g. Bumby, 2000; Erikson *et al*., 2000; Simpson *et al*., 2013), while providing more detail. Eriksson *et al.* (2000) recognized roll-up structures, mat chips and desiccated large mat fragments, sand cracks, and wrinkle structures in the Makgabeng Formation; these are all mat destruction features that are also recognized in this work. Simpson *et al.* (2013) described tufted microbial mat, biological soil crusts and gas escape features in the Makgabeng Formation. The MISS of the Makgabeng Formation and composite mat chips (a new microscopic textural feature recorded in this work) aligned with physical sedimentary structures in the Makgabeng Formation complement the existing literature which postulates a setting prone to high energy episodic inter-dune flash floods, that led to the predominance of mat destruction features (e.g. Hennes *et. al.,* 2014). The geochemistry of the Makgabeng Formation samples is generally inhomogeneous, concomitant with the inferred high energy setting which would have mixed sediments irregularly and intermittently.

For the Magaliesberg Formation, two new MISS features (pseudo petee ridges and pseudo cross-lamination) are documented for the first time, and the resolution of the known palaeoenvironmental model applied to this Formation has been greatly enhanced in its detailed comprehension of physical and biological processes. Bosch and Eriksson (2008), and Parizot *et al.* (2005) recorded variegated types of sand cracks within the mineralogically mature and texturally immature sandstone beds of the Magaliesberg Formation as well as petee ridges, and *Manchuriophycus*. These surface ornamentation features are recorded in this work as the most predominant MISS morphology in Magaliesberg Formation and are genetically related to biostabilization, emergence and inundation within the inferred showing shallow littoral palaeoenvironment. This shallow marine palaeoenvironment postulated by previous workers and in this thesis too, is further reflected by the uniform geochemistry of the Magaliesberg Formation samples, supporting mixing by wind and water actions which formed part of the braid–delta – epeiric coastline environment inferred for the Formation by Bosch and Eriksson (2008).

The overall implication of this thesis is that MISS features aligned with a study of physical sedimentary structures creates a clearer understanding of palaeoenvironmental parameters, and should in fact become a standard approach in modeling ancient depositional settings. While the MISS are no more palaeoenvironmentally specific than physically formed sedimentary structures (Schieber *et al*., 2007 and references therein); careful investigation of mat-produced features related to underlying physical processes broaden understanding of environmental parameters and enable linking of physical, chemical and biological influences into a much more holistic appreciation of ancient sedimentary basins (e.g., Noffke *et al.,* 2001a; Schieber *et al*; 2007; Eriksson *et al.,* 2012).

Conclusion

The MISS catalogue shows that there is more disparity than similarity between the MISS of the Magaliesberg and Makgabeng Formations. The MISS of the Makgabeng Formation are mostly mat destruction features related to destruction, erosion and re-deposition of mat-bound sediments and the genetic mechanism of formation classified as allochthonous and reflects high energy. The MISS of the Magaliesberg Formation is mostly surface ornamentation features that are related to distortion of mat growth, resistance of mat to reworking, mat metabolism and decay, and the genetic mechanism of formation is deemed authochtonous and reflects biostabilization.

Results show that specific palaeoenvironments can be determined by the MISS/MRS specificity. These features documented in these two Formations symbolize these two shallow water palaeoenvironments. This is attested to by geochemical, mineralogical and textural attributes.

References

Altermann, W., 2004. Precambrian stromatolites: problems in definition, classification, morphology and stratigraphy. In: Eriksson, P.G., Altermann, W., Nelson, D.R., Mueller, W.U. and Catuneanu, O. (Eds.), The Precambrian Earth: tempos and events. Elsevier, Amsterdam, pp. 564-574.

Awramik, S.M., Margulis, L., 1974. Stromatolite Newsletter 2, 5.

Awramik, S.M., 1984. Ancient stromatolites and microbial mats. In: Cohen, Y., Castenholz, R.W., Halvorson, H.O. (Eds.), Microbial Mats: Stromatolites. Alan R. Liss, New York, pp. 1-22.

Bennett P.C., Cassey, W.H., 1994. Organic acid and dissolution of silicates. In: Pittman, E. Lewan, M., (Eds.), The role of organic acids in geological processes. Springer-Verlag, Berlin, pp. 162-201.

Beraldi-Campesi, H., 2013. Early life on land and the first terrestrial ecosystems. Ecological Processes 2, 1.

Blake, R.E., Walter, L.M., 1996. Effects of organic acids on orthoclase dissolution at 80° C and ph 6. Chemical Geology, 132, 91-102.

Bosch, P., Eriksson P.G., 2008. A note on two occurrences of inferred microbial mat features preserved in the c. 2.1 Ga Magaliesberg Formation (Pretoria Group, Transvaal Supergroup) sandstones, near Pretoria, South Africa. South African Journal of Geology, 111, 251-262.

Bose, P.K., Sarkar, S., Banerjee, S., Chakraborty, S., 2007. Mat-related Features from Sandstones of the Vindhyan Supergroup in Central India. In: Schiebr J., Bose, P.K. Eriksson P.G., Banerjee S., Sarkar S., Altermann W., Catuneanu O. (Eds.), Atlas of Microbial Mat features preserved within the siliciclastic Rock Record. Elsevier Atlases in Geology 2, Elsevier, Amsterdam, pp. 181-188.

Bottjer, D.J., Hagadorn, J.W., 2007. Mat Growth Features. In: Shieber J., Bose P.K., Eriksson P.G., Banerjee S., Sarkar S., Altermann, W., Catuneanu, O. (Eds.), Atlas of Microbial Mat features preserved within the siliciclastic Rock Record. Elsevier Atlases in Geology 2, Elsevier, Amsterdam, pp. 53-71.

Buick, R., Dunlop, I.S.R., Groves, D.I., 1981. Stromatolite recognition in ancient rocks. An appraisal of irregularly laminated structures in an early chert-barite unit from North-pole, Western Australia: Alcheringia 5, 161-181.

Buick, R., 1992. The antiquity of oxygenic photosynthesis: Evidence from stromatolites in sulphate-deficient Archaean lakes. Science 255, 74-77.

Bumby, A.J., 2000. The geology of the Blouberg Formation, Waterberg and Southpansberg Groups in the area of Blouberg Mountain, Northern Province, South Africa. Unpublished PhD thesis, University of Pretoria, South Africa, 293pp.

Burger, A.J., Walraven, F., 1980. Summary of age determinations carried out during the period April 1978 to March 1979. Annual Geological Survey of South Africa 14, 109-118.

Burne, R.V., Moore, I.S., 1987. Microbialites: organosedimentary deposits of benthic microbial communities. Palaios 2, 241-254

Button, A., 1986. The Transvaal sub-basin of the Transvaal sequence. In: Anhaeusser, C.R., Maske, S. (Eds.), Mineral Deposits of Southern Africa. Geological Society of South Africa Johannesburg, pp. 811-817.

Callaghan, C.C., 1987a. The Geology of the Waterberg Group in the Southern portion of the Waterberg basin. Unpublished M.Sc. Thesis, University of Pretoria, 164p.

Callaghan, C.C., Eriksson, P.G., Snyman, C.P., 1991. The sedimentology of the Waterberg Group in the Transvaal, South Africa: an overview. Journal of African Earth Sciences 13, 121-139.

Catuneanu, O., Eriksson, P.G., 1999. The sequence stratigraphic concept and the Precambrian rock record: an example from the 2.3-2.1 Ga Pretoria Group, Kaapvaal craton. Precambrian Research 97, 215-251.

Catuneanu, O., 2007. Sequence stratigraphic context of microbial mat features. In: Shieber, J., Bose P.K., Eriksson P.G., Banerjee, S., Sarkar, S., Altermann, W., Catuneanu, O. (Eds.), Atlas of Microbial Mat features preserved within the siliciclastic Rock Record. Elsevier Atlases in Geology 2, Elsevier, Amsterdam, pp. 276-283.

Cheney, E. S., Twist, D., 1986. The Waterberg “Basin” – a reappraisal. Transval Geology Society of South Africa 89, 353-360.

Cheney, E.S., 1996. Sequence stratigraphy and plate tectonic significance of the Transvaal succession of southern Africa and its equivalent in Western Australia. Precambrian Research 79, 3-24.

Costerton, J., Stoodley, P., 2003. Microbial biofilms: protective niches in ancient and modern geomicrobiology. In: Krumbein, W.E., Paterson, D.M., Zavarzin, G.A. (Eds.), Fossil and Recent Biofilms (Preface). Kluwer Academic Publishers, Dordrecht, pp. 15-21.

Dott, R.H., 2003. The importance of eaolian abrasion in supermature quartz sandstones and the paradox of weathering on vegetation free landscapes. Journal of Geology 111, 387-405.

Drever, J.I., Vance, G.F., 1994. Role of organic acids in mineral weathering processes. In: Lewan, M.D, Pittman, E.D. (Eds.), Role of Soil Organic Acids in Geological Processes. Springer, New York, pp. 138-161.

Du Plessis, C.P., 1987. New perspectives on early Waterberg Group sedimentation from the Gatkop area, northwestern Transvaal. South African Journal of Geology 90, 395-408.

Ehrlich, H.L., 1996. How microbes influence mineral growth and dissolution. Chemical Geology 132, 1-4.

Eriksson, P.G, Shreiber, U.M., Van der Neut, M., 1991. A review of the sedimentology of the Early Proterozoic Pretoria Group, Transvaal sequence, South Africa: Implications for tectonic setting. Journal of African Earth Sciences 13, 107-119.

Eriksson, P.G., Cheney, E.S., 1992. Evidence for the transition to an oxygen-rich atmosphere during the evolution of red beds in the Lower Proterozoic sequences of southern Africa. Precambrian Research, 54.257-269.

Eriksson, P.G., Hattingh, P.J., Altermann, W., 1995a. An overview of the geology of the Transvaal sequence and the Bushveld Complex South Africa. Mineralium Deposita 30, 98-111.

Eriksson, P.G., Reczko, B.F.F., Boshoff, A.J., Schreiber, U.M., Van der Neut, M., Snyman, C.P., 1995b. Architectural elements from Lower Proterozoic braid-delta and high-energy tidal flat deposits in the Magaliesberg Formation, Transvaal Supergroup South Africa. Sedimentary Geology 97, 99-117.

Eriksson, P.G., Altermann, W., 1998. An overview of the geology of the Transvaal Supergroup dolomites. Enviromental Geology 36, 179-188.

Eriksson, P.G., Van der Merwe, R., Bumby, A.J., 1998. The Palaeoproterozoic Woodlands Formation of eastern Botswana-northwestern South Africa: lithostratigraphy and relationship with Transvaal basin inversion structures. Journal of African Earth Science 27/3-4, 349-358.

Eriksson, P.G., Mazumder, R., Roy, K.K., Bose, P.K., Altermann, W., Van der Merwe, R., 1999. The 2.7-2.0 Ga volcano-sedimentary record of Africa, India and Australia: evidence for global and local changes in sea level and continental freeboard. Precambrian Research 97, 269-302.

Eriksson, P.G., Simpson, E. L., Eriksson, K.A., Bumby, A.J., Steyn, G.L., Sarkar, S., 2000. Muddy Roll-up structures in Siliciclastic Interdune Beds of the c. 1.8 Ga Waterberg Group, South Africa. Palaios 15, 177-183.

Eriksson, P.G., Altermann, W., Catuneanu, O., Van der Merwe, R., Bumby A.J., 2001. Major influences on the evolution of the 2.67-2.1 Ga Transvaal basin, Kaapvaal craton. Sedimentary Geology 141-142, 205-231.

Eriksson, P.G., Altermann, W., Eberhardt, L., Ahrend-Heidbrinck, S., Bumby, A.J., 2002. Palaeoproterozoic epeiric sea palaeoenvironments: Silverton Formation (Pretoria Group, Transvaal Supergroup), South Africa. In: Altermann, W., Corcoran P.L. (Eds.), Precambrian Sedimentary Environments: a modern approach to ancient depositional systems. Special Publication 33, International Association of Sedimentologists, Blackwell, Oxford, United Kingdom, 351-367.

Eriksson, P.G., Catuneanu, O., 2004. Third-order sequence stratigraphy in the Palaeoproterozoic Daspoort Formation (Pretoria Group, Transvaal Supergroup), Kaapvaal craton. In: Eriksson, P.G., Altermann, W., Nelson, D.R., Mueller, W.U., Catuneanu, O. (Eds.), Precambrian Earth: Tempos and Events. Elsevier, Amsterdam, pp. 724-735.

Eriksson, P.G., Bumby, A.J., Brumer, J.J., Van der Neut, M., 2006b. Precambrian fluvial deposits: enigmatic palaeohydrological data from the c.2-1.9 Ga Waterberg Group, South Africa. Sedimentary Geology 190, 25-46.

Eriksson, P.G., Altermann, W., Hartzer, F.J., 2006a. The Transvaal Supergroup and its precursors, In: Johnson, M.R., Anhaeusser, C.R., Thomas, R.J. (Eds.), The Geology of South Africa. Geological Society of South Africa, Johannesburg and Council for Geoscience, Pretoria, pp. 237-260.

Eriksson, P.G., Porada, H., Banerjee, S., Bouougri, E., Sarkar, S., Bumby, A.J., 2007b. Mat-destruction Features. In: Shieber, J., Bose, P.K., Eriksson, P.G., Banerjee, S., Sarkar, S., Altermann, W., Catuneanu, O. (Eds.), Atlas of Microbial Mat Features Preserved within the Siliciclastic Rock Record. : Atlas in Geosciences. 2. Elsevier, Amsterdam, pp. 76-105.

Eriksson, P.G., Shieber, J., Bououguri, E., Gerdes, G., Porada, H., Banerjee, S., Bose, P.K., Sarkar, S., 2007a. Classification of Structures Left by Microbial Mats in Their Host Sediments. In: Shieber, J., Bose, P.K., Eriksson, P.G., Banerjee, S., Sarkar, S., Altermann, W., Catuneanu, O. (Eds.), Atlas of Microbial Mat Features Preserved within the Siliciclastic Rock Record. : Atlas in Geosciences. 2. Elsevier, Amsterdam, pp. 39-52.

Eriksson, P.G., Long, D., Bumby, A.J., Eriksson, K.A., Simpson, E., Catuneanu, O., Classen, M., Ntikulu, M., Mudziri, K., Brumer, J., Van Der Neut, M., 2008. Palaeohydrological data from the c. 2.0 to 1.8 Ga Waterberg Group, South Africa: discussion of a possibly unique fluvial style. South African Journal of Geology 111, 281-304.

Eriksson, P.G., Rautenbach, C.J., Wright, D.T., Bumby, A.J., Catuneanu, O., Mostert, P Van der Neut, M., 2009. Possible evidence for episodic epeiric marine and fluvial sedimentation (and implications for palaeocurrent conditions), c. 2.3-1.8 Ga, Kaapvaal craton, South Africa. Palaeogeography, Palaeoclimatology, Palaeoecology, 273, 153-173.

Eriksson, P.G., Sarkar, S., Banerjee, S, Porada, H., Catuneanu, O., Samanta, P., 2010. Palaeoenvironmental context of microbial mat-related structures in siliciclastic rocks – examples from the Proterozoic of India and South Africa. Seckbach, J., Oren, A. (Eds.), Microbial Mats: Modern and Ancient Microorganisms in Stratified Systems. : Springer, Berlin, pp. 73-108.

Eriksson, P.G., Bartman, R., Catuneanu, O., Mazumder, R., Lenhardt, N., 2012. A case study of microbial mat-related features in coastal epeiric sandstones from the Palaeoproterozoic Pretoria Group (Transvaal Supergroup, Kaapvaal craton, South Africa); The effect of preservation (reflecting sequence stratigraphic models) on the relationship between mat features and inferred paleoenvironment. Sedimentary Geology, 263, 67-75.

Farmer, J.D., 1999. Taphonomic modes in microbial fossilization. In Proceedings of the workshop size limits of very small organisms, Space Studies Board, National Research, National Academies Press, Washinghton, DC, 94-102.

Garca-Pichel, F., Castenholz, R.W., 1994. On the significance of solar ultraviolet radiation for the ecology of microbial mats. In: Stal, L.J., Caumette, P. (Eds.), Microbial Mats, Structure, Development and Environmental significance, NATO ASI series, Springer-Verlag, Berlin, pp. 77-84.

Gavish, E., Krumbein, W.E., Halevy, J., 1985. Geomorphology, mineralogy and groundwater chemistry as factors of the hydrodynamic system of the Gavish sabkha. In: Friedman, G.M. Krumbein, W.E. (Eds.), Hypersaline Ecosystems: the Gavish sabkha. Springer-Verlag, Berlin, pp. 186-217.

Gehling, J.G., 1999. Microbial mats in terminal Proterozoic siliciclastics; ediacaran death masks. Palaios, 14, 40-57.

Gehling, J.G., 2000. Environmental interpretation and a sequence stratigraphic framework for the terminal Proterozoic Ediacara Member within the Rawnsley Quartzite, South Australia. Precambrian Research 100, 65-95.

Gerdes, G., Krumbein, W.E., Holtkamp, E.M., 1985. Salinity and water activity related zonation of microbial communities and potential stromatolites of the Gavish Sabkha. In: Friedman, G.M., Krumbein, W.E. (Eds.), Ecosystems: The Gavish Sabkha. Sringer Berlin, pp. 238-266.

Gerdes, G., Klenke, T., 2003. Geologische Bedeutung okologischer Zeiträume in biogener Schischtung (Mikrobenmatten, potentielle stromatolithe). Mitt. Ges. Geol. Bergbaustaud. Österr 46, 35-49.

Gutzmer, J., Beukes, N.J., 1998. Earliest laterites and possible evidence for terrestrial vegetation in the Early Proterozoic. Geology 26, 263-266.

Hagadorn, J.W., Pfluger, F., Bottjer, D.J., 1999. Unexplored microbial worlds. Palaios 14, 1-2.

Hall. A. L., 1932. The Bushveld Igneous Complex of the central Transvaal. Memoir of Geological Survey of South Africa, 28.

Hamblin, W.K., Christiansen, E.H., 2007. Earth's dynamic systems, 10th edition Prentice Hall, Upper Saddle River, New Jersey.

Hennes, E.A., Edward, E.L., Bumby, A.J., Eriksson, P.G., Eriksson, K.A., Hilbert-Wolf, H.L., Okafor, O.J., Linnevelt, S., Fitzgerald, M., Modungwa, T., 2014. Evidence for climate shifts in the 2.0 Ga upper Makgabeng Formation erg, South Africa. Palaeogeography, Palaeoclimatology, Palaeoecology 409, 265-279.

Henry, G., Clendein, C.W., Charlesworth, E.G., 1990. Depositional facies of the Black Reef Quartzite Formation in the eastern Transvaal. Abstracts (23rd Geocongress '90) of the Geological Society of South Africa, Cape Town, 234-237.

Jansen, H., 1975a. Precambrian basins on the Transvaal craton and their sedimentological and structural features. Transvaal Geological Survey, South Africa, 78, part 1, 25-33.

Jansen, H., 1982. The geology of the Waterberg Basin in the Transvaal, Republic of South Africa. Memoir of Geological Survey of South Africa 71, 98p.

Kalkowsky, E., 1908. Oolith and stromatolith in norddeutschen Bundsandstein. Z. Deutsche Geol. Ges. 60, 68-125.

Krumbein, W.E., 1983. Stromatolites – the challenge of a term in space and time. Precambrian Research 20, 493-531.

Krumbein, W.E., Patterson, D.M., Stal, L. (Eds.), 1994. Biostabilization of sediments. Bibliotheks-und Informationsystem der Carl von Ossietzky Unversitat Oldenburg, (BIS)-Verlag, Olderburg, 526 pp.

Miall, A.D., 1985. Architectural-element analysis: a new method of facies-analysis applied to fluvial deposits. Earth science Review 22, 261-308.

Nelson, D.R., Trendall, A.F., Altermann, W., 1999. Chronological correlation between the Pilbara and Kaapvaal cratons. Precambrian Research 97, 165-189.

Nisbet, E.G., Sleep, N.H., 2001. The habitat and nature of early life. Nature, 409, 1083-1091.

Noffke, N., 1999. Erosional remnants and pockets evolving from biotic-physical interactions in a Recent lower supratidal environment. Sedimentary Geology 123, 175-181.

Noffke, N., Gerdes, G., Klenke, T., Krumbein, W.E., 2001a. Perspectives. Microbially induced sedimentary structures-a new category within the classification of primary sedimentary structures. Journal of Sedimentary Research 71 (5), 649-656.

Noffke, N., 2003c. Epibenthic cyanobacterial communities counteracting sedimentary processes within siliciclastic depositional systems (present and past). In: Patterson, D., Zavarzin, G, Krumbein, W.E. (Eds.), Biofilms through space and time. Congress Proceedings, Kluwer Academic Publishers, pp. 265-280.

Noffke, N., Gerdes, G., Klenke, T., 2003b. Benthic cyanobacteria and their influence on the sedimentary dynamics of peritidal depositional systems (siliciclastics, evaporitic salty and evaporitic carbonatic). Earth Science Review 62: 163-176.

Noffke, N., Eriksson, K.A., Hazen, R.M., Simpson, E.L., 2006b. A new window into Early Archean life: microbial mats inn earth's oldest siliciclastic deposits (3.2 Ga Moodies Group, South Africa). Geology 34, 253-256.

Noffke N., Beukes N., Gutzmer, J., Hazen, R., 2006a. Spatial and temporal distribution of microbially induced sedimentary structures: A case study from siliciclastic storm deposits of the 2.9 Ga Witwatersrand Supergroup, South Africa. Precambrian Research 146:35-44.

Noffke, N., 2010. Geobiology: Microbial Mats in Sandy Deposits from the Archean Era to Today.

Noffke, N. and Awramik, S.M., 2013. Stromatolites and MISS-Differences between relatives. GSA Today, v. 23, no. 9, doi: 10.1130/GSATG187A.1.

Parizot, M., Eriksson, P.G., Tahar, A., Sarkar, S., Banerjee, S., Catuneanu, O., Altermann, W., Bumby, A.J., Bordy, E.M., Van Rooy, L., Boshoff, J., 2005. Suspected microbial mat-related crack-like sedimentary structures in the Palaeoproterozoic Magaliesberg Formation sandstones, South Africa. Precambrian Research 138, 274-296.

Patterson D., 1994. Microbial mediation of sediment structure and behavior. In: Stal, L. and Caumette, P. (Eds.), Microbial mats. Springer Verlag, Berlin.

Pettijohn, F.J., Potter, P.E., 1964. Atlas and Glossary of Primary sedimentary Structures: Berlin, Springer-Verlag, 370 p.

Plüger, F., 1999. Matground structures and redox facies. Palaios 14: 25-39.

Porada, H., Bougougri, E. 2007b. Wrinkle structures – a critical review. Earth Science Review 81: 199-215.

Porada, H., Eriksson, P.G., 2009. Cyanobacterial mat features in the siliciclastic sedimentary record: Palaeodeserts and modern supratidal flats. In: Seckbach, J., Walsh, M., (Eds.), From Fossils to Astrobiology: Records of life on Earth and search for extraterrestrial biosignatures. Cellular Origin, Life in Extreme Habitats and Astrobiology 12, pp. 181-210.

Reczko, B.F.F., 1994. The geochemistry of the sedimentary rocks of the Pretoria Group, Transvaal Sequence, PhD thesis, University of Pretoria.

Reid, R.P., Visscher, P.T., Decho, A.W., Stolz, J.F., Bebout, B.M., Dupraz, C., MacIntyre, I.G., Pearl, H.W., Pinckney, J.L., Prufert-Bebout, L., Steppe, T,F., Desmarais, D.J., 2000. The role of microbes in accretion, lamination and early lithification of modern marine stromatolites. Nature, 406, 989-991.

Reineck, H.E., Gerdes, G., Claes, M., Dunajtschik, K., Riege, H., Krumbein, W.E., 1990. Microbial modification of sedimentary surface structures. In: D. Heiling, P. Rothe, U. Forstner and P. Stoffers. (Eds.), Sediments and Environmental Geochemistry, Springer-Verlag, Berlin, pp. 254-276.

Retallack, G.J., 2001. Soils of the past: An introduction to Palaeopedology 2nd ed. Blackwell, Oxford. 600p.

Riding, R., 2000. Microbial carbonates: the geological record of calcified bacterial-algal mats and biofilms. Sedimentology 47, 179-214.

Riding, R.E., Awramik, S.M., 2000. Microbial sediments. Springer-Verlag, Berlin, 331 pp.

Rigby, M.J., Brandl, G., Mouri, H. 2008. P-T conditions and the origin of quartzo-feldspathic veins in metasyenites from the Central Zone of the Limpopo Belt, South Africa. South Africa Journal of Geology 111, 313-332.

Ruiz Cruz M.D., 2007. Genesis and evolution of the kaolin-group minerals during and the beginning of metamorphism. In: Nieto F., Jiménez-Milán J. (Ed), ‘’Diagenesis and Low-Temperature Metamorphism. : Theory, Methods and Regional Aspects’’ Seminarios SEM, 3, pp. 41-52.

SACS (South African Committee for Stratigraphy) 1980. Stratigraphy of South Africa Part 1 (Comp. L. E. Kent), Lithostratigraphy of the Republic of South Africa.South West Africa/Namibia, and the Republics of Bophuthatswana, Trankei and Venda. The Handbook of Geological Survey of South Africa 8.

Sarkar, S., Bose, P.K., Samanta, P., Sengupta, P., Eriksson, P.G., 2008. Microbial mat mediated structures in the Ediacaran Sonia Sandstone, Rajastan, India, and their implications for Peroterozoic sedimentation: Precambrian Research, 248-263.

Sheldon, N.D., 2012. Microbially induced sedimentary structures in the ca. 1100 Ma terrestrial midcontinent rift of North America. In: Noffke, N., Chafetz, H., (Eds.), Microbial mats in siliciclastic depositional systems through time. SEPM Special Publication 101, pp. 153-162.Schieber, J., 1998b. Deposition of mudstones and shales: overview, problems and challenges. In: Schieber, J., Zimmerle, W., Sethi, P., (Eds.), Shales and mudstones, vol. 1, Basin Studies, Sedimentology and Palaontology. Schweizerbart’sche Verlagsbuchhandlung, Stuttgart, pp. 187-215.

Schieber, J., 1998a. Possible indicators of microbial mat deposits in shales and sandstones: Examples from the Mid-Proterozoic Belt Supergroup, Montana, U.S.A.: Sedimentary Geology 120, 105-124.

Schieber, J., 1999. Microbial mats n terrigeneous clastics: the challenge of identification in the rock record. Palaios 14, 3-13.

Schieber, J., 2004. Microbial mats in the siliciclastic rock record: a summary of the diagnostic features. In: Eriksson, P.G., Altermann, W., Nelson, D.R., Mueller, W.U., Catuneanu, O. (Eds.), The Precambrian Earth: Tempos and Events. Developments in Precambrian Geology 12, Elsevier, Amsterdam, pp. 663-673.

Shieber, J., Bose, P.K., Eriksson, P.G., Sarkar, S., 2007. Palaeogeography of Microbial Mats in Terrigeneous Clastics-Environmental Distribution of Associated Sedimentary Features and the Role of Geologic Time. In: Shieber, J., Bose, P.K., Eriksson, P.G., Banerjee, S., Sarkar,

S., Altermann, W., Catuneanu, O. (Eds.), Atlas of Microbial Mat Features Preserved within the Siliciclastic Rock Record. : Atlas in Geosci. 2. Elsevier, Amsterdam, pp. 267-275.

Simpson, E.L., Eriksson, K.A., Eriksson, P.G., Bumby, A.J., 2002. Eolian dune degradation and generation of massive sandstones in the Palaeoproterozoic Makgabeng Formation, Waterberg Supergroup, South Africa. Journal of Sedimentary Research 72, 40-45.

Simpson, E.L., Heness, E., Bumby, A.J., Eriksson, P.G., Eriksson, K.A., Hilbert-Wolf, H.L., Linnevelt, S., Fitzgerald M., Modungwa, T., Okafor, O.J., 2013. 2.0 Ga continental ecosystem diversity: microbial mat proxies in a palaeodesert setting. Precambrian Research 237, 36-50.

Stal, L.J., 2000. Cyanobacterial mats and stromatolites. In: Whitton, B.A., Potts. M. (Eds.), The Ecology of Cyanobacteria. Kluwer Academic Publishers, Dordrecht, pp. 61-120.

Stettler, E.H., 1991. The present thickness of sediments in the main Waterberg basin as derived from Geophysical data. Precambrian sedimentary basins of southern Africa, Terra Nova 3, Abstracts p.58.

Tankard, A. J., Jackson, M. P. A., Eriksson, K. A., Hobday, K. A., Hunter, D. R., Minter, W. E. L., 1982. Crustal evolution of Southern Africa: 3.8 billion years of earth history: with a contribution by S.C. Eriksson .Springer-Verlag New York, 523p.

Treloar. P.J., Coward, M.P., Harris, N.B.W., 1992: Himalayan-Tibetan analogies for the evolution of the Zimbabwe craton and Limpopo Belt. Precambrian Research 55, 571-587.

Tyler, N., 1979a. The stratigraphy of the early Proterozoic Buffalo Springs Group in the Thabazimbi area, west-central Transvaal. Transval Geological Society of South Africa 82, 215-226.

Tyler, N., 1979b. Stratigraphy, geochemistry and correlation of the Ventersdorp Supergroup in the Derdepoort area, west-central Transvaal. Transval Geological Society of South Africa 82, 133-147.

Van der Merwe, R., Roering, C., Smith, C.A., 1988. Slickenside analysis of the Potchefstroom Fault. South African Journal of Geology, 91, 264-274.

Van der Neut, M., 1990. Affsettingstoestandevan die Pretoria Groepgesteentes in the Pretoria-Bronkhorstspruit-Delmasgebied. Unpublished Msc thesis, University of Pretoria, South Africa, 233p.

Visser, J.N.J., 1969.‘N Sedimentologiese Studievandieserie Pretoria in Transvaal. Unpublished PhD thesis, University of the Orange Free State, South Africa, 263pp.

Vos, R. G., Eriksson, K. A., 1977. An embayment model for tidal and wave-swash deposits occurring within a fluvially dominated Proterozoic sequence in South Africa. Sedimentary Geology 18, 161-173.

Watanabe, Y., Martini, J.E.J., Ohmoto, H., 2000. Geochemical evidence for terrestrial ecosystems 2.6 billion years ago. Nature 408, 574-578.

Welch, S.A., Ullman, W.J., 1993. The effect of organic acids on plagioclase dissolution rates and stoichiometry. Geo-chim. Cosmochim. Acta 57: 2725-2736.

Welch, S.A., McPhail, D.C., 2003. Mobility of major and trace elements during biologically mediated weathering of granite. In: Roach I.C. (Ed.), Advances in Regolith, 437-440.

Wingate, M.T.D., 1998. A palaeomagnetic test of the Kaapvaal-Pilbara (Vaalbara) connection at 2.78 Ga. South African Journal of Geology 101, 257-274.

Appendix 1: Utilizing modern microbial mats as analogy for Proterozoic mats and relationship to sedimentation and accommodation